SOME REACTIONS OF NEUTRAL

SPECIES IN FLAMES

_____

A thesis

submitted in partial fulfilment

of the requirements for the Degree

of

Doctor of Philosophy in Chemistry

in the

University of Canterbury

by

J.N. Mulvihill

_____

University of Canterbury

1975

CONTENTS

ABSTRACT

The combustion of trace additives in hydrogen-nitrogen-oxygen flames has been investigated experimentally by mass spectrometric and spectroscopic analysis of the burnt gas stream and theoretically by computer simulation. Breakdown of cyanogen in a flame of composition H_2: N_2: O_2 = 4.5 : 8.0 : 1.0 gives HCN and carbon oxides. The mass spectrometric ratio of HCN to CO/CO_2 mixture in the burnt gases emerging from the reaction zone is dependent on the percentage cyanogen added to the flame, showing a slow rise from 0.25 at 0.1% to 0.30 at 1.0% cyanogen, followed by a more rapid increase to a value of approximately unity at an additive concentration of 1.5%. Computer modelling on the basis of a main primary reaction:

$$H + C_2N_2 \rightarrow HCN + CN,$$
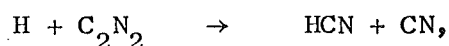
is inconsistent with these results. It is concluded that primary decomposition of C_2N_2 in hydrogen flames probably takes place by reaction with atomic oxygen:

$$O + C_2N_2 \rightarrow NCO + CN,$$
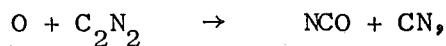
carbon oxides being formed from CN and NCO radicals by the fast processes:

$$CN + O_2 \rightarrow NCO + O,$$

$$NCO + O \rightarrow CO + NO,$$

$$NCO + H \rightarrow CO + NH.$$
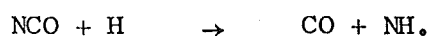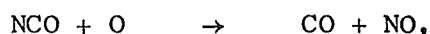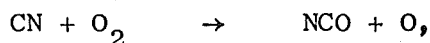
Production of HCN would then be limited to relatively slow reactions, giving calculated yields of HCN lower than the corresponding yields of carbon oxides, as observed experimentally.

Mass spectrometric measurement of HCN and NO profiles in a flame containing 1.1% cyanogen and 2.0% nitric oxide is used to determine a value for the rate of reaction of NO with CN radicals at the burnt gas temperature:

$$CN + NO \rightarrow N_2 + CO,$$

$$k = 7.5 \times 10^9 \ m^3 \ kgmol^{-1} \ s^{-1} \ at \ 1500 \ K.$$
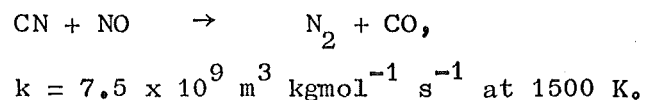
The reaction of NO with NH radicals is studied in a flame containing 0.90% nitric oxide and up to 1.15% ammonia. Results indicate that the reaction rate is sufficiently fast to reach equilibrium within the combustion zone, while isotopic labelling of the reactant NO and mass spectrometric analysis of the burnt gas stream gives evidence for the formation of molecular nitrogen as the predominant stable product.

Metal cyanide dissociation energies are determined for the alkali metals Li, Na, K, Rb and Cs. In the presence of known concentrations of HCN and H atoms, spectroscopic measurement of the proportion of metal combined to form metal cyanide enables a value to be calculated for the equilibrium constant of the reaction:

$$M + HCN \rightleftharpoons MCN + H.$$
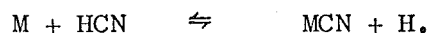
Statistical methods are then used to obtain the enthalpy of reaction at absolute zero and thus the dissociation energy of the metal cyanide.

CHAPTER I

INTRODUCTION

I. GENERAL INTRODUCTION

The studies described in this thesis have been carried out using a fuel-rich hydrogen-nitrogen-oxygen flame as the basic reaction system. Accurate, quantitative measurements in such systems have become possible since the development of the shielded, laminar-flow burner. In this design, the unburnt gases are mixed before entering the burner and pass up to the flame through bundles of fine stainless steel or silica tubes. Thus it is ensured that the gas flow in the flame is laminar. Primary combustion takes place in a flat, disc-shaped reaction zone about 1 mm thick, after which the burnt gases pass outward at approximately constant temperature and velocity for a distance of 2 to 3 cm. At this point, perturbations occur as the central "experimental" flame and the outer "shield" flame begin to merge.

The shielded stream of hot burnt gases in the central flame forms a high-temperature flow reactor in which the time scale in the usual reaction rate expressions is replaced by a scale of distance along the flame. A time interval of 0.001s corresponds to a distance of approximately 1 mm. In the present work, mass spectrometric sampling has been used to determine concentration profiles through the burnt gas region for stable species such as HCN and NO, while flame photometric methods have been used to obtain temperature profiles and concentration profiles for unstable species such as H atoms. Results from these two techniques have been combined to give information on reaction rates and equilibria in the burnt gases.

Over the past few years, advances in computing techniques, together with a more detailed understanding of the chemical and physical processes occurring in the reaction zone of a flame, have led to the development of computer programmes to simulate these processes. The results give calculated concentration profiles through the reaction zone for both stable and unstable species. Similar profiles are obtained for temperature, average molar enthalpy and other flame parameters. Hence it is possible to test a proposed reaction mechanism for a flame of known unburnt composition by comparing the computer results calculated on the basis of this mechanism with values derived from experimental measurements in the reaction zone and through the burnt gas region. The simulation programme used in this work was developed by Professor L.F. Phillips of this department from the hydrogen-bromine flame programme of Spalding and Stephenson. Beginning with a converged solution of the programme for a hydrogen-nitrogen-oxygen flame containing no additives, calculations have been carried out for the same flame containing trace quantities of cyanogen. A model reaction scheme is proposed to describe the breakdown of the additive in the flame. Using this mechanism, computer simulated profiles through the reaction zone are obtained for components such as HCN, CO and NO and are compared with the measured concentrations of these species in the burnt gas region immediately above the reaction zone, as derived from mass spectrometric sampling and flame photometry.

A major part of the thesis deals with the addition of small quantities of compounds such as cyanogen, nitric oxide or metal salts to the basic reaction system. Additives in flames must be considered from two aspects:

(i) the effect of the flame on the additive, in particular

the compounds formed by the additive with species already present in the flame gases;

(ii) the effect of the additive on flame parameters such as temperature, burning velocity and free radical concentrations. Thus when about 0.5% gaseous cyanogen is added to a hydrogen-nitrogen-oxygen flame, breakdown of C_2N_2 in the reaction zone gives HCN and carbon oxides. One effect on the flame is to produce a reduction of approximately 5% in the peak H atom concentration. If the proportion of additive is increased to about 1.5%, the flat reaction zone begins to lift away from the burner face, which indicates that the cyanogen is causing a major perturbation of the reaction system and that results derived from measurements in the burnt gas region may no longer be considered to refer to a hydrogen-nitrogen-oxygen flame containing trace amounts of cyanogen. This phenomenon, known as "flame-lift", is illustrated in plates I and II on pages 6-7.

II. SUMMARY OF THE THESIS

The introduction to this study is followed by a short review on the production of odd-nitrogen oxides in combustion processes.

Chapter III describes the burner and flow system, together with the apparatus and techniques used for flame analysis.

A series of experiments concerned with the collection and identification of solid oxide particles formed in hydrogen-nitrogen-oxygen flames by metals such as chromium and vanadium is discussed in Chapter IV. Adsorption of gaseous sulphur dioxide on the surface of metal oxide particles is also considered.

Chapter V deals with the breakdown of cyanogen in the reaction zone of a fuel-rich hydrogen-nitrogen-oxygen flame. Gaseous cyanogen is added in small amounts, up to about 1.5% of the unburnt gas

PLATE I

Flame Z8 (H_2 : N_2 : O_2 = 4.5 : 8.0 : 1.0)

Containing 0.5% Cyanogen

The reaction zone appears as a flat, disc-shaped region immediately above the burner face.

PLATE II

Flame Z8 ($H_2 : N_2 : O_2 = 4.5 : 8.0 : 1.0$)

Containing 1.5% Cyanogen

The additive concentration is now sufficiently high to cause a visible distortion of the reaction zone, an effect known as "flame-lift".

composition, the combustion products being analysed in the burnt gas region by mass spectrometric methods. The experimental results are discussed in terms of a proposed mechanism for the combustion of cyanogen. A similar study of the burnt gas stream in the same hydrogen-nitrogen-oxygen flame containing 1.1% cyanogen and 2.0% nitric oxide gives an estimate for the rate of reaction of NO with CN radicals at the burnt gas temperature.

Metal cyanide dissociation energies $D_o^o(M - CN)$ for the alkali metals Li, Na, K, Rb and Cs form the subject of Chapter VI. Optical measurement of the ratio [MCN] / [M] in the burnt gas region is combined with mass spectrometric measurement of [HCN] at the same point in the flame to give the equilibrium constant for metal cyanide formation, which in turn yields $D_o^o(M - CN)$.

Chapter VII is concerned with computer simulation of the processes occurring in the breakdown of cyanogen in the reaction zone of a fuel-rich hydrogen-nitrogen-oxygen flame. Using the model reaction scheme of Chapter V, together with additional data from the literature, calculations are carried out for a flame containing up to 1.0% cyanogen and the results are compared with those obtained by experimental analysis of the burnt gas stream.

In Chapter VIII the reaction of NO with NH radicals is investigated. Mass spectrometric measurement of the NO profile in a hydrogen-nitrogen-oxygen flame containing small quantities of both nitric oxide and ammonia indicates that the process is sufficiently fast to reach completion in the reaction zone. Isotopic labelling is used in identification of the reaction products.

Conclusions arising from the work discussed in the preceding chapters are summarised at the end of the thesis.

CHAPTER II

THE PRODUCTION OF ODD-NITROGEN OXIDES IN COMBUSTION PROCESSES

I. INTRODUCTION

Oxides of nitrogen emitted from combustion systems are known to play a major role in the formation of photochemical smog. As a result, the production of odd-nitrogen oxides in combustion processes has been extensively investigated in recent years, particularly with regard to the concentrations of NO_x pollutants in exhaust gases released to the atmosphere.

The predominant nitrogen oxide formed in combustion is nitric oxide, which is derived from one of two sources:

(i) "thermal" NO is produced by high-temperature oxidation of atmospheric nitrogen;

(ii) "fuel" NO is formed by oxidation of chemically bound nitrogen in the fuel.

In either case, the rate of nitric oxide production is dependent on the concentration of atomic oxygen, which in the combustion zone is known to be in excess of its equilibrium value. Super-equilibrium radical concentrations may be determined experimentally. In carbon monoxide-air flames, Malte and Pratt[41] have observed excess O atom concentrations in the range 0.1 to 1.0 mole percent by spectroscopic measurement of CO + O continuum chemiluminescence. Alternatively, radical concentrations may be calculated from the measured concentrations of stable species. This approach, which assumes partial equilibrium of the fast flame reactions:

$$H + O_2 \rightleftharpoons OH + O \ldots \ldots (1),$$

$$O + H_2 \rightleftharpoons OH + H \ldots \ldots (2),$$

$$H_2 + OH \rightleftharpoons H_2O + H \ldots \ldots (3),$$
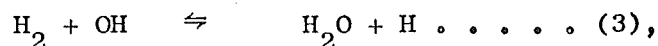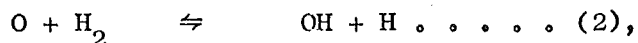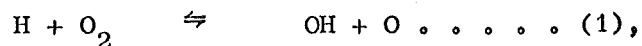
has been applied to kinetic models for nitric oxide formation in methane-air flames.[42, 43]

II. PRODUCTION OF "THERMAL" NO FROM ATMOSPHERIC NITROGEN

(1) Results in Hydrogen-Air and Carbon Monoxide-Air Flames

It is now well established that in flames of air with hydrogen or carbon monoxide production of "thermal" NO at temperatures in the range 2000 K to 2500 K is dominated by the Zeldovich[44] mechanism:

$$O + N_2 \rightleftharpoons NO + N \ldots \ldots (4),$$

$$N + O_2 \rightleftharpoons NO + O \ldots \ldots (5),$$
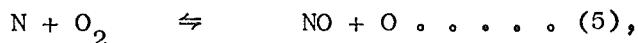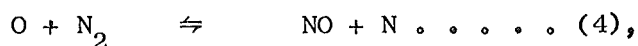
which under fuel-rich conditions is extended to include the process:

$$N + OH \rightleftharpoons NO + H \ldots \ldots (6).$$

Reactions involving N_2O become significant at temperatures below about 2000 K:

$$N_2 + O_2 \rightleftharpoons N_2O + O \ldots \ldots (7),$$

$$N_2 + OH \rightleftharpoons N_2O + H \ldots \ldots (8),$$

$$N_2O + O \rightleftharpoons NO + NO \ldots \ldots (9).$$
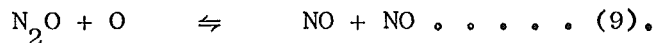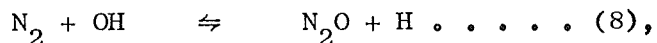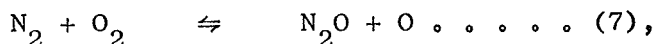
However, in most practical combustion systems, the N_2O mechanism makes a relatively small contribution to the total rate of nitric oxide formation.[45] The Zeldovich exchange reactions have been successfully used to predict rates of NO_x production in the jet-stirred combustion of hydrogen-air and carbon monoxide-air mixtures,[46] in hydrogen-air diffusion flames[47] and in the shock-induced combustion of hydrogen-nitrogen-oxygen mixtures.[45]

Kinetic models based on either the high temperature

Zeldovich mechanism or the low temperature N_2O mechanism are

dependent on the presence of super-equilibrium concentrations of

atomic oxygen in the combustion zone. This has been demonstrated

in a number of different investigations. In the jet-stirred

combustion of hydrogen-air and carbon monoxide-air mixtures,

Engleman and co-workers[46] have compared measured rates of

NO_x formation with the corresponding rates calculated on the

basis of reactions (4) to (6). Rate constants were taken from the

compilation of Baulch and co-workers.[37] The extended Zeldovich

mechanism was found to give close agreement between calculated and

experimental yields of nitrogen oxides only when excess O atom

concentrations in the reaction zone were correctly evaluated.

Similar results have been obtained by Malte and Pratt[41] for the

N_2O mechanism. Nitric oxide formation in the jet-stirred

combustion of carbon monoxide with moist air was predicted by

reactions (7) to (9) provided the values of temperature and O atom

concentration for the kinetic model were determined experimentally.

Measured concentrations of atomic oxygen were significantly higher

than the calculated equilibrium concentrations.

(2) Results in Hydrocarbon-Air Flames

In the post-combustion zone of hydrocarbon-air flames,

production of "thermal" NO is consistent with the Zeldovich

mechanism.[48, 49] However, in the vicinity of the combustion zone,

particularly for high values of fuel to air equivalence ratio, the

measured rates of nitric oxide formation exceed those calculated

on the basis of the Zeldovich exchange reactions.[48] This

"prompt" NO has been attributed by some workers to super-equilibrium

radical concentrations in the reaction zone. Bowman[50] has compared

experimental data on nitric oxide formation in shock-induced

methane combustion[51] and in methane-air and ethylene-air flames[48]

with rates of NO_x production predicted by the Zeldovich mechanism

for calculated non-equilibrium concentrations of atomic oxygen.

Satisfactory agreement was obtained for methane combustion in

fuel-lean and moderately fuel-rich mixtures. In premixed

methane-air flames, Sarofim and Pohl[43] have concluded that the

Zeldovich reactions give calculated rates of nitric oxide formation

which are a reasonable approximation to the measured yields of

"thermal" NO provided super-equilbrium radical concentrations are

calculated by assuming partial equilibrium of reactions (1) to (3).

A similar conclusion has been reached by Thompson, Brown and Beer[42]

from a study of the factors affecting fuel-lean methane combustion.

Fenimore[48] was the first to propose that the fast, transient

formation of nitric oxide in the primary reaction zone of

hydrocarbon flames could be due to the production of nitrogenous

intermediates by reaction of hydrocarbon fragments with molecular

nitrogen. "Prompt" NO was observed by this author in methane,

propane and ethylene flames. Since a comparable effect was not

detected in hydrogen or carbon monoxide flames, it was suggested

that rapid formation of nitrogen oxides could be caused by

processes of the type:

$$CH + N_2 \rightleftharpoons HCN + N \ldots \ldots (10),$$

$$C_2 + N_2 \rightleftharpoons 2CN \ldots \ldots (11),$$
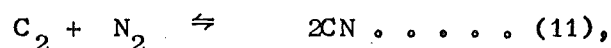
followed by oxidation of N atoms to nitric oxide by reaction with

OH radicals:

$$N + OH \rightleftharpoons NO + H \ldots \ldots (6).$$

A number of recent studies have supported this mechanism.

Iverach, Basden and Kirov[52] have measured rates of nitric oxide

production in methane, propane, ethylene and acetylene flames,

comparing the results with rates of NO_x formation calculated on the

basis of N atom and NO generation by the processes:

$$CH + N_2 \quad \rightleftharpoons \quad HCN + N \ . \ . \ . \ . \ . \ (10),$$

$$C + N_2 \quad \rightleftharpoons \quad CN + N \ . \ . \ . \ . \ . \ (12),$$

$$N + OH \quad \rightleftharpoons \quad NO + H \ . \ . \ . \ . \ . \ (6).$$
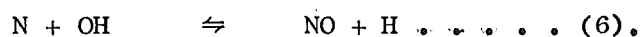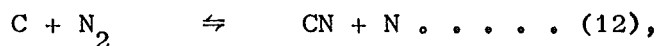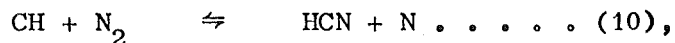
Parallel calculations were carried out for nitric oxide formation as

predicted by the Zeldovich reactions (4) to (6). In hydrocarbon

flames with fuel to air equivalence ratios greater than 1.15,

nitric oxide production rates in the combustion zone were modelled

by the Zeldovich mechanism only for unacceptably high concentrations

of atomic oxygen, whereas a satisfactory model was obtained using

reactions (10), (12) and (6) for concentrations of atomic nitrogen

greater by no more than a factor of two than the corresponding

equilibrium concentrations. Similar results have been reported by

Engleman and co-workers[46] for NO_x formation in propane-air flames.

Over the composition range 50% to 150% stoichiometric air, the

Zeldovich mechanism was found to underpredict the measured yields

of nitrogen oxides by a factor of four in lean mixtures and by an

order of magnitude in rich mixtures, a discrepancy which was

considered too large to be attributed solely to super-equilibrium

O atom concentrations in the reaction zone. It was concluded

that breakdown of the hydrocarbon could be giving rise to readily

oxidised nitrogenous intermediates.

Direct experimental evidence for the production of HCN or

CN species from hydrocarbon fuels has been obtained in propane-air

flames,[53] where HCN was detected in the burnt gas stream at

concentrations ranging from 0.3 ppm for a fuel to air equivalence

ratio of 1.10 to 8.0 ppm for an equivalence ratio of 1.35. Formation

of nitric oxide from nitrogenous intermediates has also been

demonstrated in two-stage methane combustion.[54] Analysis of the

gas composition after primary combustion showed the presence of the

intermediates NH_3 and HCN, while addition of nitric oxide to the

fuel resulted in an increase in the concentrations of NH_3 and HCN

in the gas stream from the primary combustion chamber, together

with a comparable increase in the total NO_x concentration in the

exhaust gases from the secondary combustion chamber.

A survey of these and other similar investigations indicates

that a number of mechanisms contribute to the production of "thermal"

NO in hydrocarbon flames. The Zeldovich reactions:

$$O + N_2 \rightleftharpoons NO + N \ldots \ldots (4),$$

$$N + O_2 \rightleftharpoons NO + O \ldots \ldots (5),$$

$$N + OH \rightleftharpoons NO + H \ldots \ldots (6),$$
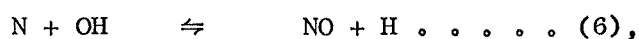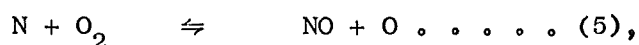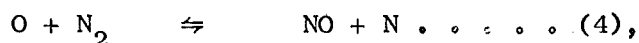
appear to dominate in the post-flame region. In the combustion

zone, particularly under fuel-rich conditions, there is evidence

for a significant contribution from "prompt" NO, produced by a

mechanism involving CN or NH intermediates. Present results are

consistent with reactions of the type:

$$CH + N_2 \rightleftharpoons HCN + N \ldots \ldots (10),$$

$$C + N_2 \rightleftharpoons CN + N \ldots \ldots (12),$$
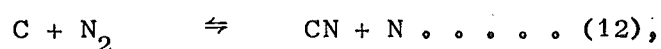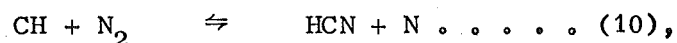
followed by oxidation of atomic nitrogen and possibly CN radicals

to nitric oxide. In addition, nitrogen dioxide may play a role in

the formation of "prompt" NO. From a study of NO_x production in

methane-air flames, Merryman and Levy[55] have proposed a mechanism

in which nitric oxide, formed in the combustion zone by oxidation of

CN or NH radicals, is rapidly converted to nitrogen dioxide by

reaction with HO_2 radicals:

$$CN/NH + O_2 \rightleftharpoons NO + CO/OH \ldots \ldots (13),$$

$$NO + HO_2 \rightleftharpoons NO_2 + OH \ldots \ldots (14).$$
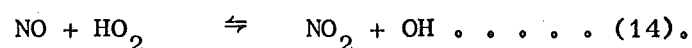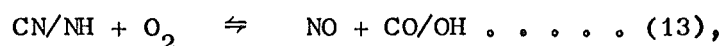
Nitric oxide is regenerated in the post-flame region by the process:

$$NO_2 + O \; \rightleftharpoons \; NO + O_2 \; . \; . \; . \; . \; . \; (15).$$
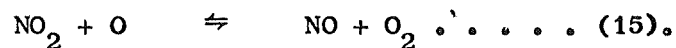
III. PRODUCTION OF "FUEL" NO FROM CHEMICALLY BOUND NITROGEN

The production of nitric oxide from nitrogen-containing fuels is considered to follow a two-stage kinetic scheme. Breakdown of the primary nitrogen compound gives a series of nitrogen-containing intermediates, which may react either with a species OX to form nitric oxide or with a species NX, generally nitric oxide itself, to form molecular nitrogen:

primary nitrogen compound

↓

intermediates,

e.g. HCN, CN, NH_2, NH, N

↓ OX   NX ↓

NO N_2

Fenimore[56] has studied the formation of nitric oxide in premixed ethylene flames containing small quantities of pyridine, ammonia, methylamine or methacrylonitrile. The measured yields of nitric oxide were found to follow the equation:

$$\frac{[NO]}{X} = 1 - e^{-([NO] + [N])/2X} \; . \; . \; . \; . \; . \; (16),$$

where [NO] is the observed concentration of nitric oxide in the burnt gas, [N] is the concentration which would be observed if all the added nitrogen were converted to nitric oxide and X is the maximum concentration of nitric oxide formed as [NO] becomes independent of [N]. Plots of $\log_{10}$ ([NO]/[N]) versus $\log_{10}$ ([N]/X) gave two asymptotes:

(i)   at low additive concentrations,

[NO] = [N];

(ii)   at high additive concentrations,

$$[NO] = X.$$

These results were interpreted by assuming that all nitrogen added

to the flame passes through an intermediate I, which reacts either

with a species R to give nitric oxide:

$$I + R \quad \rightarrow \quad NO + \ldots \ldots (17),$$

or with nitric oxide itself to give molecular nitrogen:

$$I + NO \quad \rightarrow \quad N_2 + \ldots \ldots (18).$$
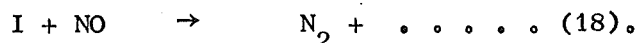
The equation for nitric oxide production by reactions (17) and (18)

was shown to give a solution of the same form as the experimental

curve (16). At low initial proportions of additive, all added

nitrogen would be expected to form nitric oxide:

$$k_{18} [NO] \ll k_{17}[R],$$

$$[NO] = [N];$$

while at high initial proportions of additive the concentration of

nitric oxide in the flame gases would reach a maximum:

$$k_{18} [NO] = k_{17} [R],$$

$$[NO] = \frac{k_{17} [R]}{k_{18}} = X.$$

The parameter X was found to be dependent on flame temperature

and composition. Plots of $\log_{10}X$ versus 1/T gave straight lines

of the form:

$$\log_{10}X = A - \frac{E}{2.303RT} \quad \ldots \ldots (19),$$

where the constants A and E were determined by the fuel to oxidant

equivalence ratio in the unburnt gas. For equivalence ratios in

the range 1.72 to 2.00, the temperature dependence E was calculated

to be approximately 285 kJ mol^{-1}, a figure which is close to the

temperature dependence of the equilibrium:

$$H_2O \quad \leftrightarrows \quad OH + \tfrac{1}{2}H_2 \ldots \ldots (20).$$
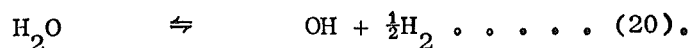
Therefore, it was suggested that the species R could be the OH radical. Since the value of X was characteristic of a given flame and independent of the nature or concentration of nitrogen-containing additive, the intermediate I was considered to be the same species, whether derived from aromatic nitrogen in pyridine, from an amine group in ammonia or methylamine, or from the CN group of methacrylonitrile. This was taken as evidence for a carbon-free intermediate, probably atomic nitrogen.

Similar results have been obtained by de Soete[57] for "fuel" NO production from ammonia, nitric oxide and cyanogen in flames of ethylene and oxygen premixed with helium or argon. Profiles of stable species in the near flame zone were used to determine the overall rates of "fuel" NO and N_2 formation. Comparison of the rate constants with those for the corresponding steps of the Zeldovich mechanism:

$$N + O_2 \;\rightleftharpoons\; NO + O \;.\;.\;.\;.\;.\;. \;(5),$$

$$N + NO \;\rightleftharpoons\; N_2 + O \;.\;.\;.\;.\;. \;(4r),$$
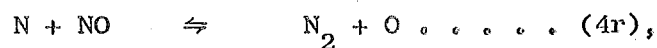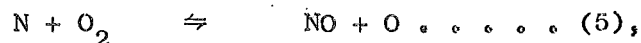
indicated that atomic nitrogen is likely to be the final indispensable intermediate in the production of nitric oxide from nitrogen-containing fuels.

Appleton and Heywood[58] have used a continuous flow combustor to study the formation of nitrogen oxides from atomised liquid fuels. The measured yields of "fuel" NO from nitrogen-containing additives were consistent with a kinetic scheme in which pyrolysis of the primary nitrogen compound gives CN and NH intermediates, which are oxidised to atomic nitrogen and nitric oxide by the fast exchange reactions:

$$CN + O \quad \rightleftharpoons \quad N + CO \ . \ . \ . \ . \ . \ (21),$$

$$NH + O \quad \rightleftharpoons \quad N + OH \ . \ . \ . \ . \ . \ (22),$$

$$NH + O \quad \rightleftharpoons \quad NO + H \ . \ . \ . \ . \ . \ (23),$$

$$N + O_2 \quad \rightleftharpoons \quad NO + O \ . \ . \ . \ . \ . \ (5).$$
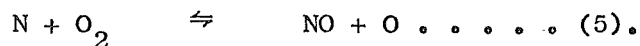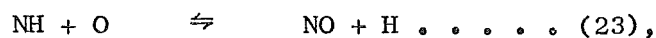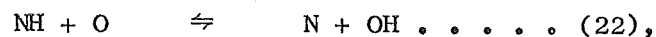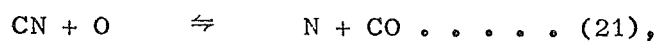
These processes occur in competition with the reduction of nitric

oxide by reactions of the type:

$$NH + NO \quad \rightleftharpoons \quad N_2 + OH \ . \ . \ . \ . \ . \ (24),$$

$$N + NO \quad \rightleftharpoons \quad N_2 + O \ . \ . \ . \ . \ . \ (4r).$$
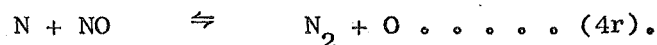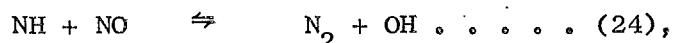
In terms of this mechanism, the degree of oxidation of

nitrogen-containing intermediates to nitric oxide would be expected

to depend on the availability of atomic oxygen, fuel-lean conditions

giving higher rates of nitric oxide production than fuel-rich

conditions. Experimentally, the highest yields of nitrogen oxides

were obtained, as predicted, from fuel-lean flames with good

fuel-air mixing.

According to the data published by these and other groups

of workers, the formation of nitric oxide from nitrogen-containing

fuels may take place through a number of intermediate species,

depending on the structure of the primary nitrogen compound.

However, the final yield of "fuel" NO will be determined by the

relative rates of the processes:

$$I + R \quad \rightarrow \quad NO + \ . \ . \ . \ . \ . \ (17),$$

$$I + NO \quad \rightarrow \quad N_2 + \ . \ . \ . \ . \ . \ (18),$$
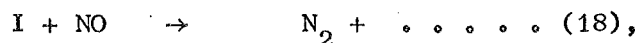
where the intermediate I is generally atomic nitrogen or CN or NH

radicals. The reactant R may represent several different

oxygen-containing species. Fenimore has suggested an important

contribution from hydroxyl radicals:

$$N + OH \quad \rightleftharpoons \quad NO + H \ . \ . \ . \ . \ . \ (6),$$
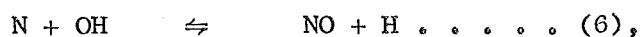
while de Soete and Appleton and Heywood have assumed the predominant

reactants to be atomic and molecular oxygen:

$$NH + O \quad \rightleftharpoons \quad NO + H \ldots \ldots (23),$$

$$N + O_2 \quad \rightleftharpoons \quad NO + O \ldots \ldots (5).$$
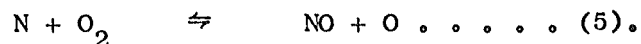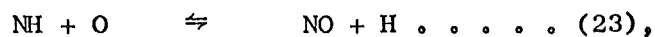
IV. PRODUCTION OF NITROGEN DIOXIDE IN COMBUSTION PROCESSES

Although nitrogen dioxide is considered to form less than 5% of the total nitrogen oxides emitted from most combustion systems,[59-61] this compound has been observed in proportions as high as 80% in exhausts from gas turbines.[62] Significant concentrations of nitrogen dioxide have also been reported in recent laboratory experiments. Cernansky and Sawyer[63] have determined NO_x and NO_2 profiles in a turbulent propane-air diffusion flame, while Merryman and Levy[55] have carried out similar measurements in laminar methane-air flames, the results in both cases indicating that nitrogen dioxide is formed by rapid oxidation of nitric oxide in the presence of super-equilibrium radical concentrations. Thus nitrogen dioxide may play a more important part than previously expected in the production of nitrogen oxides in combustion processes.

Merryman and Levy have shown their results to be consistent with a mechanism in which the initial formation of nitric oxide from either atmospheric or chemically bound nitrogen takes place in the reaction zone by oxidation of CN or NH intermediates:

$$CN/NH + O_2 \quad \rightleftharpoons \quad NO + CO/OH \ldots \ldots (13).$$
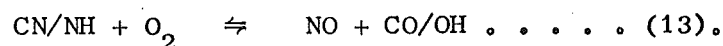
In the visible flame region, nitric oxide is rapidly converted to nitrogen dioxide by reaction with HO_2 radicals:

$$NO + HO_2 \quad \rightleftharpoons \quad NO_2 + OH \ldots \ldots (14).$$
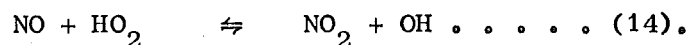
As the radical concentrations decline to equilibrium in the post-flame region, nitric oxide is regenerated by reduction of nitrogen dioxide:

$$NO_2 + O \quad \rightleftharpoons \quad NO + O_2 \ldots \ldots (15),$$
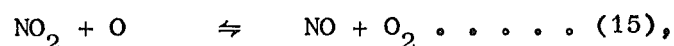
while further production of nitric oxide occurs through the Zeldovich reactions.

The chemistry of nitrogen oxides in hydrocarbon flames is therefore more complicated than would be expected from the simple Zeldovich mechanism. Although the Zeldovich reactions undoubtedly contribute to NO_x formation, particularly in the post-flame zone, recent investigations such as those of Fenimore and Merryman and Levy indicate that in the combustion zone nitric oxide is produced largely by oxidation of CN, NH or N intermediates. Super-equilibrium radical concentrations lead to further oxidation of nitric oxide to nitrogen dioxide. Since the nitrogenous intermediates may be derived either by reaction of hydrocarbon fragments with molecular nitrogen or by pyrolysis of nitrogen-containing fuels, the results imply a similar kinetic scheme for the production of both "thermal" and "fuel" NO.

CHAPTER III

EXPERIMENTAL

I. THE BURNER

The burner used in the present work was similar to that
described by McEwan.[1] As shown in figure 1, the core consisted
of approximately 500 stainless steel hypodermic tubes (gauge 20)
glued together. The central 100 tubes were supplied with gas plus
additives for the "experimental" flame, while the surrounding 200
tubes were supplied with gas of the same composition but without
additives for the "shield" flame. The remaining 200 tubes could
be supplied with hydrogen for an additional "outer shield" flame
if this was required. Inside the burner, there were three compart-
ments separated by neoprene "O" rings on brass washers. The
stainless steel tubes were glued to the washers with araldite,
after which the araldite was overlaid with sealing wax to prevent
leakage between compartments caused by the glue expanding away from
the brass. Cooling water was circulated through the upper chamber.

The burner was mounted vertically on a movable table, which
could be raised or lowered by turning a screw. From the pitch of
the screw thread (26 turns per inch), it was possible to adjust the
burner position to an accuracy of $\pm$ 0.25 mm over a range of about
10 cm. In this way, distance measurements in the burnt gas region
of a given flame could be converted to a time scale by calculating
the flow rate of the burnt gas from the rate of supply of the
unburnt gas, the cross-sectional area of the central flame, the
unburnt gas temperature and the final flame temperature.
Calculations of this type assume a planar flame front. In the present

FIGURE I   22

Burner Design for the Production of Premixed Laminar-Flow Flames
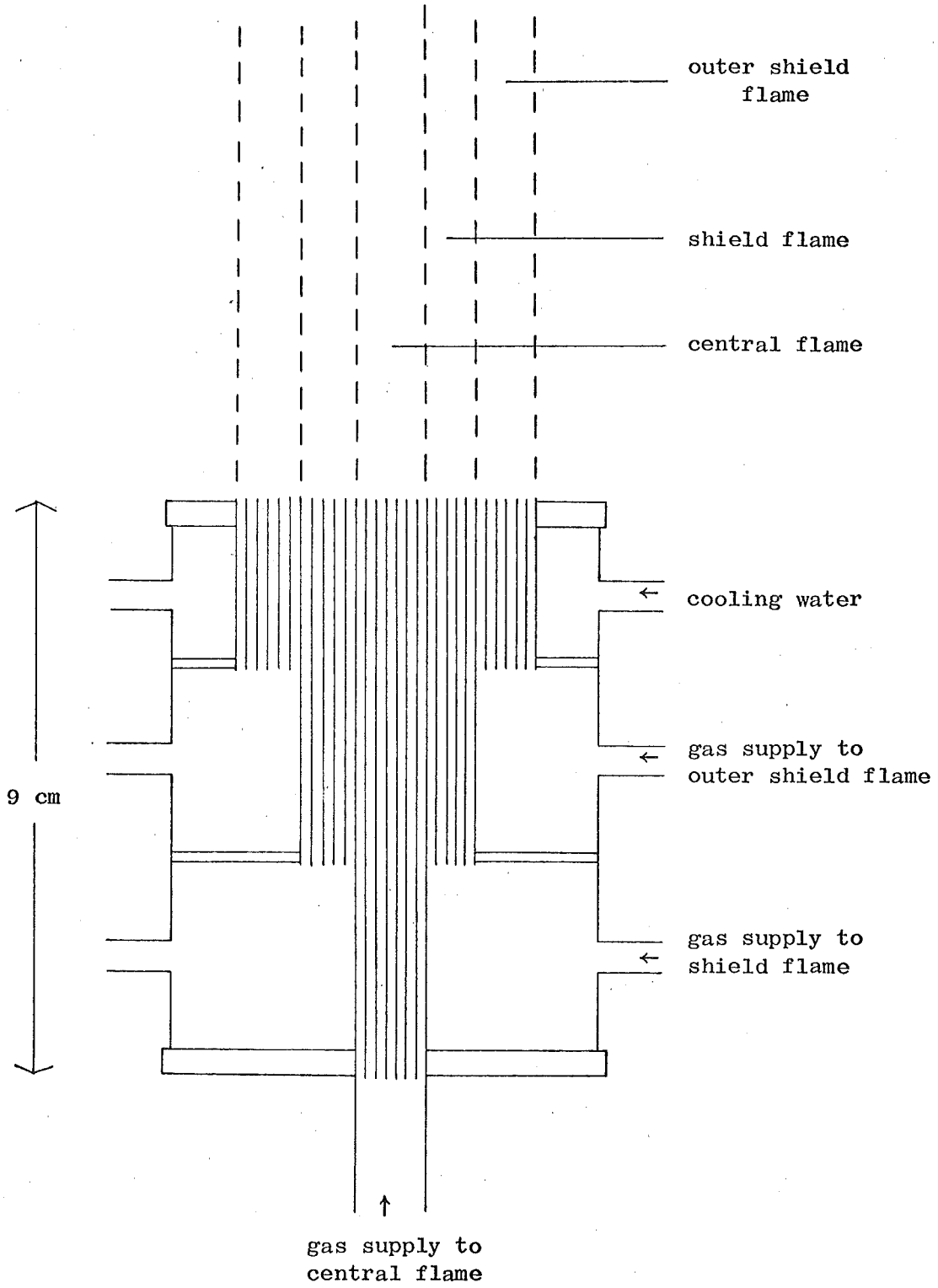
work this assumption may be considered reasonable, since the measurements were carried out within 0.005s of the reaction zone.

Actual distance resolution in the flame was limited to approximately 0.5 mm. This corresponds in optical work to the finite solid angle of light received from the flame,[2] while in mass spectrometric sampling it corresponds to the finite external diameter of the probe tip.

II. FLAMES : COMPOSITION AND CONTROL

Figure 2 shows the flow line for the supply and control of gases to the burner. Flow rates were measured by capillary flow-meters with dibutyl phthalate as the manometric liquid. In most cases, these capillary flowmeters were calibrated using commercial Rotameter flowmeters, but for gas flows less than about $1 \text{ cm}^3 \text{ s}^{-1}$ it was necessary to use a bubble meter made from a 100 ml burette. Agreement between the two methods where their ranges overlapped was within 5%.

Commercial hydrogen, nitrogen, argon and compressed air were taken from cylinders without further purification. For a given hydrogen-nitrogen-oxygen flame, the unburnt gas composition was determined by assuming that air is exactly 20% oxygen and 80% nitrogen. Mixing of the gases prior to the burner took place in small (~ 50 cm^3) mixing chambers.

As has been done in previous work,[2] the flames were classified according to their unburnt composition. A family of flames is a group with the same, usually integral, nitrogen to oxygen ratio. In fuel-rich flames, the hydrogen to oxygen ratio generally takes the values 2.5, 3.0, 3.5, 4.0 and 4.5, denoted by the letters F, K, P, U and Z respectively. The family number is indicated by

FIGURE II   24

Flow Line for the Supply and Control of Gases to the Flame
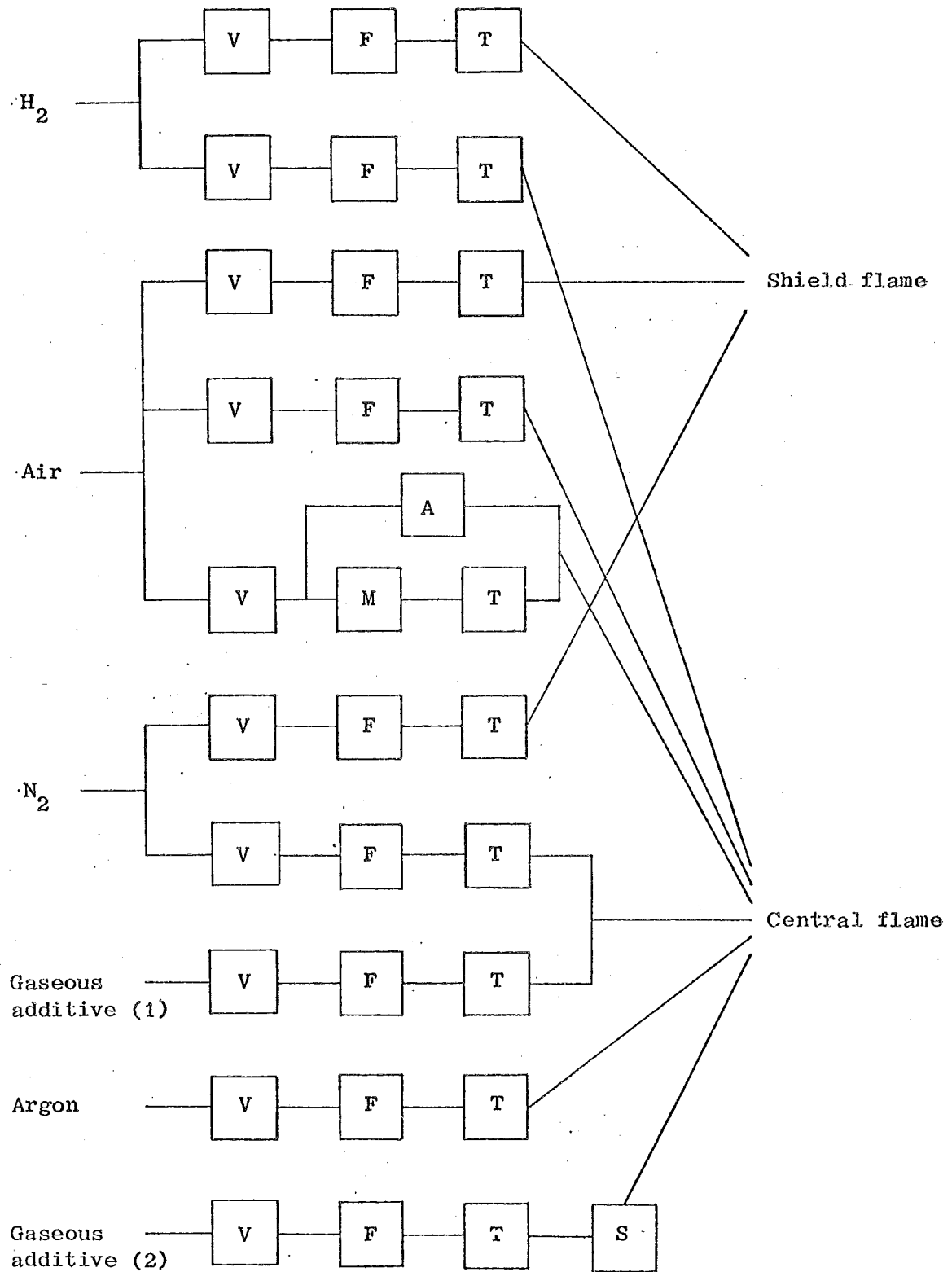
V: needle valve   S: stopcock

F: capillary flowmeter   M: mercury manometer

T: trap   A: atomiser

the nitrogen to oxygen ratio as a suffix. For example, flame Z8

has unburnt composition H_2: N_2: O_2 = 4.5 : 8.0 : 1.0, while flame

P6 has H_2: N_2: O_2 = 3.5 : 6.0 : 1.0. Most of the experiments des-

cribed in the present work were carried out in the fuel-rich flame

Z8, which has a final temperature of about 1500 K in the burnt

gas region.

III. ADDITIVES

(1) Gases

Gaseous additives were introduced directly into the unburnt

gas stream. Nitric oxide, nitrous oxide, cyanogen and carbon

monoxide were taken from cylinders (Matheson Gases), while gaseous

ammonia and sulphur dioxide were obtained from cylinders

(New Zealand Industrial Gases) of liquefied ammonia and sulphur

dioxide respectively. Flow rates were measured with capillary

flowmeters. Addition to the unburnt gas supply could be carried

out in two ways:

  (i) by mixing with the nitrogen flow to the central flame;

  (ii) by introduction into the premixed unburnt gases for the

    central flame just before they entered the burner.

The second inlet close to the burner was fitted with an off-on

stopcock which was used when it was necessary to minimise the time

interval between introduction of the additive into the gas stream

and its appearance in the flame. Using flame Z8, unburnt gas flow

81.0 cm^3 s^{-1}, response times of about one second could be obtained.

In the work involving simultaneous addition of nitric oxide and

ammonia, maintenance of a steady flow of nitric oxide was achieved

by using a Matheson 14-660 gas regulator, constructed of

corrosion-resistant stainless steel.

FIGURE III   26

Atomiser for Addition of Aqueous Metal Salt

Solutions to the Flame

aqueous metal salt
solution, liquid level
controlled by height
of adjacent reservoir

to liquid
reservoir

air supply to
central flame
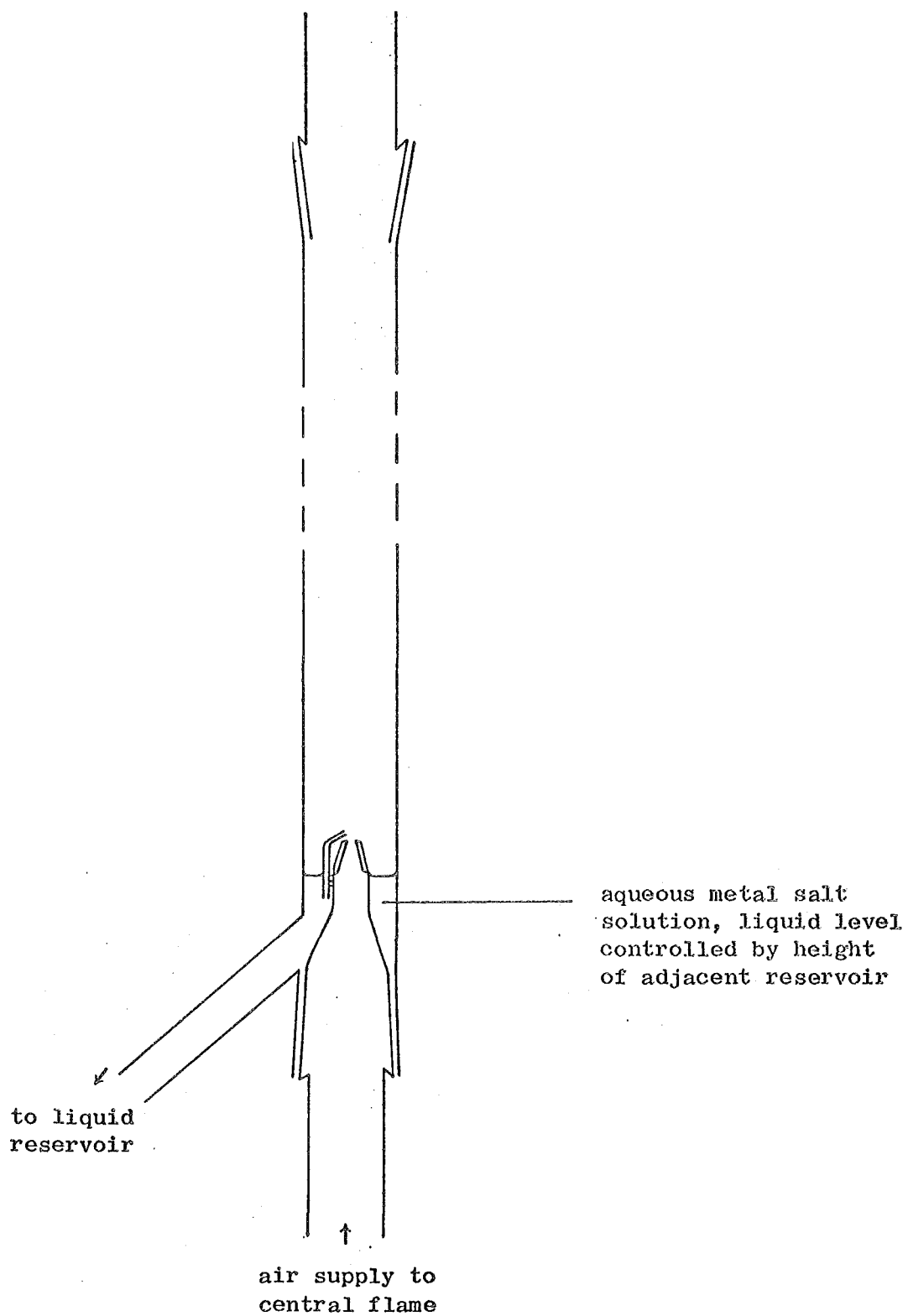
Escape of dangerous additive gases and their combustion products into the laboratory was prevented by constructing a four-sided metal enclosure with forced ventilation to surround both the burner and the quartz probe used for mass spectrometric sampling. Quartz windows (2 in x 2 in) on opposite walls of the enclosure provided a light path for optical measurements. On a third side of the metal surround, a hinged trapdoor gave access to the burner, while for major adjustments to the burner or mass spectrometric sampling system it was possible to demount and completely remove the protective enclosure.

(2) Metals

Metals were added to the unburnt gases as fine sprays of aqueous solutions of their salts. Generally, the simple nitrates or chlorides of the metals were used, as these are known to be completely and rapidly fragmented in the reaction zone, unlike the more stable phosphates and sulphates.[3] Figure 3 gives a diagram of the atomiser. This was based on the design described by Phillips[2] and was operated by diverting part of the air stream to the central flame through the atomiser jet. The final concentration of metal atoms in the burnt gas was of the order of one part in 10^6.

IV. MASS SPECTROMETRIC SAMPLING

Concentrations of stable species in the burnt gas region were determined by continuous flow sampling and mass spectrometric analysis. A quartz microprobe, made by drawing 1 mm external diameter tubing down to produce an orifice about 25 μ in diameter, was positioned horizontally in the flame. A similar probe has

been used by Sutton[4] in hydrogen-nitrogen-oxygen and

hydrogen-nitrogen-nitrous oxide flames. In general, it has been

shown that satisfactory results may be obtained provided the

orifice diameter of the probe is less than $100\,\mu$.[5-7]

The sampling system is illustrated in figure 4. Differential

pumping was used to maintain a pressure of no more than a few torr

in the flow line from the porous silicon-carbide plug, which

restricted the rate at which gases were extracted from the flame,

to the inlet to the variable leak. Thus it was ensured that the

pressure in the sampling line was sufficiently low to quench the

flame reactions. Condensation of water in the high pressure region

from the probe tip to the porous plug was eliminated by heating the

tube electrically to approximately $100^{\circ}C$.

The mass spectrometer was an E.A.I. quadrupole mass filter,

model 150A, set up to cover the mass range 1 to 150 amu. A

Granville-Phillips diaphragm type variable leak regulated the

fraction of the sample gas stream passing into the mass filter and

hence controlled the pressure in the ionisation chamber, which was

measured with an ionisation gauge (Edwards High Vacuum). The output

from the electron multiplier of the mass spectrometer was monitored

with a Keithley high-speed picoammeter and chart recorder.

Peak heights in the mass spectrum were found to be particularly

sensitive to the emission current recorded at the anode of the

ionisation chamber. This was therefore maintained at a steady value

of $100\,\mu A$. Total gas pressure in the ionisation chamber during

analysis of a sample was normally in the range 2×10^{-5} to 6×10^{-5}

torr. Pressure fluctuations could be taken into account by adding

argon to the flame at a constant known flow rate of the order of 1%

of the unburnt gas composition, the mass spectrometric peak heights

being related to the corresponding argon-40 peak heights at the same

FIGURE IV   29

Continuous Flow Sampling System for Mass Spectrometric

Analysis of the Burnt Gas Stream

quartz probe (internal
pressure 760 torr)

porous
silicon-carbide
plug

probe tip in central
flame (orifice
             diameter 25μ)

|← 10 cm →|

pyrex
tubing

burner
face

nichrome wire for
electrical heating

35 cm

capillary tube (orifice
diameter 1 mm)

teflon
vacuum
valve

V

to mass filter (pressure in ionisation
chamber 2 x 10^{-5} to 6 x 10^{-5} torr)

araldite seals

to
vacuum
pump
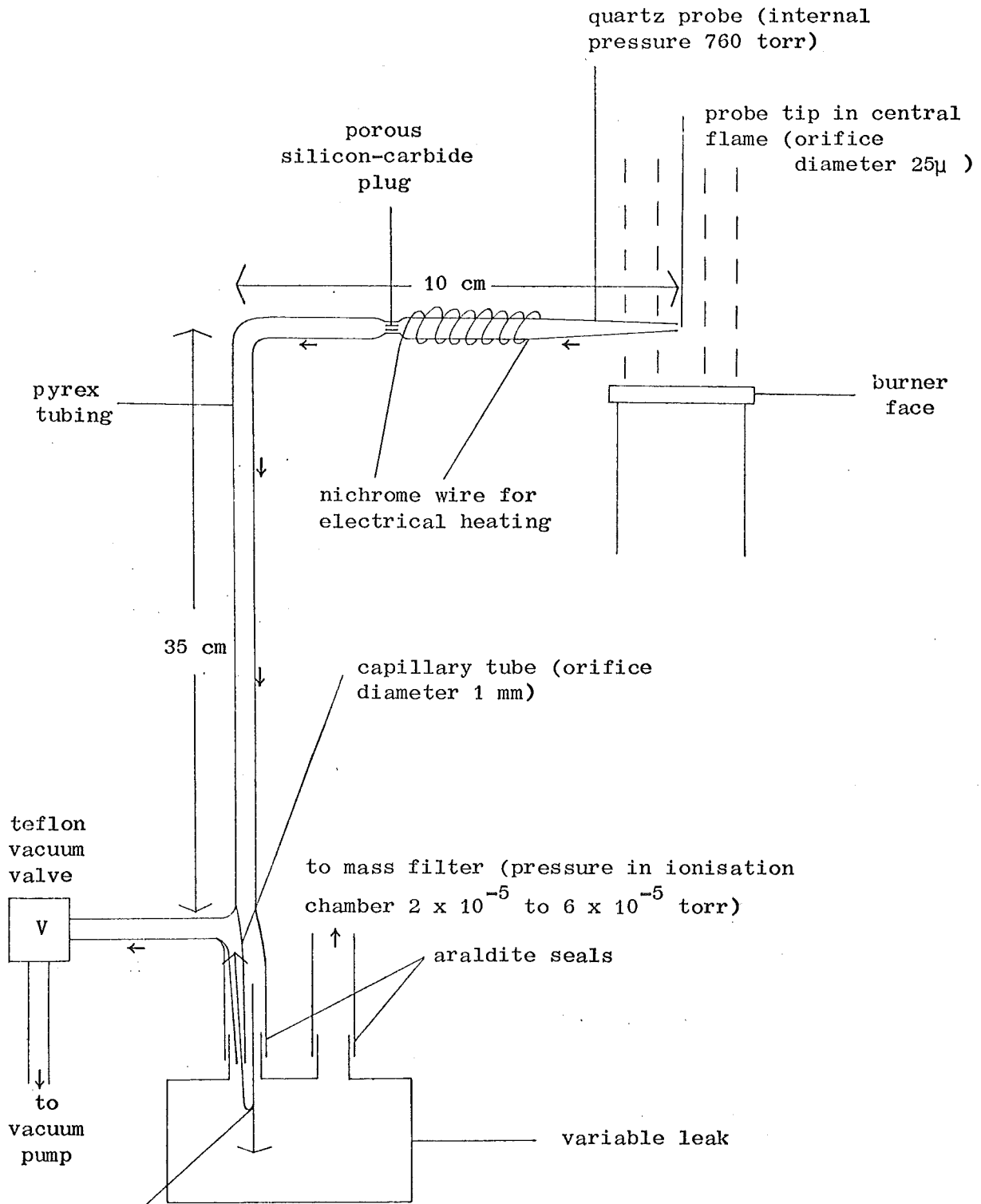
variable leak

gas stream divides: small fraction passes on into variable leak

and remainder is drawn off by vacuum pump

direction of gas flow: →

point in the flame.

The probe and sampling line were supported on a rigid frame-work close to the burner. When taking samples, the position of the probe tip relative to the plane of the reaction zone was determined by first raising the burner until the probe could be seen to lie just within the reaction zone and then slowly lowering the burner by the required number of turns of the calibrated thread. Concentration profiles through the burnt gas region were obtained by scanning the appropriate parts of the mass spectrum at each sampling position. Using this technique, distance resolution in the profiles was limited to about 0.5 mm, the finite external diameter of the probe tip.

V. PHOTOMETRIC MEASUREMENTS

Photometric techniques were used to determine the concen-trations of unstable species in the burnt gas region. The absorption-emission system, which is shown in figure 5, was of the same design as that used by Dr M.J. McEwan[1] of this department. Light from the flame was analysed by a Jarrell-Ash grating monochromator. This was generally used in conjunction with an E.M.I. 9558 Q photomultiplier. However, in work on the dissociation energy of caesium cyanide, the E.M.I. 9558 Q was found to have insufficient sensitivity at longer wavelengths to detect the caesium emission lines at 852.1 nm and 894.3 nm. Hence in these experiments it was replaced by an R.C.A. 7102 red-sensitive photomultiplier.

Referring to figure 5, the background source for absorption measurements was a hollow cathode lamp (lithium or sodium-potassium), which was run from a stabilised 500 volt power supply, using a lamp

A: background source

B: burner

C: quartz lens

D: spectrometer

E: photomultiplier

F: light chopping disc

G: 6-volt bulb

H: 90 AV photocell

N: phase-sensitive detector

M: microammeter

O: amplifier

P: 300 volt power supply

Q: photomultiplier power supply
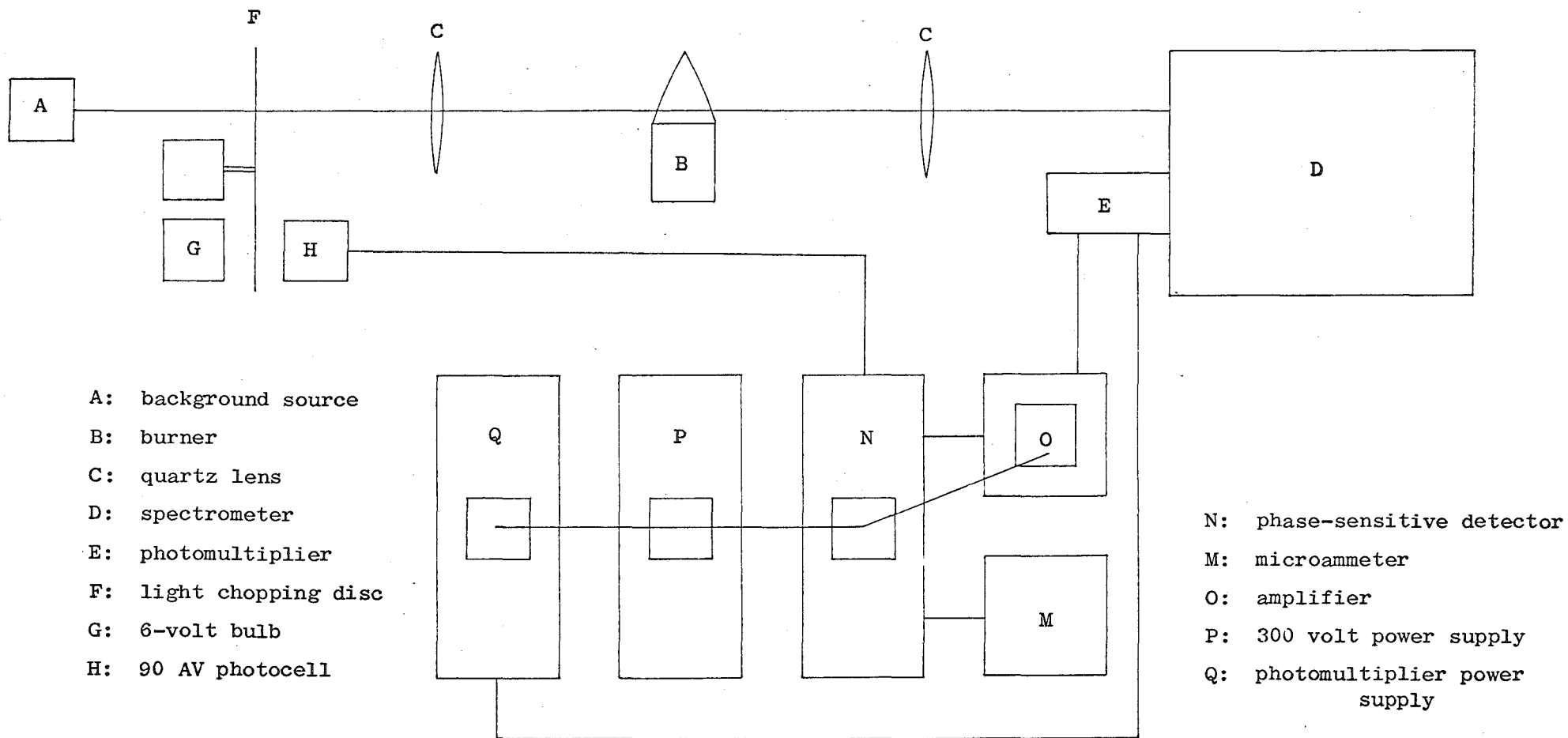
FIGURE V

Photometric System as used for Absorption Measurements

current of 12 mA for the lithium and about 20 mA for the

sodium-potassium lamp. Light from the background source was

focused by a quartz lens to form an image in the flame. A second

quartz lens then focused the transmitted light from the flame onto

the spectrometer slit. To prevent the photomultiplier responding

to emission from the flame, a rotating sectored disc driven by a

synchronous motor was arranged to cut the background light at a

frequency of 600 cycles per second, a 6-volt bulb and 90 AV

photocell providing a reference signal of the same frequency as the

light signal from the flame. The a.c. output from the photomultiplier

was amplified and passed to a phase-sensitive detector. This

detector combined the reference and photomultiplier signals to give

a rectified output which was displayed on a microammeter and was

directly proportional to the light intensity at the photomultiplier.

Stabilised power supplies, denoted P and Q in figure 5, provided

300 volts positive and 450 to 950 volts negative respectively.

In emission measurements, light modulation was not required.

The phase-sensitive detector was therefore replaced by a Keithley

high-speed picoammeter, which amplified the d.c. signal from the

photomultiplier to give a reading once again directly proportional

to the light intensity at the spectrometer slit.

To reduce the dark current arising from random thermal

emission of electrons in the R.C.A. 7102 photomultiplier, the

electron tube was cooled by conduction. A diagram of the apparatus

is given in figure 6. Liquid nitrogen was poured into a reservoir,

which was supported on a flexible rubber membrane inside the

upper part of a second chamber containing the photomultiplier.

The reservoir was in thermal contact with a brass ring fitted

round the nose of the electron tube. Condensation of water

vapour inside the cryostat was avoided by evacuating the entire

FIGURE VI   33

Photomultiplier Cryostat

liquid nitrogen port

rubber membrane

to vacuum pump

liquid nitrogen
reservoir

brass rod

O

O

brass cooling
ring

P   Q
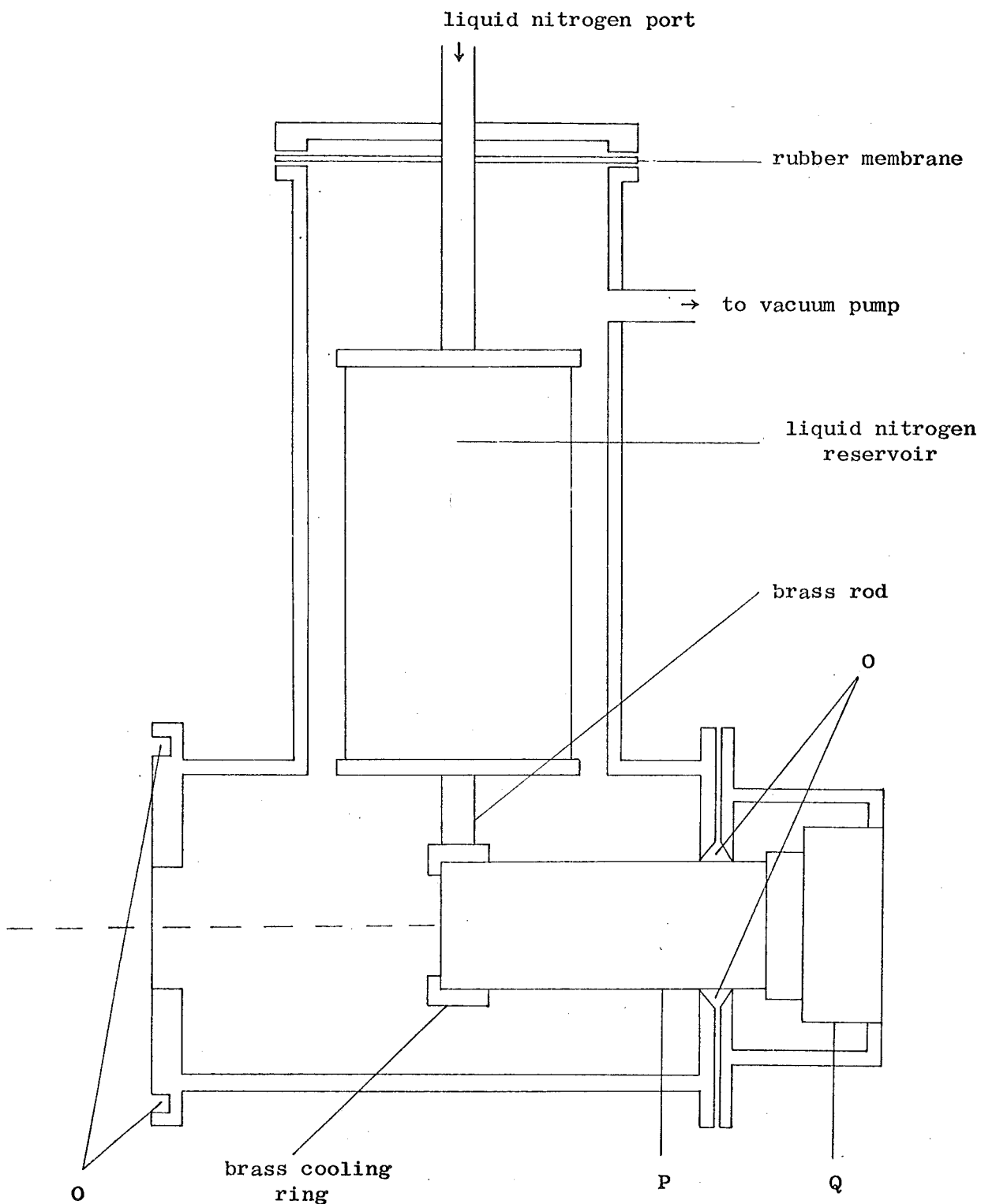
O: position of neoprene "O" ring

P: photomultiplier tube

Q: tube socket with potted resistors

— — — · —   light path from spectrometer

volume with an Edwards single-stage vacuum pump, using neoprene
"O" rings to seal the connections to atmosphere. It was possible
to reduce the dark current by a factor of 10^5, while still
maintaining the cathode voltage at its maximum value of -950 volts
in order to obtain maximum sensitivity from the photomultiplier.
The cooling apparatus, built by Mr R. Gillard of this department,
was based on a commercial design marketed by Jarrell-Ash Company
Limited.

VI. TEMPERATURE MEASUREMENTS

Temperature profiles through the burnt gas region were
obtained by the sodium D-line reversal method.[8] An N.P.L. calibrated
optical pyrometer was used to determine the colour temperature in
the red of the image of a tungsten strip filament, these brightness
temperatures in the red being corrected to the yellow from the
emissivity data of de Voss.[9] The filament lamp was run from the
a.c. mains supply through a variac and a welding transformer.
Line reversals were determined photometrically, using the optical
scheme described in figure 5, with the tungsten strip filament as
the background source and the Jarrell-Ash monochromator with an
E.M.I. 9558 Q photomultiplier. The light chopping disc was removed
and the d.c. output from the photomultiplier was monitored with a
Keithley high-speed picoammeter.

Since the sodium reversal temperature is strictly the
electronic excitation temperature,[10] the profiles obtained by
sodium reversal show a sharp upward curve in the reaction zone due
to chemiluminescent excitation of the sodium atoms and it is only
downstream from the reaction zone that the reversal temperature may
be regarded as a measure of the true thermal temperature of the burnt

FIGURE VII

Temperature Profile for Flame Z8 (H_2: N_2: O_2 = 4.5 : 8.0 : 1.0)

as Determined by the Sodium Reversal Method
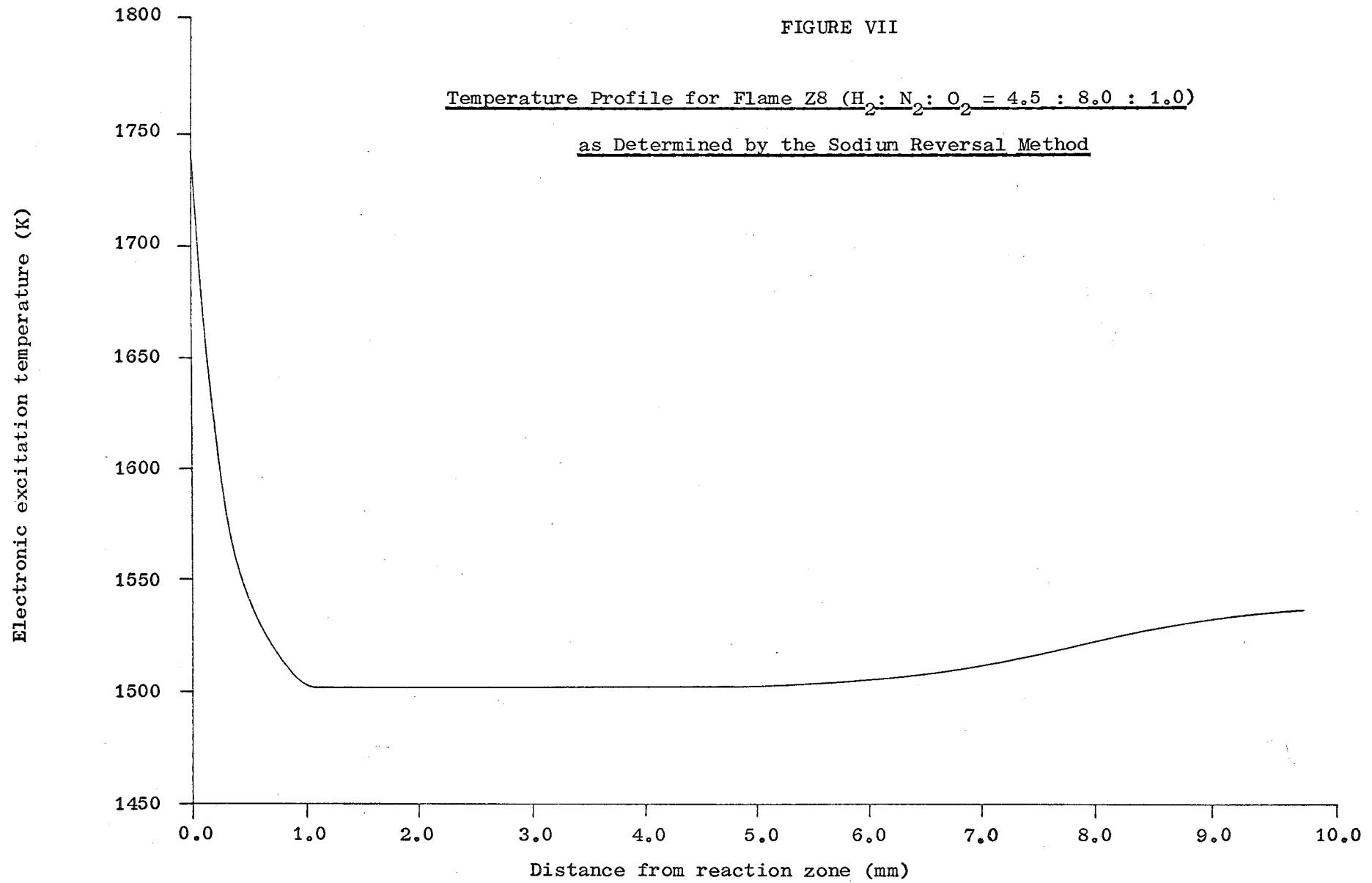
gases. All the flames used in the present work gave final temperatures in the burnt gas region not lower than 1500 K. Under these conditions, the sodium emission at distances greater than about 1 mm above the reaction zone may be considered to arise solely from thermal excitation, with a negligible contribution from chemiluminescent effects.[11]

It is possible to obtain the reversal temperatures to within $\pm$ 10 K. Similarly, assuming the pyrometer to be without error, there is an uncertainty of $\pm$ 10 K in the calibration of the tungsten strip filament. An error margin of $\pm$ 30 K therefore appears to give a reasonable estimate of the accuracy of the flame temperatures in the present work. Figure 7 shows an example of a typical profile for flame Z8 (H_2 : N_2 : O_2 = 4.5 : 8.0 : 1.0). Comparison of this and other temperature profiles with those obtained by Phillips[2] in flames of the same composition has in all cases given agreement to within $\pm$ 30 K.

CHAPTER IV

METAL OXIDE PARTICLES IN HYDROGEN-NITROGEN-OXYGEN FLAMES

I.   INTRODUCTION

Transition metals which possess high-melting refractory

oxides have been known for a number of years to form solid

particles when added as aqueous sprays to hydrogen-nitrogen-oxygen

flames.[3]   In 1967, Kallend[12] observed a continuous emission

from particles obtained by adding 0.01 M vanadyl sulphate solution

to fuel-rich hydrogen-nitrogen-oxygen flames ranging in temperature

from 1600 K to 2000 K. The particle composition was assumed to be

V_2O_3 (melting point 2243 K), V_3O_4 (melting point 2240 K) or a

mixture of these two oxides. A more detailed study by Kelly and

Padley[13] used electron microscopy to investigate the structure of

particles collected by passing a carbon-coated copper grid through

hydrogen-nitrogen-oxygen flames containing an aqueous spray of

1M chromic acid. Spherical particles about 0.6μ in diameter were

observed. These were thought to originate each from a single

aqueous droplet of chromic acid, particle formation occurring in the

reaction zone through rapid contraction and dehydration of the

spherical droplets.

Following these early studies, attention was focused on the

role of metal oxide particles in the catalysis of radical

recombination in hydrogen-nitrogen-oxygen flames. Surface temper-

atures of uranium oxide particles were measured by Bulewicz and

Padley.[14] Particle temperatures greater than the ambient gas

temperature were attributed to heat released by surface-catalysed

recombination reactions such as:[12,14,15]

$$H + H + Surface \rightarrow H_2 + Surface \ . \ . \ . \ . \ . \ (1).$$
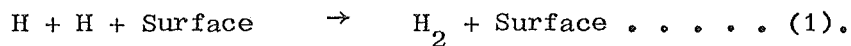
In the work on catalytic effects, the particles were assumed to be oxides, but there was no report of any study being carried out to establish in more detail the chemical composition or physical structure of these oxides. The first aim of the present work was therefore to determine the chemical composition of the particles formed by a series of transition metals. Changes in composition with changes in flame temperature or hydrogen to oxygen ratio were to be investigated, together with any corresponding variations in catalytic activity.

II. CHEMICAL COMPOSITION OF METAL OXIDE PARTICLES

Chromium, vanadium and iron were the three transition metals selected for an initial study of the chemical composition of oxide particles in hydrogen-nitrogen-oxygen flames. Aqueous sprays of chromic nitrate (saturated $Cr(NO_3)_3$), vanadyl trichloride (0.3M $VOCl_3$) and ferric nitrate (0.1M $Fe(NO_3)_3$) were used. These were added separately to a series of flames, Z8, Z7 and Z6, in which the hydrogen to oxygen ratio was held constant ($H_2 : O_2 = 4.5 : 1.0$), while the temperature was steadily increased (Z8< Z7 <Z6). Addition was also carried out to three isothermal flames, Z8.0, U8.5 and P9.0. In this series, equal calculated adiabatic flame temperatures were obtained by using unburnt compositions which give the same partial pressure of water vapour in the burnt gases.

In each case, a sample of the metal oxide formed in the flame was collected by placing a length of silica tubing of 1 mm external diameter in the burnt gas stream 5 mm above the reaction zone. A visible coating of particles was obtained on the exterior of the

silica. After about 10 minutes, the tubing was removed from the

flame and a small portion of the sample was transferred to a grease-

coated soda-glass fibre for analysis by X-ray powder diffraction.

The powder diffraction patterns were compared with those listed

in the A.S.T.M. Data File[16] for known metal oxides.

Chromium oxide particles collected from all seven flames gave

diffraction lines in close agreement with those listed for the

oxide Cr_2O_3. As a further check, the diffraction patterns from the

particle samples were compared with that obtained by photographing

a prepared sample of Cr_2O_3 under the same conditions. A typical

set of results is listed in table I. The d-values for corresponding

powder lines as given by the particle sample and by the prepared

Cr_2O_3 agree within experimental error with those given for the same

lines by the A.S.T.M. Data File. Hence it may be concluded that the

chromium oxide particles consisted of at least 90% Cr_2O_3.

Similar results were obtained for vanadium. Particles

collected from both series of flames gave diffraction patterns which

were in every case almost identical to that listed in the

A.S.T.M. Data File for the oxide V_2O_3. The d-values for a sample

from flame Z6 are given in table II. Comparison with the literature

values, which agree well within the expected margin of error,

establishes the oxide composition as 90% V_2O_3. With iron as the

metal additive, analysis of the particle samples by powder

diffraction did not give sufficient evidence to determine the

chemical composition of the iron oxide formed in the flames. One

possibility appeared to be a mixture of the oxides FeO and Fe_2O_3.

In summary, from this short qualitative study of metal oxide

particles in hydrogen-nitrogen-oxygen flames, it was concluded that

the metals chromium and vanadium form solid oxides of composition

Cr_2O_3 and V_2O_3 respectively. These two oxides are isomorphous, both

TABLE I

d-values for Powder Diffraction Lines of Cr_2O_3

	d (Å)		I/I_1 (%)	hkl
(a)	(b)	(c)	(c)	(c)
3.61($\pm$0.01)	3.63($\pm$0.01)	3.633	75	012
2.66	2.67	2.666	100	104
2.48	2.48	2.480	95	110
2.26		2.264	12	006
2.17	2.18	2.176	40	113
1.88	1.90	2.048	10	202
1.82	1.82	1.8156	40	024
1.68	1.68	1.672	90	116
		1.579	14	112
1.47	1.47	1.465	25	214
1.44	1.44	1.4314	40	300
1.30		1.2961	20	

(a) Particle sample from flame Z6 (H_2: N_2: O_2 = 4.5 : 6.0 : 1.0).

(b) Prepared Cr_2O_3 sample.

(c) A.S.T.M. Data File.

TABLE II

d-values for Powder Diffraction Lines of V_2O_3

d (Å)		I/I_1 (%)	hkl
(a)	(b)	(b)	(b)
3.65($\pm$0.01)	3.65	60	$\bar{1}$02
2.72	2.70	80	104
2.48	2.47	60	110
	2.32	2	006
2.18	2.18	20	113
	2.03	2	202
1.83	1.83	25	$\bar{2}$04
1.70	1.69	100	116
	1.61	2	$\bar{2}$10
	1.57	3	$\bar{1}$08
1.47	1.47	25	214
1.43	1.43	30	300
	1.33	10	$\bar{2}$16

(a)   Particle sample from flame Z6 (H_2: N_2: O_2 = 4.5 : 6.0 : 1.0).

(b)   A.S.T.M. Data File.

possessing a corundum structure.[17] Iron oxide particles formed

under the same conditions appeared to be of mixed composition. Over

the ranges studied, the chromium and vanadium oxides showed no

detectable change in chemical composition with changes in flame

temperature (T = 1500 K for Z8 to T = 1630 K for Z6) or hydrogen to

oxygen ratio (H_2: O_2 = 3.5 : 1.0 for P9.0 to 4.5 : 1.0 for Z8.0).

In each case, the particles consisted of the solid metal oxide with

the highest thermodynamic stability. These results suggest the

solid oxide produced by a particular metal in hydrogen-nitrogen-

oxygen flames is characteristic of the metal and independent of

flame temperature or composition, provided the final temperature in

the burnt gas region is lower than the melting point of the oxide.

This conclusion is supported by the results of Nielsen, Hamilton

and Walsh[18] in natural gas-air flames.

III. ADSORPTION OF SULPHUR DIOXIDE AT THE SURFACE OF METAL OXIDE

PARTICLES

The role of sulphur dioxide in air pollution is now well

established.[19] Removal of sulphur dioxide from waste gases released

to the atmosphere is part of many industrial processes, particularly

those which involve the combustion of sulphur-containing fuels.

One possibility would be to adsorb the gas at the surface of solid

particles, which could then be removed from the gas stream by

filtration or electrostatic precipitation.

As part of the present work on metal oxide particles in

hydrogen-nitrogen-oxygen flames, an attempt was made to determine

whether or not adsorption of sulphur dioxide would occur at the

surface of the particles formed in these flames by the transition

metals chromium, vanadium and iron. Measurements were carried out

using flames Z8 and Z6. Gaseous sulphur dioxide was added at a steady flow rate in the range 0.1% to 1.0% of the unburnt composition, while the metals were introduced as before as aqueous sprays of chromic nitrate (saturated $Cr(NO_3)_3$), vanadyl trichloride (0.3M $VOCl_3$) and ferric nitrate (0.1M $Fe(NO_3)_3$). The concentration of sulphur dioxide in the burnt gas stream was followed by continuous flow sampling and mass spectrometric analysis. With maximum sensitivity at the output of the mass spectrometer, the proportion of added sulphur dioxide was reduced to a minimum level which still enabled the mass 48-SO and mass 64-SO_2 peaks to be clearly distinguished from the background. The mass spectrum was scanned before, during and after the introduction of the metal additive. However, in no case was there a significant decrease in the peak height at mass 48 or at mass 64 which could be attributed to the presence of solid oxide particles in the flame gases.

According to these results, no adsorption of sulphur dioxide was detected at the surface of the metal oxide particles. Two explanations may be put forward. Firstly, since the solid oxides formed by transition metals in hydrogen-nitrogen-oxygen flames are high-melting, stable oxides, it is unlikely that any interaction would occur at the particle surface which would lead either to physical adsorption of sulphur dioxide molecules or to chemical reaction to form a sulphate. Secondly, when a metal is added to a flame as a fine spray of an aqueous salt solution, the maximum concentration of metal atoms in the burnt gas region is about one part in 10^4,[2] while the proportion of metal oxide particles would be still lower. In order to detect sulphur dioxide in the burnt gases by mass spectrometric sampling, it was necessary to maintain a concentration of at least 0.5% or five parts in 10^3. With a ten-fold or greater excess of sulphur dioxide over metal oxide, even

a strong interaction with the surface of the solid oxide particles would reduce the proportion of sulphur dioxide in the gas stream by less than 10%. The mass spectrometer was operated at maximum sensitivity. Under these conditions, a 10% fluctuation in peak heights in the mass spectrum could well be attributed to experimental error and a decrease in sulphur dioxide concentration of less than 10% would pass undetected.

On the basis of the information already obtained, it was decided to discontinue the study of metal oxide particles. An extension of the investigations described in this chapter appeared unlikely to reveal any further useful data, either with regard to the structure and chemical composition of the solid metal oxides, or the interaction of the oxide particles with gaseous flame additives such as sulphur dioxide.

CHAPTER V

THE BREAKDOWN OF CYANOGEN IN A FUEL-RICH

HYDROGEN-NITROGEN-OXYGEN FLAME

I. INTRODUCTION

The combustion of small amounts of cyanogen in premixed

hydrogen-nitrogen-oxygen flames has been investigated

spectroscopically by Rentzepis and Sugden.[20] Using a basic flame

of composition H_2 : N_2 : O_2 = 4.0 : 4.0 : 1.0 and final temperature

2100 K at atmospheric pressure, emission and absorption spectra

were recorded for the addition of about 1% cyanogen to the unburnt

gas stream. CN, NO, NH, OH and CH species were detected in the

reaction zone. In the burnt gas region, NO, NH and OH were observed.

Bulewicz, Padley and Smith[21] have carried out a similar

spectroscopic study of the behaviour of trace quantities of cyanogen

in hydrogen flames, while the effect of cyanogen on ionisation in

carbon monoxide flames has been discussed by Van Tiggelen, Peeters

and Vinckier.[22]

Rentzepis and Sugden interpreted their results in terms of

an initial attack on C_2N_2 by atomic hydrogen:

$$H + C_2N_2 \rightarrow HCN + CN \quad \ldots \ldots \text{(1)},$$

followed by further reaction of CN radicals with molecular hydrogen:

$$CN + H_2 \rightleftharpoons HCN + H \quad \ldots \ldots \text{(2)}.$$

To account for the appearance of NO* in the early reaction zone, a

reaction of CN with molecular oxygen was proposed:

$$CN + O_2 \rightarrow CO + NO \quad \ldots \ldots \text{(3a)},$$

or: $$CN^* (A^2\Pi) + O_2 \rightarrow CO + NO^* (^2\Sigma^+) \quad \ldots \ldots \text{(3b)}.$$
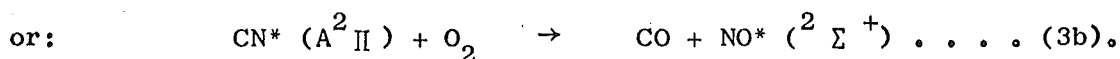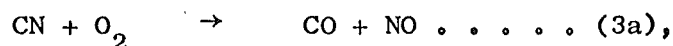
Production of NH radicals in the later reaction zone was thought

to occur by reaction of CN with OH:

$$CN + OH \rightarrow CO + NH \ldots \ldots (4),$$
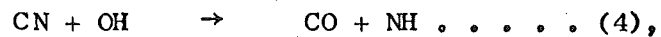
while the formation and destruction of CH in the reaction zone was

attributed to reactions (5) and (6) respectively:

$$CN + NH \rightarrow CH + N_2 \ldots \ldots (5),$$

$$CH + OH \rightarrow CO + H_2 \ldots \ldots (6).$$
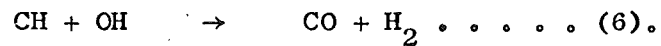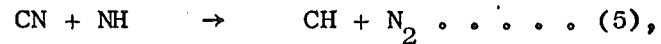
Further removal of NO and NH would take place by:
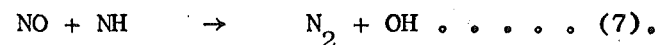
$$NO + NH \rightarrow N_2 + OH \ldots \ldots (7).$$

In the present work, mass spectrometric sampling has been

used to determine the concentrations of stable species in the burnt

gas region of a fuel-rich hydrogen-nitrogen-oxygen flame containing

up to 1.5% cyanogen. Evidence is obtained that the carbon atoms

introduced as C_2N_2 are converted largely to carbon oxides rather than

HCN. Therefore, it appears that formation of CN radicals from C_2N_2

occurs through processes which involve little or no production of

HCN, while the reaction of CN with molecular oxygen,

process (3), is considerably faster than the competing reaction of

CN with molecular hydrogen. A single step four-centre process as

represented in (3), is unlikely to be rapid. However, it is to be

expected that the reaction of CN radicals with molecular oxygen takes

place by way of an intermediate NCO radical:

$$CN + O_2 \rightarrow NCO + O \ldots \ldots (8),$$

$$NCO + O \rightarrow CO + NO \ldots \ldots (9).$$
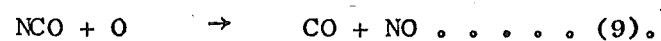
II. BREAKDOWN OF THE ADDITIVE : DETERMINATION OF STABLE COMBUSTION

PRODUCTS

(1) Sampling Procedure for Mass Spectrometric Analysis

The measurements described in this chapter were carried out

in flame Z8 (H_2: N_2: O_2 = 4.5 : 8.0 : 1.0). Using a total unburnt

gas flow, excluding additives, of $81.0 \text{ cm}^3 \text{ s}^{-1}$, cyanogen was

admitted at varying flow rates in the range 0.0 to $1.3 \text{ cm}^3 \text{ s}^{-1}$.

The upper limit of additive concentration for reproducible

experimental results was determined by the onset of "flame-lift",

a distortion of the visible reaction zone which was observed at

cyanogen flows greater than about $1.4 \text{ cm}^3 \text{ s}^{-1}$. An internal standard

was provided by addition of argon at $1.0 \text{ cm}^3 \text{ s}^{-1}$.

Gas samples for mass spectrometric analysis were withdrawn

from the burnt gas region using the quartz probe and continuous flow

sampling system described in Chapter III. At a given cyanogen

concentration, the mass spectrum was recorded as a function of

distance from the reaction zone. Starting from an initial position

0.5 mm above the reaction zone, samples were taken at 0.5 mm intervals

to a distance of 10.0 mm, peaks being recorded as the average of

three scans at each sampling position. Background corrections were

applied where necessary. Pressure fluctuations in the flow line

and in the ionisation chamber of the mass spectrometer were taken

into account by expressing the peak heights relative to the

corresponding mass 40 - argon peaks.

Further experiments were carried out to record the mass

spectrum as a function of cyanogen concentration. The probe position

in the burnt gas region was held constant, generally in the range

2.0 to 6.0 mm above the reaction zone, while the flow rate of added

cyanogen was varied from 0.0 to $1.3 \text{ cm}^3 \text{ s}^{-1}$. At each particular

flow, the mass peak heights relative to argon were determined as

before.

(2) Profiles of Stable Species in the Burnt Gas Region

Addition of up to 1.5% cyanogen to flame Z8 resulted in the

breakdown of the additive to HCN and carbon oxides. In the mass

spectrum of samples from the burnt gas region, a peak due to CO_2 was observed at mass 44, while HCN and its fragmentation product CN gave rise to two peaks at masses 27 and 26 respectively. Carbon monoxide was assumed to be present in concentrations given by the water-gas equilibrium:

$$CO_2 + H_2 \rightleftharpoons CO + H_2O \quad \ldots \ldots \quad (10).$$
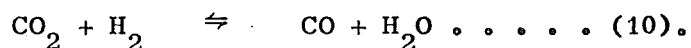
Direct detection of carbon monoxide by measurement of the mass 28-CO peak was not possible, since this was obscured by a strong background N_2 peak at the same mass number. Nitric oxide was observed in low concentrations immediately above the reaction zone. The mass 30-NO peak appeared in samples taken 1.0 mm from the reaction zone, but the peak height never exceeded 5% of the corresponding mass 27-HCN peak and decreased to zero within 3.0 mm.

No significant changes in peak height were observed at mass 44 or at masses 26 and 27 as the distance of the sampling position above the reaction zone was varied from 0.5 to 8.0 mm. This indicated steady concentrations of HCN and carbon oxides through the burnt gas region. From the rapid decay of the weak NO peak at mass 30, the concentration of nitric oxide in the burnt gases was reduced to zero within 3.0 mm or approximately 0.001s of the reaction zone. A possible mechanism of nitric oxide removal is discussed later. According to the mass spectrometric profile, nitric oxide produced in the breakdown of cyanogen was destroyed by a fast process occurring in the reaction zone and in the first millisecond of the burnt gas stream.

(3) <u>Relative Yields of HCN and CO/CO_2 Mixture from C_2N_2</u>

The ratio of the mass 27-HCN and mass 44-CO_2 peaks in the burnt gas stream was found to vary with the initial proportion of cyanogen in the unburnt gases supplied to the flame. This indicated

a variation in the relative yields of HCN and CO/CO$_2$ mixture from C$_2$N$_2$. At a given flow rate of added cyanogen, the peak height at mass 27 is directly proportional to the yield of HCN in the burnt gases, while the peak height at mass 44 may be related to the total yield of carbon oxides.

From reaction (3), the carbon oxide first formed in the combustion of cyanogen is carbon monoxide, further oxidation to carbon dioxide occurring through the water-gas reaction (10). The final concentration of carbon dioxide in the burnt gas region is given by:

$$[CO_2] = \frac{K_{10} [H_2O]}{[H_2]} [CO] \quad . \quad . \quad . \quad . \quad . \quad (11).$$

Provided the proportion of cyanogen is less than about 1.5%, the concentrations of the bulk constituents H$_2$ and H$_2$O may be regarded as unchanged by the presence of the additive, while the flame temperature, as discussed in Chapter VII, is unlikely to vary by more than 10%. Hence the factor $K_{10} [H_2O] / [H_2]$ may be considered constant for a given flame. As a result, the mass 44-CO$_2$ peak in samples from the burnt gas stream will be proportional to the total yield of carbon oxides arising from breakdown of cyanogen in the reaction zone.

Calibration of the mass 44 peak was carried out in separate experiments using carbon monoxide as the additive. The peak height in samples taken, for example, 4.0 mm above the reaction zone was recorded for initial concentrations of carbon monoxide ranging from 0.0% to 2.5% of the unburnt gas composition. Figure 8 shows a typical calibration curve. This was constructed by plotting the measured value of the peak height at mass 44 as a function of the concentration of carbon monoxide in the burnt gases emerging from the reaction zone, calculated as if there were no conversion to

FIGURE VIII   50

Measured Intensity of Mass 44-CO_2 Peak versus

Calculated Concentration of Carbon Oxides in the Burnt

Gas Region of Flame Z8

Sampling distance: 4.0 mm above reaction zone.

Concentration of carbon oxides in burnt gas (atm x 10^{-2})
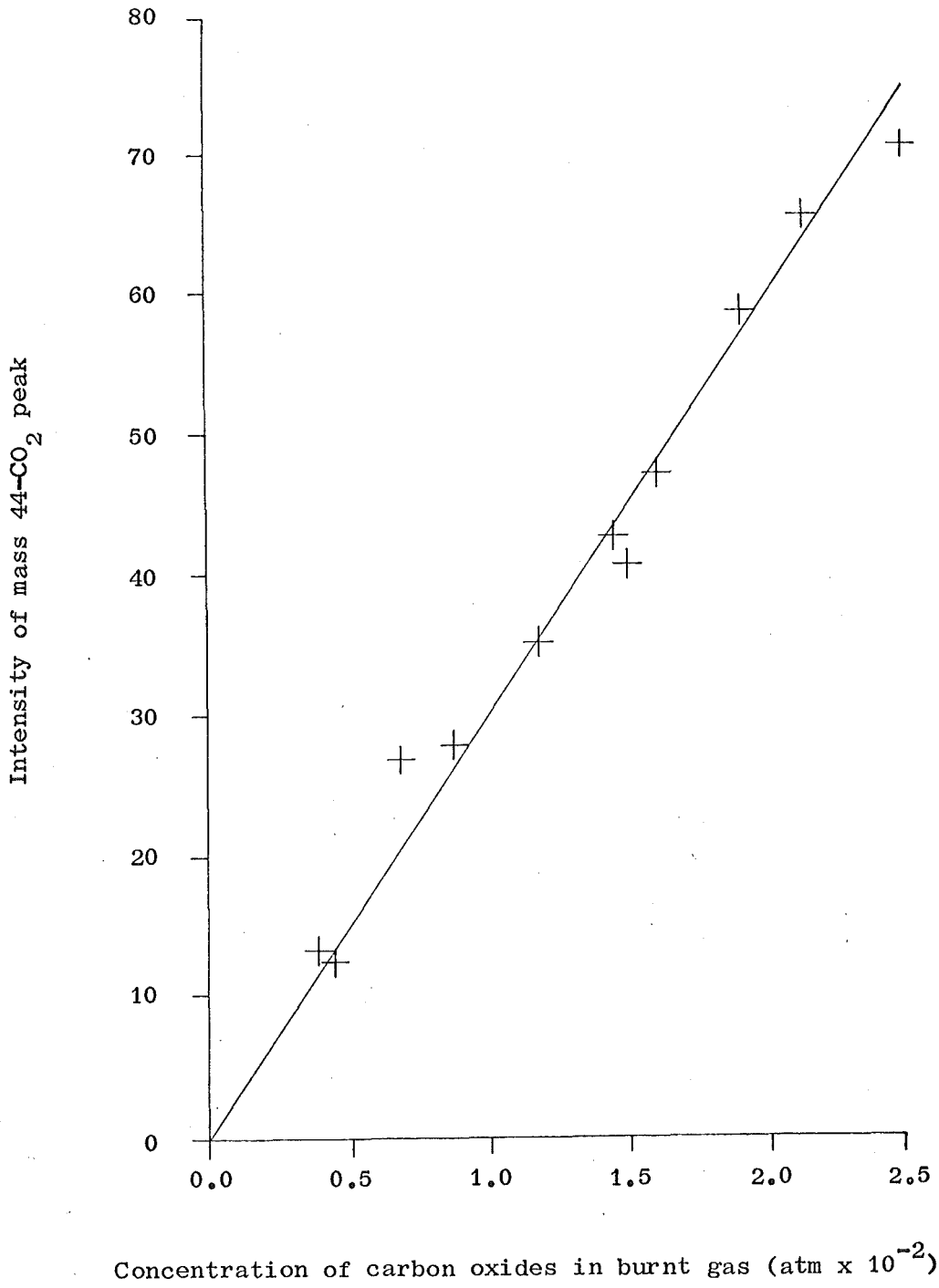
carbon dioxide.

Experiments to determine the yields of HCN and carbon oxides from cyanogen were always carried out immediately after calibration of the sampling system with carbon monoxide. The probe position was maintained at the same distance from the reaction zone. Peak heights at mass 27 and mass 44 were measured for varying initial proportions of cyanogen from 0.0% to 1.5% of the unburnt gas flow. The values for the mass 44-CO_2 peak were converted directly to the corresponding values for the concentration of carbon oxides in the burnt gas region. At the end of the experimental run, three points on the calibration curve were checked.

Assuming that all the carbon atoms introduced as cyanogen form either HCN or carbon oxides, initial values for the mole fraction of HCN in the burnt gases were obtained by subtracting the measured concentrations of CO/CO_2 mixture from the corresponding concentrations calculated on the basis of complete conversion of cyanogen to carbon oxides. The mass 27-HCN peaks were each divided by the mole fraction of HCN at the same cyanogen flow. This gave a series of ratios of peak height to HCN concentration. Final values for the mole fraction of HCN in the burnt gas stream were then determined by dividing the measured mass 27-HCN peaks by the average ratio of peak height to HCN concentration.

A check was made for CO or CO_2 impurities in the cyanogen added to the flame. Hydrogen was passed through the burner at a flow rate of about 27 cm^3 s^{-1}, samples for mass spectrometric analysis being withdrawn from the gas stream at a distance of 5.0 mm above the burner face. Cyanogen was introduced at varying flows up to 1.3 cm^3 s^{-1}. The mass 26-CN and mass 52-C_2N_2 peaks were observed, but it was not possible to detect a peak at mass 28 due to CO or a peak at mass 44 due to CO_2. A similar check was carried out for CO_2

FIGURE IX   52

Relative Yields of HCN and Carbon Oxides from C_2N_2 in the

Burnt Gas Region of Flame Z8

Sampling distance: 4.0 mm above reaction zone.

FIGURE IX   52

Relative Yields of HCN and Carbon Oxides from C_2N_2 in the

Burnt Gas Region of Flame Z8

Sampling distance: 4.0 mm above reaction zone.

Percentage C_2N_2 in unburnt gas
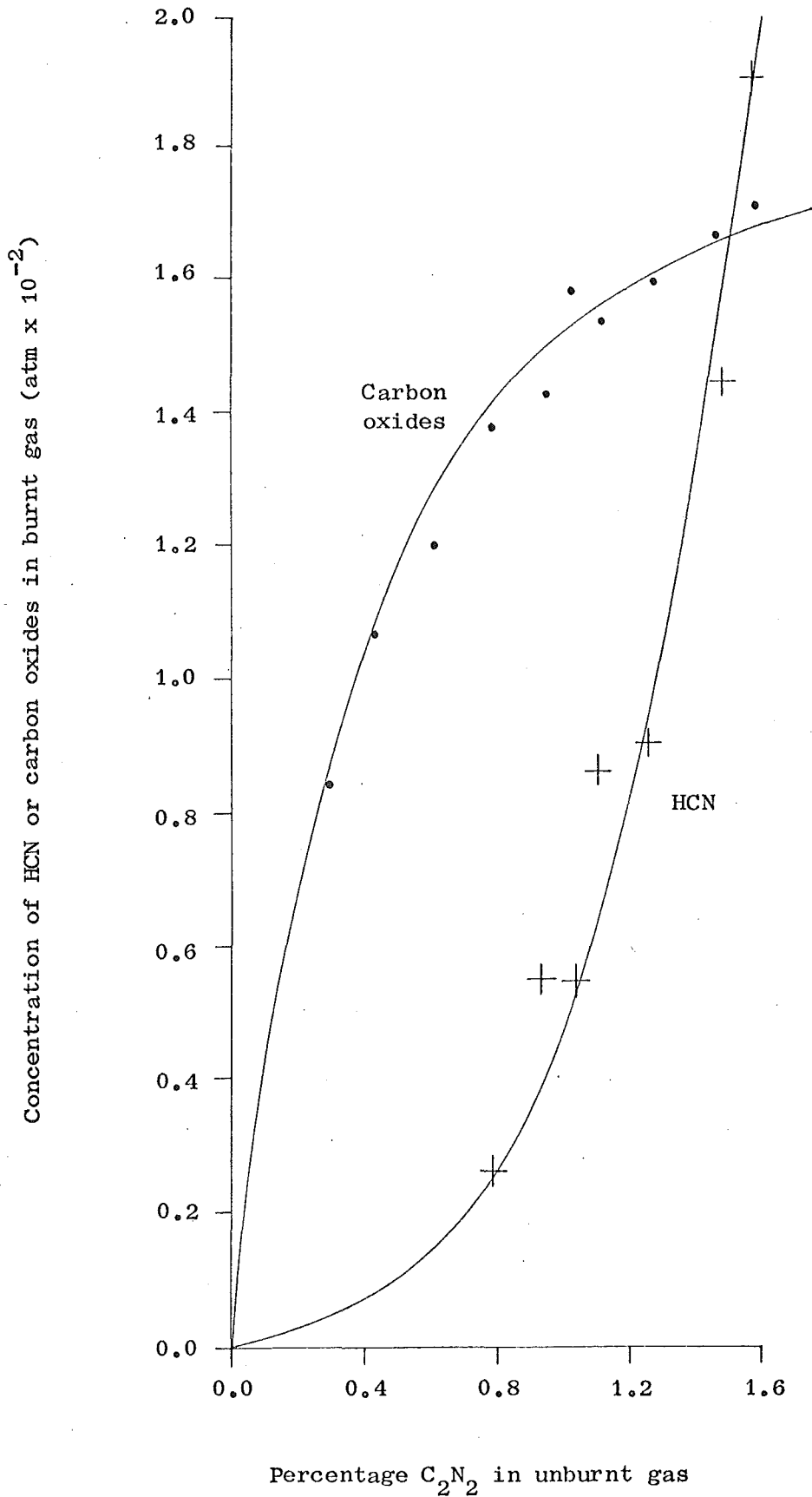
impurities in the carbon monoxide. Dry nitrogen was used as the diluent gas, carbon monoxide being added as in the calibration experiments at flows up to 2.0 $cm^3 s^{-1}$. Once again, the mass spectrum showed no significant mass 44-CO_2 peak. Hence the experimental results for the relative yields of HCN and CO/CO_2 mixture from C_2N_2 cannot have been in error due to carbon oxide impurities in the additive gases.

The mole fractions of HCN and CO/CO_2 mixture in the burnt gas region were plotted as a function of percentage cyanogen added to the flame. Figure 9 shows the curves for samples taken 4.0 mm above the reaction zone. According to these results, at low cyanogen concentrations the additive is converted largely to carbon oxides and it is only as the precentage cyanogen in the flame rises above 1.0% that the ratio of HCN to carbon oxide product reaches a value of 1:3, finally increasing to approximately 1:1 at 1.5% cyanogen. Little change was observed with changes in sampling position. Relative yields of HCN and CO/CO_2 mixture in samples taken at 2.0 mm and 6.0 mm distance from the reaction zone were in close agreement with the curves of figure 9.

(4) Model Reaction Scheme for the Breakdown of Cyanogen

Breakdown of cyanogen in the reaction zone of flame Z8 leads to the formation of HCN and carbon oxides in varying proportions according to the percentage cyanogen in the flame. Carbon oxides predominate at cyanogen concentrations below 1.5%. In terms of the mechanism proposed by Rentzepis and Sugden,[20] this implies that the main primary reaction:

$$H + C_2N_2 \rightarrow HCN + CN \quad . \quad . \quad . \quad . \quad . \quad (1),$$

is followed by a rapid reaction of CN radicals with molecular oxygen:

$$CN + O_2 \rightarrow NCO + O \quad . \quad . \quad . \quad . \quad . \quad (8).$$

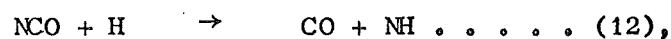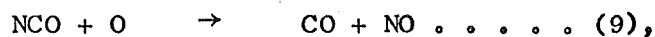The competing reaction of CN with molecular hydrogen:

$$CN + H_2 \rightleftharpoons HCN + H \ldots \ldots (2),$$
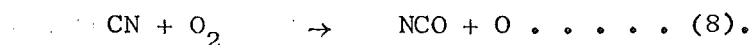
will be relatively unimportant. Carbon monoxide will be produced from NCO by the fast processes:

$$NCO + O \rightarrow CO + NO \ldots \ldots (9),$$

$$NCO + H \rightarrow CO + NH \ldots \ldots (12),$$

after which further oxidation of CO to CO_2 will occur by reactions of the type:

$$CO + OH \rightleftharpoons CO_2 + H \ldots \ldots (15).$$
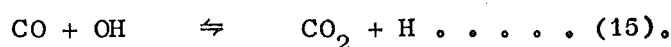
In the burnt gas stream, the ratio of CO to CO_2 will be maintained by the water-gas equilibrium:

$$CO_2 + H_2 \rightleftharpoons CO + H_2O \ldots \ldots (10).$$
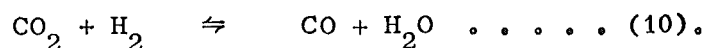
Computer simulation of the combustion of cyanogen in flame Z8 has shown that this mechanism leads to approximately equal values for the calculated yields of HCN and CO/CO_2 mixture from C_2N_2. The computer modelling work is discussed in detail in Chapter VII. Results indicate that the proposed reaction scheme is unable to account for a ratio of HCN to carbon oxide product which is less than unity, even if conversion of CN to CO by reactions (8) and (9) takes place at temperatures where there is no significant competition from reaction (2). Thus the mechanism is inconsistent with the HCN concentrations observed in mass spectrometric sampling. To account for yields of HCN lower than the corresponding yields of carbon oxides, formation of CN and NCO radicals from C_2N_2 must occur through processes which involve little or no production of HCN. The most likely reaction sequence is:

$$O + C_2N_2 \rightarrow NCO + CN \ldots \ldots (16),$$

$$CN + O_2 \rightarrow NCO + O \ldots \ldots (8).$$
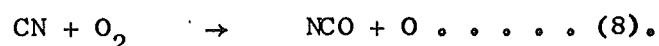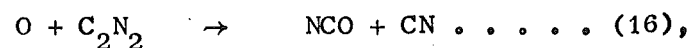
Therefore, according to the present work, primary decomposition of C_2N_2 in hydrogen-nitrogen-oxygen flames takes place by reaction with

atomic oxygen:

$$O + C_2N_2 \quad \rightarrow \quad NCO + CN \; . \; . \; . \; . \; . \; (16),$$
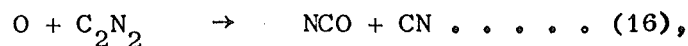
rather than by reaction with atomic hydrogen:

$$H + C_2N_2 \quad \rightarrow \quad HCN + CN \; . \; . \; . \; . \; . \; (1).$$
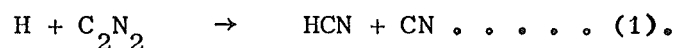
Production of CO from CN by reactions (8) and (9) would be expected to give concentrations of NO in the burnt gases comparable to the concentrations of carbon oxides. Experimentally, the NO yield is less than 5% of the corresponding CO yield. Hence NO must be removed by a fast process which reaches completion within one or two milliseconds of the reaction zone. A possible reaction is:

$$NO + NH \quad \rightarrow \quad products \; . \; . \; . \; . \; (13).$$
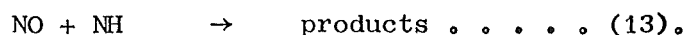
According to the results of computer simulation, NH is present in the reaction zone in concentrations greater than those of CN, while values of the rate constant k_{13} given in the literature are of the order of $2 \times 10^{10} \, m^3 \, kgmol^{-1} \, s^{-1}$,[40] comparable to the rates of fast processes such as:

$$NCO + O \quad \rightarrow \quad CO + NO \; . \; . \; . \; . \; . \; (9),$$

$$k_9 = 7.9 \times 10^9 \, m^3 \, kgmol^{-1} \, s^{-1} \text{ at } 298 \text{ K.}[23]$$
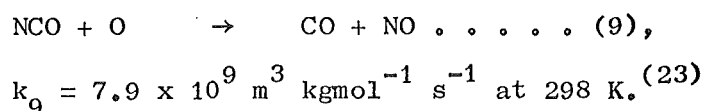
The main alternative to reaction (13) is removal of NO by reaction with CN radicals:

$$CN + NO \quad \rightarrow \quad N_2 + CO \; . \; . \; . \; . \; . \; (14).$$
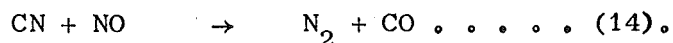
However, Boden and Thrush[27] have shown that at 687 K, close to the mean temperature of the reaction zone, reaction (14) is slower than the competing process (8), the reaction of CN with O_2, by at least one order of magnitude. Process (14) is therefore too slow to account for the observed destruction of NO in the reaction zone.

III. THE REACTION OF CN WITH NO

(1) Profiles of HCN and NO in the Burnt Gas Region of a Flame

Containing Cyanogen and Nitric Oxide

In flame Z8 (H_2: N_2: O_2 = 4.5 : 8.0 : 1.0), the sodium

reversal temperature in the burnt gas region remained essentially

constant at 1500 K for a distance of about 10 mm from the reaction

zone. The detailed temperature profile is given in figure 7. When

either cyanogen or nitric oxide was added separately to the flame,

the measured concentration of HCN or NO in the burnt gases was

constant for distances from 0.5 mm to 8.0 mm above the reaction zone.

However, when both additives were present, there was a steady

decrease in the HCN and NO profiles. This was attributed to removal

of CN and NO by reaction (14):

$$CN + NO \rightarrow N_2 + CO \ldots \ldots (14),$$
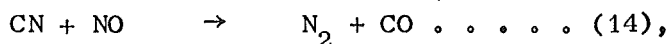
the concentration of CN radicals being maintained by the

equilibrium (2):

$$CN + H_2 \rightleftharpoons HCN + H \ldots \ldots (2).$$

Profiles of HCN and NO were determined by mass spectrometric

sampling. In a flame containing 1.1% cyanogen and 2.0% nitric oxide,

the mass 27-HCN and mass 30-NO peaks were recorded in samples taken

at 0.5 mm intervals along the burnt gas stream, starting 0.5 mm

above the reaction zone and continuing for a distance of 3.0 mm.

The peak heights gave relative concentrations of HCN and NO.

Absolute concentrations of HCN were obtained by assuming the mass 27

peak at the first sampling position 0.5 mm from the reaction zone

to correspond to the known concentration of HCN at this point in a

flame containing 1.1% cyanogen but no nitric oxide. At the remaining

sampling positions, the mass 27-HCN peaks were scaled accordingly.

Calibration of the mass 30-NO peak was carried out in the

absence of cyanogen. Using samples taken 2.0 mm above the reaction zone, the peak height was recorded for varying initial proportions of nitric oxide up to 2.0% of the unburnt composition. NO is essentially unaffected by passage through a pure hydrogen-nitrogen-oxygen flame. Hence, at each particular flow rate of added nitric oxide, the concentration of NO in the burnt gas region was calculated from the known percentage of NO in the unburnt gas. An average ratio of peak height to NO concentration was determined. In the flame containing both nitric oxide and cyanogen, this average ratio was used to convert the measured mass 30-NO peaks to the corresponding absolute concentrations of NO in the burnt gas stream.

HCN and NO profiles from two separate experiments are presented in figure 10. In each case, the experimental run was carried out directly after calibration of the sampling system with nitric oxide, while a number of calibration points were checked at the end of the run. The mole fractions of HCN and NO were plotted as a function of distance from the reaction zone. Conversion to the time scale of figure 10 was carried out by calculating the linear velocity of the burnt gas stream, using a cross-sectional area of 1 cm^2, initial and final gas temperatures of 298 K and 1500 K respectively, and a total unburnt gas flow of 81.0 cm^3 s^{-1}. A distance of 1.0 mm corresponded to a time interval of 2.45 x 10^{-4}s.

(2) Calculation of the Rate of Reaction of CN with NO at 1500 K

From the concentration profiles of HCN and NO given in figure 10, a value may be calculated for the rate constant k_{14} at the burnt gas temperature. The differential equation for the rate of removal of HCN is:

FIGURE X   58

Mole Fraction Profiles of HCN and NO in the Burnt

Gas Region of Flame Z8

Initial additive concentrations in the unburnt composition:

$1.1\% \ C_2N_2$;   2.0% NO.
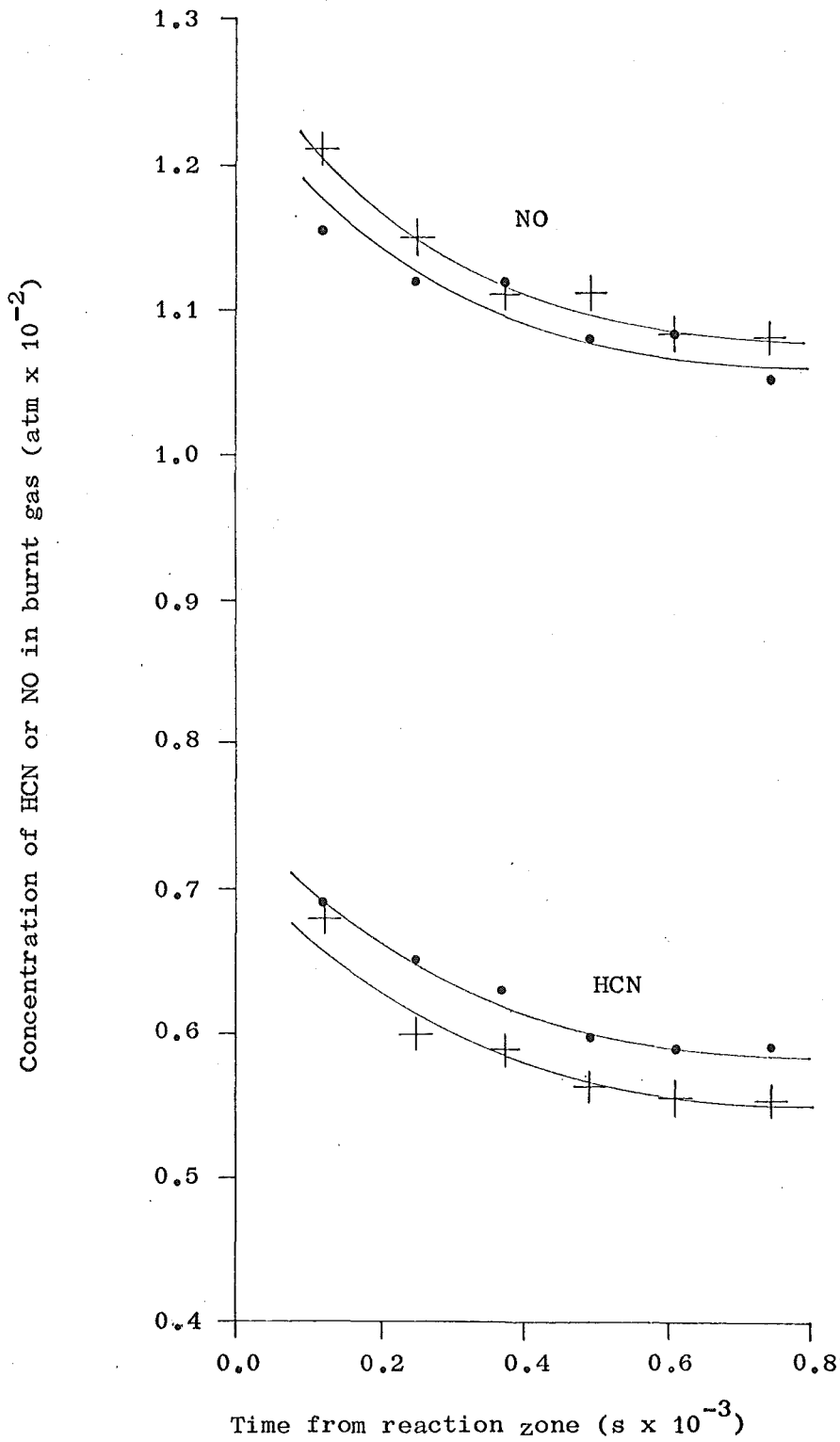
Run (1): ┼   ┼   Run (2): •   ∘

$$\frac{-d\ [HCN]}{dt} = k_{14}\ [CN][NO],$$

$$= k_{14}\ [HCN]\ [NO]\ [H]\ /\ K_2\ [H_2].$$

This may be written as:

$$\frac{dx}{dt} = k_{14}\ (a-x)(b-x)\ [H]/\ K_2\ [H_2]\ \ldots\ldots\ (15),$$

where (a-x) and (b-x) are the concentrations of HCN and NO

respectively. The time dependence of [H] is of the form:

$$\frac{1}{[H]} = \frac{1}{[H]_o} + k't\ \ldots\ldots\ (16).$$

Substituting for [H] in equation (15) and integrating from time

zero to time t gives:

$$k''\ \log_e\ [a(b-x)/b(a-x)] = k(b-a)\ \log_e\ [1 + k''t]\ \ldots\ (17),$$

where: $k = k_{14}\ [H]_o/K_2\ [H_2]$ and $k'' = k'\ [H]_o$.

Relative hydrogen atom concentrations were determined by

spectroscopic measurement of the decrease in CuH band intensity

with distance from the reaction zone in a flame containing no added

cyanogen or nitric oxide. The values were scaled to the absolute

[H] as measured by the Li/LiOH method. Details of this work are

discussed in Chapter VI, section III, while the final curve for the

variation of 1/[H] with time from the reaction zone is shown in

figure 15. From the slope and intercept of the profile:

$$k' = 5.5\ x\ 10^4\ atm^{-1}\ s^{-1},$$

$$[H]_o = 1.62\ x\ 10^{-2}\ atm.$$

In the presence of cyanogen, a slight decrease was observed in the

value of $[H]_o$, together with a corresponding increase in k', both

changes amounting to about 10% for additive concentrations in the

range 1.0% to 1.5%. Similar results were obtained by computer

simulation. Hence, to calculate the rate constant k_{14} for a flame

containing 1.1% cyanogen and 2.0% nitric oxide, the values of k'

and $[H]_o$ were taken as:

$$k' \quad = \quad 6.0 \times 10^4 \ atm^{-1} \ s^{-1},$$

$$[H]_o \quad = \quad 1.46 \times 10^{-2} \ atm.$$

The equilibrium constant K_2 was obtained from partition functions, using data from the JANAF tables,[25] together with a value of 418 kJ mol^{-1} for the enthalpy of formation of gaseous CN at absolute zero.[24] At 1500 K, this gave $K_2 = 79.9$. Since there is some disagreement in the literature as to the most reliable figure for the enthalpy of formation of CN,[24] the major uncertainty in the present calculation of k_{14} probably arises from the uncertainty in the value of K_2.

Concentrations of HCN and NO were taken from figure 10. By substitution in equation (17), the final result for k_{14} was determined as the mean of ten values:

$$k_{14} = 7.5 \times 10^9 \ m^3 \ kgmol^{-1} \ s^{-1} \ at \ 1500 \ K,$$

with a standard deviation of $1.0 \times 10^9 \ m^3 \ kgmol^{-1} \ s^{-1}$. Cumulative errors of measurement are estimated to introduce an uncertainty of about 40%. This value is consistent with the result of Boden and Thrush at 687 K:[27]

$$k_{14} = (3 \pm 2) \times 10^8 \ m^3 \ kgmol^{-1} \ s^{-1},$$

while the two figures may be combined to give the following pre-exponential factor and activation energy for the reaction of CN with NO:

$$CN + NO \quad \rightarrow \quad N_2 + CO \quad \ldots \ldots \quad (14),$$
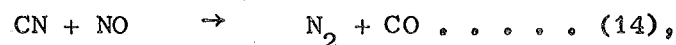
$$k_{14} = 1.08 \times 10^{11} \ e^{-(3.36 \times 10^4 \ kJ \ kgmol^{-1})/RT} \ m^3 \ kgmol^{-1} \ s^{-1}.$$

CHAPTER VI

DISSOCIATION ENERGIES OF ALKALI METAL CYANIDES

I. INTRODUCTION

When an aqueous spray of an alkali metal salt is added to a

hydrogen-nitrogen-oxygen flame containing about 0.5% cyanogen,

formation of the alkali metal cyanide takes place. The proportion

of the metal remaining as free atoms may be determined by flame

photometry. In the presence of known concentrations of HCN and H

atoms, a value may thus be obtained for the equilibrium constant for

metal cyanide formation. Combination of the equilibrium constant

with the partition functions for reactants and products, derived

from known or estimated spectroscopic data, gives the enthalpy of

reaction at absolute zero, which is then used to calculate the

dissociation energy of the metal cyanide.

Measurements of this type were applied some time ago to

the formation of metallic halides in hydrogen flames.[28] In the

case of metal cyanides, the method has not previously been used

due to the uncertainty in the proportion of added cyanogen which is

present as HCN at any point in the flame. Absolute yields of HCN

have now been determined by mass spectrometric sampling. As

described in Chapter V, the concentrations of carbon oxides and

HCN in the burnt gas stream have been measured as a function of

the percentage cyanogen added to the flame. Using these results,

it has become possible to evaluate the equilibrium constant for

metal cyanide formation.

In the presence of cyanogen, the concentration of metal

atoms in the burnt gas stream depends on the equilibrium:

$$M + HCN \quad \rightleftharpoons \quad MCN + H \quad \ldots \ldots (1).$$

It is also necessary, in principle, to take into account the

equilibrium leading to hydroxide formation:

$$M + H_2O \quad \rightleftharpoons \quad MOH + H \quad \ldots \ldots (2).$$

The equilibrium constants K_1 and K_2 are given by:

$$K_1 = \frac{[MCN][H]}{[M][HCN]} \quad \ldots \ldots \ldots \ldots (3),$$

$$K_2 = \frac{[MOH][H]}{[M][H_2O]} \quad \ldots \ldots \ldots \ldots (4).$$

If $[M]_T$ is the total metal added to the flame,

$$[M]_T = [M] + [MOH] + [MCN],$$

$$= [M](1 + K_2[H_2O]/[H] + K_1[HCN]/[H]) \quad \ldots \ldots (5),$$

while in the absence of cyanogen, denoting the metal atom

concentration by $[M]_O$,

$$[M]_T = [M]_O + [MOH],$$

$$= [M]_O (1 + K_2[H_2O]/[H]) \quad \ldots \ldots \ldots (6).$$

Elimination of $[M]_T$ between equations (5) and (6) gives the result:

$$\frac{[M]_O}{[M]} = 1 + \frac{K_1[HCN]}{[H] + K_2[H_2O]} \, .$$

Provided the concentration of metal is sufficiently low for there

to be no significant self-absorption, this expression may be written:

$$\frac{I_O}{I} = 1 + \frac{K_1[HCN]}{[H] + K_2[H_2O]} \quad \ldots \ldots \ldots (7),$$

where I and I_O are the intensities of thermal emission in the

presence and absence of HCN respectively. Thus the equilibrium

constant K_1 for a given alkali metal may be determined from a

plot of $(I_O/I - 1)$ versus HCN concentration for a flame containing

known concentrations of H and H_2O.

63

II. DETERMINATION OF D_O^O (M - CN), M = Li, Na, K, Rb, Cs.

(1) <u>Measurement of Metal Atom Concentrations by Emission</u>

<u>Spectroscopy</u>

The present study of alkali metal cyanides was carried out

in flame Z8 (H_2: N_2: O_2 = 4.5 : 8.0 : 1.0). Aqueous solutions of

0.01M lithium acetate, sodium chloride, potassium chloride,

rubidium chloride and caesium bromide were added separately to

the flame. Using the optical system described in Chapter III,

the emission intensity at the metallic resonance lines was recorded

for varying initial concentrations of cyanogen over the range

0.0% to 1.5% of the unburnt composition. The wavelengths observed

were: Li, 670.8 nm; Na, 589.3 nm; K, 769.9 nm; Rb, 780.0 nm;

Cs, 852.1 nm. Spectroscopic measurements were made at a distance

of 4.0 mm from the reaction zone, a region in which the metal

emission is largely thermal rather than chemiluminescent, the

equilibrium concentration of CN radicals being sufficiently low

to rule out excitation by reactions such as:

$$M + H + CN \rightarrow M^* + HCN \ldots \ldots (8).$$
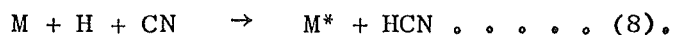
Cyanogen was introduced into the unburnt gas stream

immediately prior to the burner, the inlet being controlled by an

off-on stopcock. In this way, it was possible to reduce to about

three seconds the delay from the time at which cyanogen was added

at a new concentration to the time at which the corresponding change

in intensity was detected at the spectrometer. The proportion of

cyanogen in the unburnt gas was increased in steps of approximately

0.1% up to 1.5%. At each particular additive concentration,

measurement of the emission intensity at the metallic resonance line

gave a value of (I_o/I -1), which was then plotted against the

percentage cyanogen in the unburnt composition. All five alkali

FIGURE XI   64

Graph of $(I_o/I - 1)$ versus Cyanogen Concentration for Lithium

Emission in the Burnt Gases of Flame Z8

Percentage C_2N_2 in unburnt gas

FIGURE XII   65
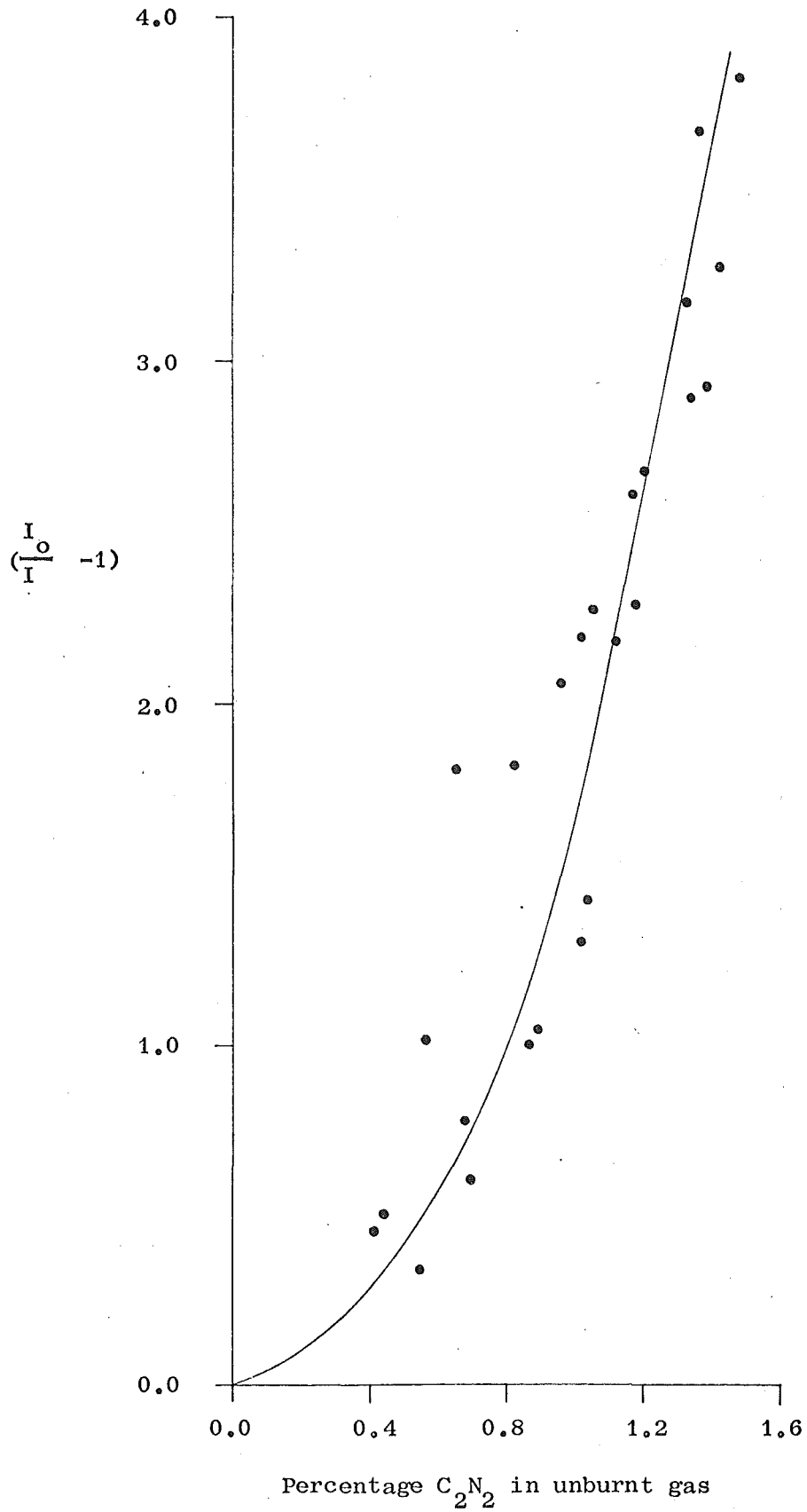
Graph of (I$_o$/I -1) versus Cyanogen Concentration for Sodium

Emission in the Burnt Gases of Flame Z8

Percentage C$_2$N$_2$ in unburnt gas
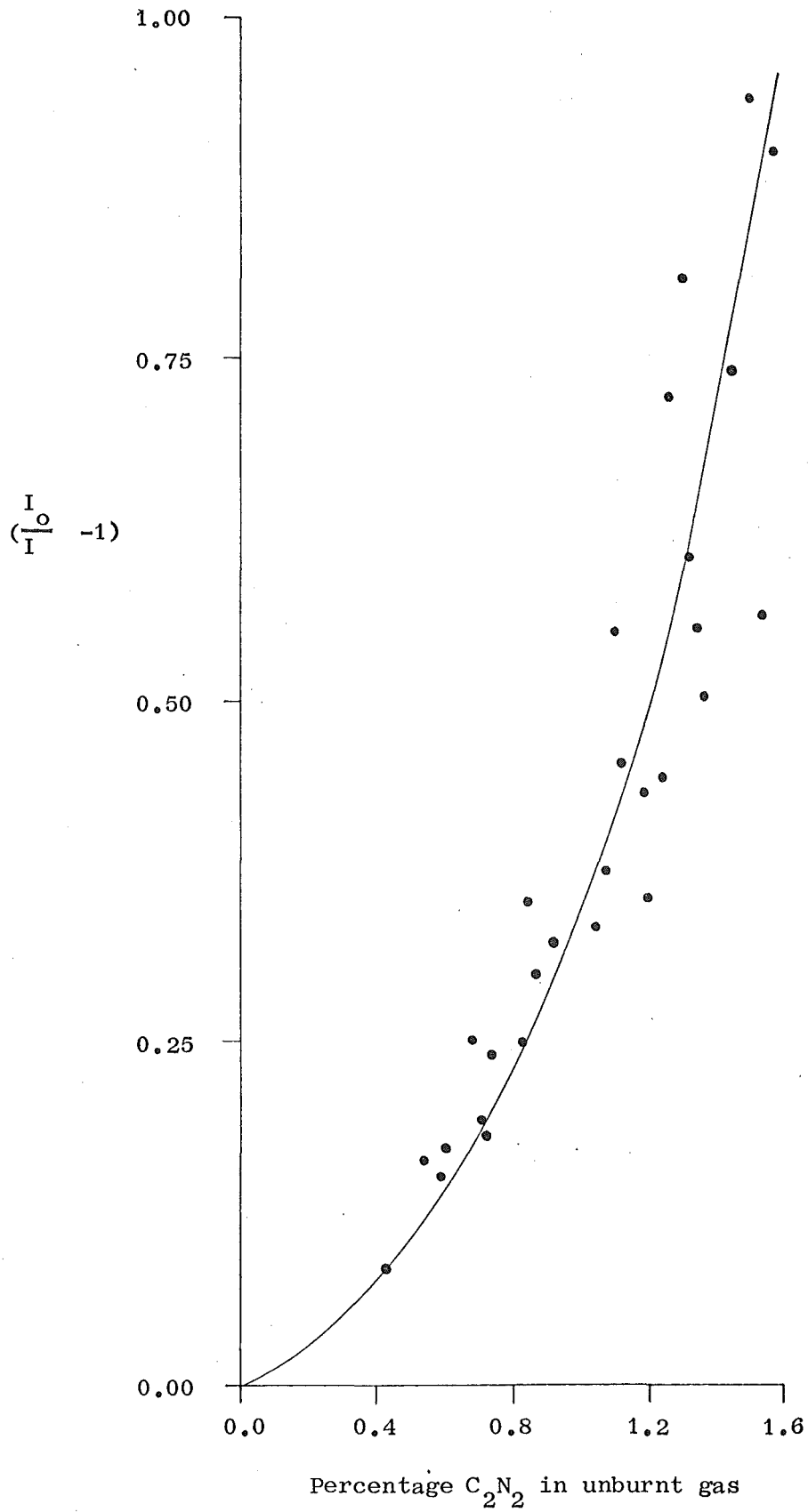
metals gave similar graphs of $(I_o/I -1)$ as a function of percentage

cyanogen added to the flame, the curves for lithium and sodium

being shown in figures 11 and 12.

(2) Calculation of the Equilibrium Constants K_1 for Metal Cyanide Formation

Graphs of $(I_o/I -1)$ versus HCN concentration were obtained

by combining the photometric results with the mass spectrometric

profile, given in figure 9, for HCN concentration as a function

of percentage cyanogen in the unburnt gas. A separate graph was

constructed for each alkali metal. At intervals of 0.1% cyanogen,

the values of $(I_o/I -1)$ were plotted against the corresponding

values of [HCN] as determined from a curve drawn through the

experimental points of figure 9. Extrapolation of the curve at

low cyanogen flows was carried out so as to give the best straight

line plots of $(I_o/I -1)$ versus HCN concentration.

Results for lithium and sodium are presented in figure 13,

while those for potassium, rubidium and caesium appear in figure 14.

In each case, the graph of $(I_o/I -1)$ as a function of HCN

concentration in the burnt gas region is a straight line at values

of [HCN] which correspond to 1.0% or less cyanogen in the unburnt

gas. At higher cyanogen concentrations, negative deviations from

linearity are observed. This effect is probably due to "flame-lift".

As illustrated in plate II on page 7, a movement of the reaction zone

away from the burner surface would tend to move a region of more

intense emission into the field of view of the monochromator, giving

higher intensity readings and lower values of $(I_o/I -1)$.

The slope of the linear portion of the curve of $(I_o/I -1)$

versus HCN concentration is given by:

$$\text{Slope} = \frac{K_1}{[H] + K_2 [H_2O]} \quad \ldots \ldots (9).$$

FIGURE XIII   67

Graphs of $(I_o/I -1)$ versus HCN Concentration in the Burnt Gases

of Flame Z8:   Results for Lithium and Sodium

HCN concentration in burnt gas (atm x 10^{-3})

FIGURE XIV   68
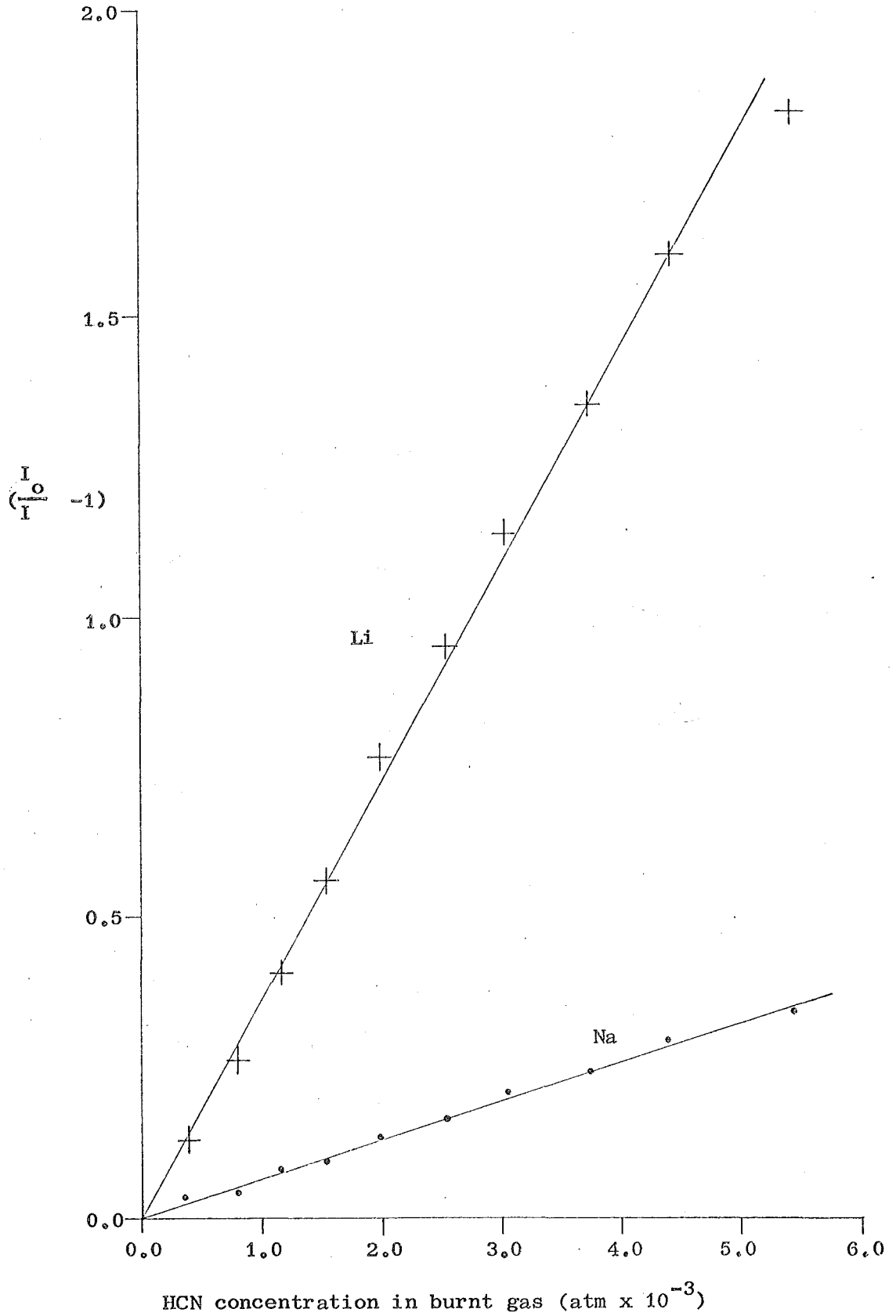
Graphs of $(I_o/I -1)$ versus HCN Concentration in the Burnt

Gases of Flame Z8 :   Results for Potassium, Rubidium and Caesium

HCN concentration in burnt gas $(atm \times 10^{-3})$
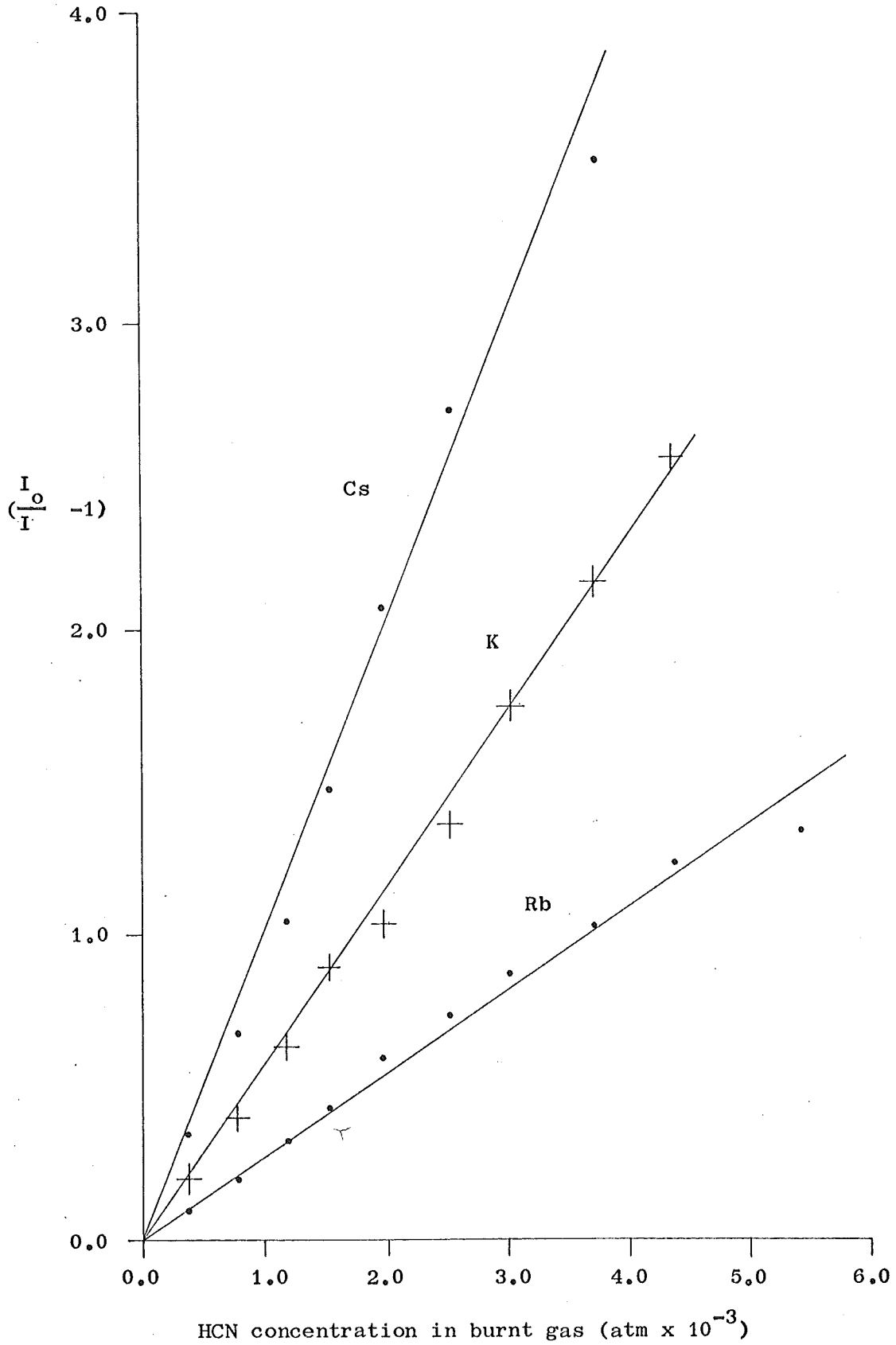
Calculated slopes for the curves of figures 13 and 14 are listed in

table III. To determine the corresponding equilibrium constants K_1

for metal cyanide formation, values are required for the equilibrium

constants K_2 and for the concentrations of H and H_2O in the burnt

gas stream. In flame Z8, the final temperature of the burnt gases

is approximately 1500 K. This is relatively cool for a hydrogen

flame, with the result that K_2 is negligible except in the case

of lithium, where $K_2 = 0.011^{(2)}$ and $[H_2O] = 0.16$ atm gives:

$$K_2 [H_2O] = 1.76 \times 10^{-3} \text{ atm.}$$

The measurement of H atom concentrations is discussed in section III

of this chapter. At a distance of 4.0 mm above the reaction zone,

absolute [H] as determined by the Li/LiOH method was 7.1×10^{-3} atm

in the absence of cyanogen. Addition of cyanogen caused a slight

reduction in H atom concentrations. However, since the observed

decrease was less than 10% for cyanogen flows below 1.0% of the

unburnt composition, a constant value of [H] was assumed for the

purposes of calculating K_1. Table III gives the equilibrium

constants K_1 and K_2 for M = Li, Na, K, Rb, Cs. The values of K_1 at

1500 K may be regarded as a measure of the extent to which metal

atoms M are combined to form metal cyanide MCN at the temperature

of the burnt gas region.

(3)   Calculation of the Dissociation Energies of Metal

Cyanides

Values of ΔH_0^o (1), the enthalpy change for reaction (1) at

absolute zero, were calculated from the equilibrium constants K_1 for

metal cyanide formation. Data for partition functions were taken

from the JANAF tables.[25]   In the case of lithium, rubidium and

caesium, molecular parameters for the metal cyanide were estimated

from those given in reference (25) for sodium and potassium cyanide.

Table IV lists the final molecular parameters for all five alkali

metal cyanides. Assuming a constant value of r_{C-N}, values of r_{M-C}, M = Li, Rb, Cs, were obtained from covalent radii, while vibration frequencies, $\nu_{1,2,3}$ (MCN), M = Li, Rb, Cs, were calculated by the method of Herzberg.[29]

Metal cyanide dissociation energies D_o^o (M-CN) were determined from the relation:

$$D_o^o \text{ (M-CN)} = D_o^o \text{ (H-CN)} - \Delta H_o^o \text{ (1)} \quad \ldots \ldots \quad (10).$$

Using a figure of $418 \pm 4 \text{ kJ mol}^{-1}$ for the enthalpy of formation of $CN_{(g)}$ at absolute zero,[24] together with the JANAF figures for the enthalpies of formation of $HCN_{(g)}$ and $H_{(g)}$, a value of $499 \pm 13 \text{ kJ mol}^{-1}$ was calculated for D_o^o (H-CN). The limit of error in ΔH_o^o (1) was taken as $\pm 9 \text{ kJ mol}^{-1}$. This corresponded to an uncertainty factor of two in the equilibrium constants K_1, which appeared to be a reasonable estimate of the uncertainty introduced by errors of experimental measurement. A total error limit of $\pm 22 \text{ kJ mol}^{-1}$ was therefore assigned to the values of D_o^o (M-CN).

Results from the present work for ΔH_o^o (1) and D_o^o (M-CN), M= Li, Na, K, Rb, Cs, are given in table III. In the case of sodium and potassium, the values of D_o^o (M-CN) may be compared with the corresponding values calculated from the enthalpies of formation listed in the JANAF tables for $M_{(g)}$, $MCN_{(g)}$ and $CN_{(g)}$, M= Na, K. Agreement is not close, but lies within the combined limits of experimental error. There appears to be no marked trend in D_o^o (M-CN) as M varies, while in comparison with the fluorides and chlorides the energy range covered by the dissociation energies of the alkali metal cyanides is small.[30]

TABLE III

Data used to Determine Dissociation Energies of Alkali Metal Cyanides

M	Slope (atm^{-1})	K_1 (1500 K)	K_2 (1500 K)	ΔH^o_o (1) (kJ mol^{-1}) (a)	D^o_o (M-CN) (kJ mol^{-1}) (b)
Li	356	3.17	0.011[2]	2 ± 9	497 ± 22	
Na	64.1	0.455	-	24 ± 9	474 ± 22	446 ± 13
K	548	3.89	-	2 ± 9	497 ± 22	442 ± 31
Rb	272	1.93	-	12 ± 9	487 ± 22	
Cs	1000	7.09	-	-2 ± 9	501 ± 22	

$[H_2O] = 0.16$ atm, $[H] = 7.1 \times 10^{-3}$ atm.

(a): Present values.

(b): Values calculated from data given in the JANAF tables.[25]

(2): Reference (2).

TABLE IV

Molecular Parameters used in Partition Function Calculations

$\underline{M}$	$\underline{r}_{(M\text{-}C)}$ (pm)	$\underline{r}_{(C\text{-}N)}$ (pm)	ν_1 (cm^{-1})	ν_2 (cm^{-1})	ν_3 (cm^{-1})
Li	179	116	410	267	2200
Na	199.2	116	400	239	2176
K	229.4	116	370	207	2158
Rb	248	116	340	202	2125
Cs	268	116	322	198	2100

III. MEASUREMENT OF HYDROGEN ATOM CONCENTRATIONS

(1) Absolute [H] in Flame Z8 from the Li/LiOH Method

The Li/LiOH method to determine H atom concentrations

depends on measurement of the proportion of lithium combined as

lithium hydroxide according to the equilibrium:

$$Li + H_2O \rightleftharpoons LiOH + H \quad \cdots \cdots (2).$$
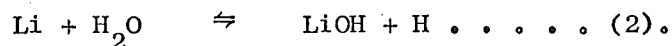
If $[Li]_T$ is the total lithium added to the flame,

$$\frac{[LiOH]}{[Li]} = (\frac{[Li]_T}{[Li]} - 1).$$

Hence the equilibrium ratio of metal hydroxide to free metal atoms

is given by:

$$(\frac{[Li]_T}{[Li]} - 1) = \frac{K_2[H_2O]}{[H]},$$

where K_2 is the equilibrium constant of reaction (2). Since sodium

hydroxide is not formed to any significant extent in hydrogen flames,

the ratio $[Li]_T/[Li]$ may be obtained by comparison of the

intensities of the sodium and lithium resonance lines under the same

flame conditions. At known values of K_2 and $[H_2O]$, the concentration

of H atoms may therefore be calculated from the relation:

$$\frac{1}{[H]} = (\frac{[Li]_T}{[Li]} - 1) \frac{1}{K_2[H_2O]} \quad \cdots \cdots (11).$$

Absolute concentrations of H atoms were determined in the

burnt gas region of flame Z8 at distances of 4.0 mm and 6.0 mm

above the reaction zone. Photometric measurements were made with the

absorption system described in Chapter III. A mixed aqueous solution

of 0.005M lithium acetate and 0.001M sodium chloride was added to

the flame, intensity readings being taken at 670.8 nm using the

lithium hollow cathode lamp and at 589.3 nm using the sodium-

potassium lamp. Values of $[Li]_T/[Li]$ were calculated from the

formula:

$$\frac{[Li]_T}{[Li]} = \frac{5 \ f_{Li} \ \sqrt{a_{Li}} \ M_{Li} \ \log_e \left(\frac{I_o}{I}\right)_{Na}}{f_{Na} \ \sqrt{a_{Na}} \ M_{Na} \ \log_e \left(\frac{I_o}{I}\right)_{Li}} \quad \ldots \ldots (12).$$

In this expression, f is the transition probability and a the

absorption coefficient of the selected metallic resonance line,

while M is the atomic weight of the metal and the factor 5 arises

from the relative concentrations of lithium and sodium in the

atomiser solution. Intensities of transmitted light in the presence

and absence of the metal additive are denoted I and I_o respectively.

The transition probabilities and absorption coefficients for the

lithium 670.8 nm lines and the sodium 589.3 nm line were taken

from Gaydon and Wolfhard.[31]

Using the measured values of $[Li]_T/[Li]$ at 4.0 mm and 6.0 mm

from the reaction zone, the corresponding values of 1/[H] were

calculated according to equation (11). The equilibrium constant

K_2 was obtained from data given by Phillips.[2] Extrapolation of

K_2 values tabulated over the temperature range 2620 K to 2405 K gave:

$$K_2 = 1.13 \times 10^{-2} \text{ at } 1500 \text{ K.}$$

Hence, in the burnt gas stream of flame Z8:

$$K_2 \ [H_2O] = 1.81 \times 10^{-3} \text{ atm.}$$

This figure is expected to be somewhat low, since the equilibrium

data of Phillips was calculated on the basis of a dissociation

energy for lithium hydroxide of 427 kJ mol^{-1}, whereas a value of

430 kJ mol^{-1} is now considered to be more reliable.[26] Therefore,

the H atom concentrations quoted in the present work are probably

too low by a factor of one or two percent.

Results for [H] and 1/[H] in flame Z8 at distances of 4.0 mm

and 6.0 mm from the reaction zone are presented in the table below.

These values, which give absolute H atom concentrations as

determined by the Li/LiOH method, were used to scale the profile of

relative H atom concentrations obtained by measurement of CuH

emission intensities in the same flame at distances ranging from

0.5 mm to 10.0 mm above the reaction zone.

Distance from Reaction Zone	$\dfrac{1}{[H]}$	$[H]$
(mm)	(atm^{-1})	(atm)
4.0	1.41×10^{2}	7.09×10^{-3}
6.0	1.87×10^{2}	5.35×10^{-3}

(2) Relative [H] in Flame Z8 from the Copper Hydride Method

Addition of an aqueous copper salt solution to a hydrogen

flame leads to the production of excited CuH*:

$$Cu + H \quad \rightarrow \quad CuH^* \; \circ \; \circ \; \bullet \; \circ \; \circ \; (13),$$
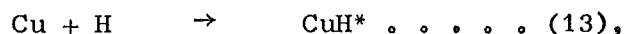
the transition to the ground state being accompanied by molecular

emission:

$$CuH^* \quad \rightarrow \quad CuH + h\nu \; \circ \; \circ \; \bullet \; \bullet \; \circ \; (14).$$
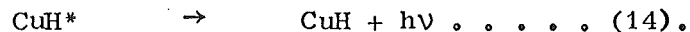
The kinetics of CuH* formation have been investigated by Bulewicz

and Sugden.[32] These authors showed that the intensity of

molecular emission is directly proportional to the concentration of

H atoms in the flame gases, with the result that measurements of

CuH emission intensity may be used to determine relative H atom

concentrations.

The variation of H atom concentration with time is of the

form:

$$\frac{1}{[H]} = \frac{1}{[H]_{o}} + k't \; \circ \; \bullet \; \bullet \; \circ \; \circ \; (15).$$

Hence a plot of $1/[H]$ versus time from the reaction zone is a straight

line with intercept $1/[H]_{o}$ and slope k'. Since the intensity of

CuH emission is proportional to the H atom concentration, a similar

straight line graph is obtained when $1/I_{CuH}$ is plotted as a function

of time from the reaction zone. The intensity profile is a profile

of relative H atom concentration. Measurement of the absolute

concentration of H atoms at any point on this graph enables the

remaining points to be scaled, giving a profile of absolute H atom

concentration with time from the reaction zone.

Relative H atom concentrations in the burnt gas region of

flame Z8 were determined by the copper hydride method. Using the

flame photometric system described in Chapter III, the CuH emission

intensity at 428.0 nm was recorded at intervals of 0.5 mm over the

range 0.5 mm to 10.0 mm above the reaction zone. Copper was added

to the flame as an aqueous solution of 0.01 M copper nitrate. The

straight line graph of $1/I_{CuH}$ versus distance from the reaction

zone was calibrated by comparison with the values of $1/[H]$ at

4.0 mm and 6.0 mm as determined by the Li/LiOH method. This gave

the corresponding plot of $1/[H]$ against distance from the reaction

zone. Figure 15 shows the final profile of absolute H atom

concentration in the burnt gas stream of flame Z8, presented in

linear form as a graph of $1/[H]$ versus time.

(3)   Effect of Cyanogen on H Atom Concentrations

Addition of cyanogen to a hydrogen-nitrogen-oxygen flame

would be expected to lead not only to breakdown of the additive to

HCN and carbon oxides but also to small changes in flame radical

concentrations. Measurements of H atom concentrations in the

presence of cyanogen have confirmed this prediction.

In flame Z8, a quantitative estimate of the effect of

cyanogen on H atom concentrations in the burnt gas region was

obtained by observing the change in CuH emission intensity caused

by introduction of the additive into the unburnt gas stream. Copper

was added to the flame as an aqueous spray of 0.01 M copper nitrate

solution. Using the optical system described in Chapter III, the

FIGURE XV

Profile of Absolute H Atom Concentration in the Burnt

Gas Stream of Flame Z8
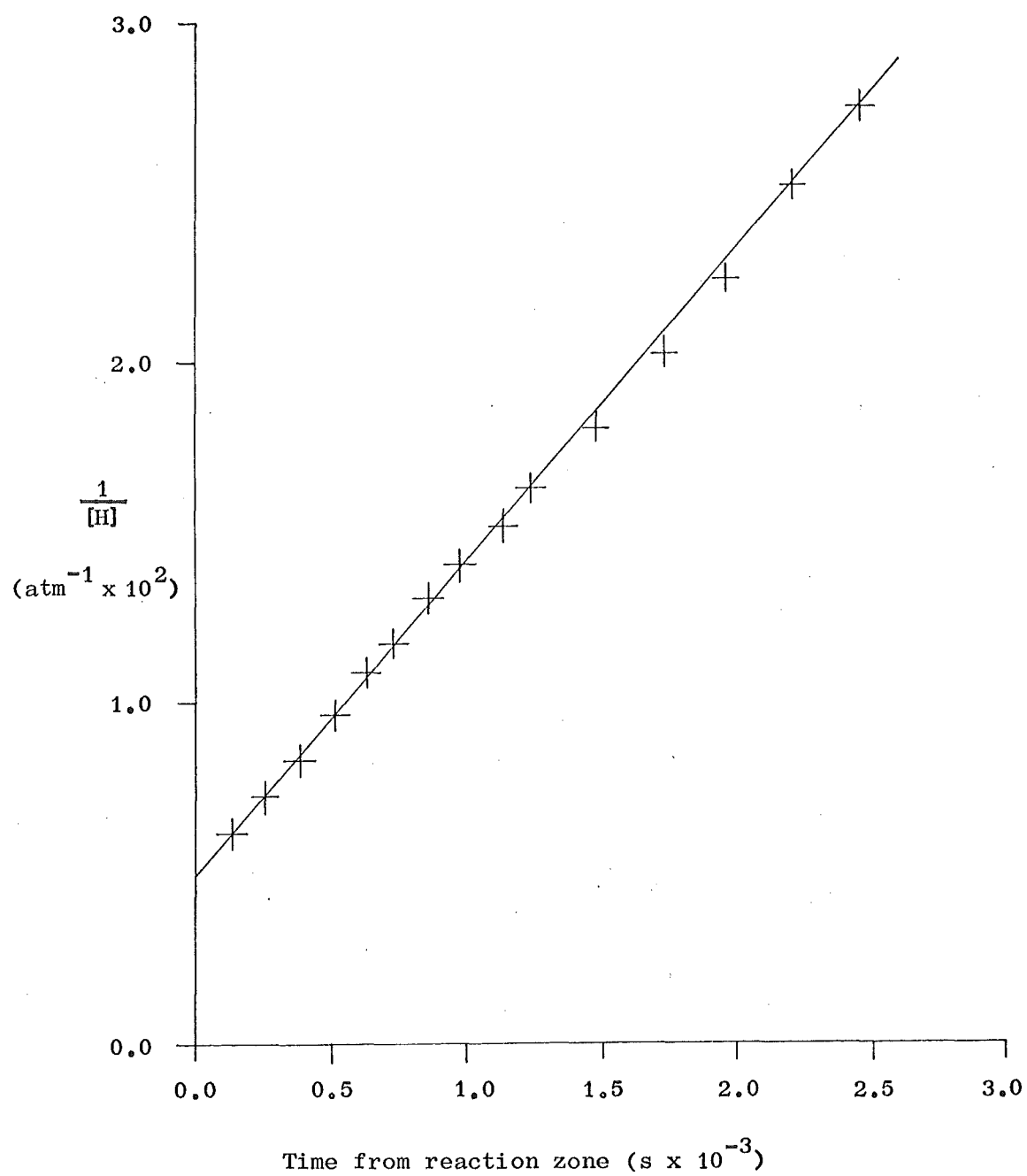
emission intensity at 428.0 nm was recorded for varying initial

concentrations of cyanogen over the range 0.0% to 1.5% of the unburnt

composition. Readings were taken at distances of 4.0 mm, 6.0 mm and

8.0 mm from the reaction zone.

To check for the possible formation of cuprous cyanide,

measurements of emission intensity were made at the copper resonance

lines at 324.8 nm and 327.4 nm. The cyanogen concentration was

varied as before from 0.0% to 1.5%. Since no significant decrease

in metallic emission was observed with increasing percentage

cyanogen in the flame, the concentration of copper atoms in the burnt

gases was assumed to be unaffected by the presence of cyanogen.

Formation of cuprous cyanide by the reaction:

$$Cu + HCN \rightleftharpoons CuCN + H \ldots \ldots (1),$$
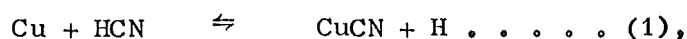
was therefore negligible. This implies that the measurements of

CuH emission intensity at 428.0 nm would not be significantly

affected by overlap with the CN band system in the wavelength range

421.6 nm to 358.4 nm, while changes in the intensity of CuH emission

could be taken as directly proportional to changes in H atom

concentration.

In the absence of cyanogen, absolute H atom concentrations in

flame Z8 at distances of 4.0 mm, 6.0 mm and 8.0 mm from the reaction

zone were taken from figure 15. At each point, the ratio of H atom

concentration to CuH emission intensity was calculated. This

calibration factor, determined in the absence of cyanogen, was used

to scale the remaining intensity readings in the presence of cyanogen,

giving a plot of absolute H atom concentration versus percentage

cyanogen added to the flame. Results are presented in figure 16.

The profiles of H atom concentration in the burnt gas stream as

a function of percentage cyanogen in the unburnt gas are given for

FIGURE XVI   79

Absolute H Atom Concentrations in the Burnt Gas Region of

Flame Z8 as a function of Percentage Cyanogen added

to the Flame

Distance from reaction zone: (a)   4.0 mm;

(b)   6.0 mm;

(c)   8.0 mm.
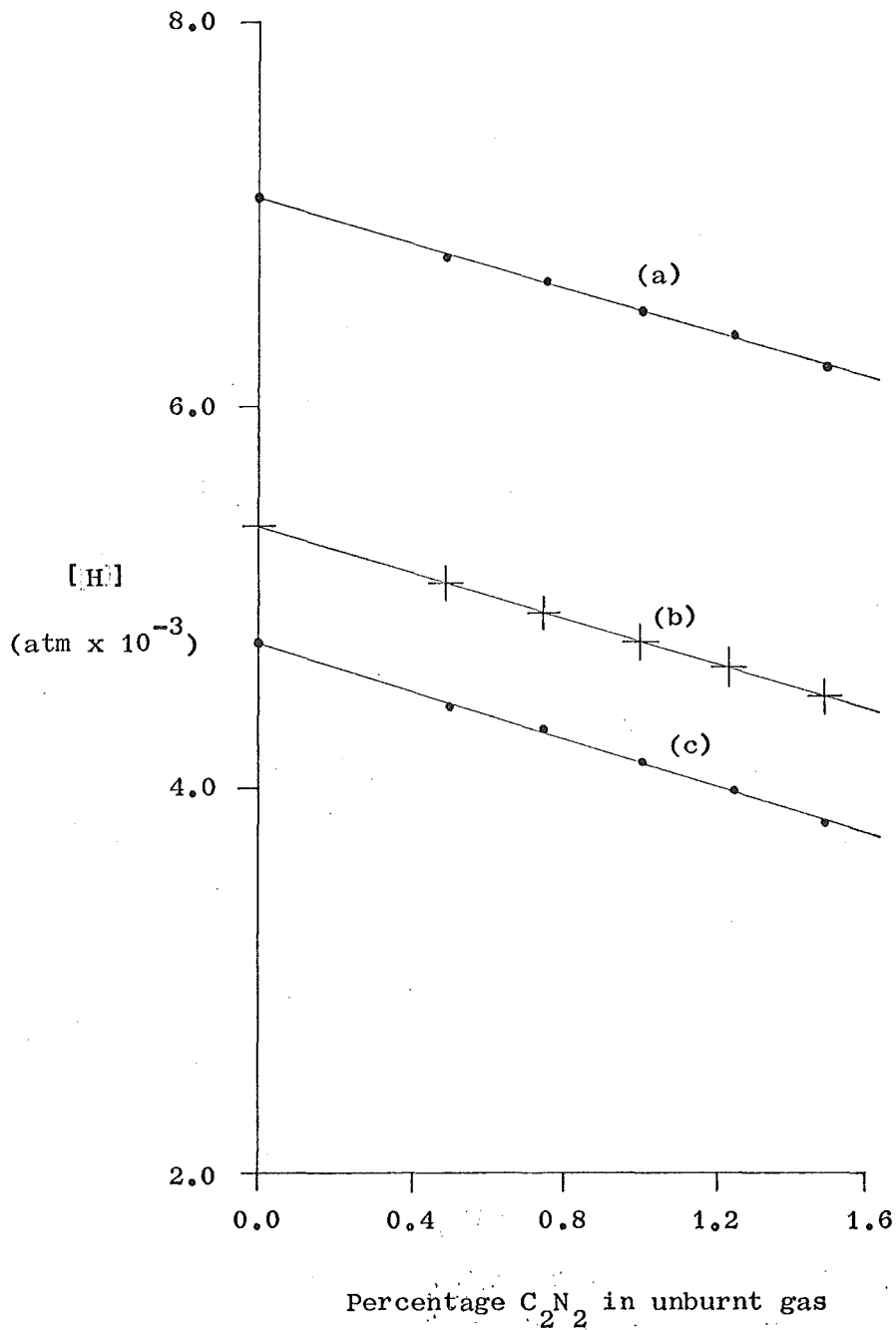
flame Z8 at distances of 4.0 mm, 6.0 mm and 8.0 mm above the reaction

zone. A similar curve is obtained in all three cases. As the

proportion of cyanogen in the unburnt composition is increased,

there is a linear decrease in the measured H atom concentration

in the burnt gas region. At 1.0% cyanogen, the total reduction in

H atom concentration is approximately 10%.

CHAPTER VII

COMPUTER SIMULATION OF THE BREAKDOWN OF

CYANOGEN IN HYDROGEN-NITROGEN-OXYGEN FLAMES

I. INTRODUCTION

The mathematical equations to describe the processes

occurring in the reaction zone of a flame are derived from the

laws of conservation of energy and mass flux, together with the

differential equations of chemical kinetics, molecular diffusion

and thermal conduction. Many attempts have been made to solve

these equations analytically. However, with advances in computing

techniques, attention has now focused on the development of computer

programmes which use an iterative procedure to calculate numerical

solutions of the flame equations.

In the present work, the programme used to simulate the

processes taking place in the reaction zone of a hydrogen-nitrogen-

oxygen flame was developed by Professor L.F. Phillips of this

department from a programme written by Spalding and Stevenson[33]

for the hydrogen-bromine flame. This was in turn derived from

the general boundary-layer programme of Patankar and Spalding.[34]

Calculations for the hydrogen-nitrogen-oxygen flame were carried

out on a Burroughs B6718 computer, programme code and data files

being stored on magnetic tape.

II. SIMULATION PROGRAMME FOR THE BASIC HYDROGEN-NITROGEN-OXYGEN

FLAME

(1) Outline of the Calculation Procedure

The computer simulation was based on a model reaction scheme

for the hydrogen-nitrogen-oxygen flame. This specified the chemical reactions to be taken into account, together with molecular parameters for stable and unstable chemical species and rate constants for the forward and reverse reactions. Concentration profiles for the first iteration were obtained by the steady state approximation. The main section of the programme then continued the calculation, giving at each iteration profiles through the reaction zone for temperature, density, mean molecular weight, average molar enthalpy and the diffusion coefficients and mass and mole fractions of all chemical species. Similar profiles were determined for thermal conductivity and heat capacity. Simultaneous differential equations were solved for the concentrations of all components except nitrogen, whose concentration was fixed by the requirement that the sum of mass fractions for all components is unity.

The reaction zone was covered by a 36-point grid. Cold and hot boundaries, corresponding to 1% and 99% fuel consumption, were set at points 9 and 27 respectively. Subroutines were used to determine entrainment rates at the boundaries of the reaction zone, to calculate source terms for chemical species and enthalpy, to obtain steady state radical concentrations and to solve simultaneous differential equations by the Patankar-Spalding procedure. A further subroutine provided for input data concerning trace additives. At each grid point, rate constants for the reaction mechanism were evaluated according to the calculated temperature at the same point in the flame.

(2)   Model Reaction Scheme

The reaction scheme used to model the basic hydrogen-nitrogen-oxygen flame containing no additives was the set of twelve reactions listed in table V. This mechanism has been

TABLE V

Model Reaction Scheme for the Basic

Hydrogen-Nitrogen-Oxygen Flame

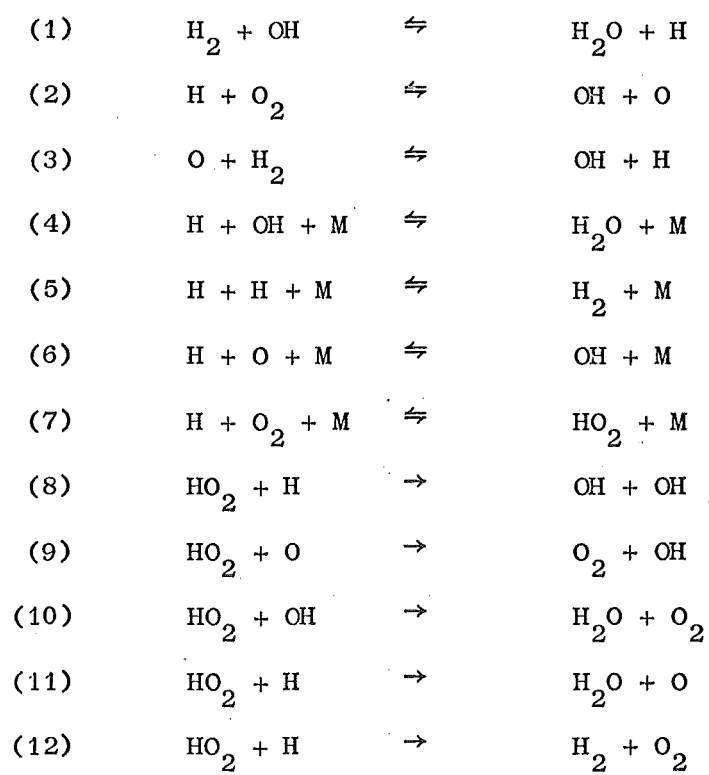| (1) | $H_2 + OH$ | $\rightleftharpoons$ | $H_2O + H$ |
(2)	$H + O_2$	$\rightleftharpoons$	$OH + O$
(3)	$O + H_2$	$\rightleftharpoons$	$OH + H$
(4)	$H + OH + M$	$\rightleftharpoons$	$H_2O + M$
(5)	$H + H + M$	$\rightleftharpoons$	$H_2 + M$
(6)	$H + O + M$	$\rightleftharpoons$	$OH + M$
(7)	$H + O_2 + M$	$\rightleftharpoons$	$HO_2 + M$
(8)	$HO_2 + H$	$\rightarrow$	$OH + OH$
(9)	$HO_2 + O$	$\rightarrow$	$O_2 + OH$
(10)	$HO_2 + OH$	$\rightarrow$	$H_2O + O_2$
(11)	$HO_2 + H$	$\rightarrow$	$H_2O + O$
(12)	$HO_2 + H$	$\rightarrow$	$H_2 + O_2$

TABLE VI

Rate Parameters for Reactions (1) to (12)

Reaction	Pre-exponential Factor $(m^3 \ kgmol^{-1} \ s^{-1})$	Activation Energy $(kJ \ kgmol^{-1})$
Forward (1)	2.19×10^{10}	2.155×10^4
Reverse (1)	1.12×10^{11}	8.557×10^4
Forward (2)	2.05×10^{11}	6.910×10^4
Reverse (2)	1.20×10^{10}	0.000
Forward (3)	1.74×10^{10}	3.954×10^4
Reverse (3)	7.81×10^9	3.953×10^4
Forward (4)	4.50×10^9	0.000
Reverse (4)	1.00×10^{14}	4.908×10^5
Forward (5)	$5.00 \times 10^{12} T^{-1}$	0.000
Reverse (5)	$7.63 \times 10^{16} T^{-1}$	4.521×10^5
Forward (6)	5.00×10^9	0.000
Reverse (6)	2.20×10^{10}	4.358×10^5
Forward (7)	1.98×10^9	-6.280×10^3
Reverse (7)	8.60×10^9	1.978×10^5
Forward (8)	7.00×10^{10}	0.000
Forward (9)	2.50×10^{10}	0.000
Forward (10)	3.00×10^9	0.000
Forward (11)	7.00×10^9	0.000
Forward (12)	1.00×10^{10}	0.000

employed in similar work by Dixon-Lewis and co-workers.[35] Rate
parameters for the forward reactions were taken from the rate set D
of Stephenson and Taylor,[36] while parameters for the reverse
reactions, with the exception of reaction (5), were calculated from
equilibrium constants, using free energy data from the JANAF
tables.[25] A complete list of forward and reverse rate constants
for reactions (1) to (12) is given in table VI. In the case of
reaction (5), since results for the burning velocity and peak
radical concentrations were found to be particularly sensitive to
the value of the reverse rate constant k_{-5}, parameters for k_{-5} were
chosen from the range of values tabulated by Baulch and co-workers.[37]

In the case of flame Z8 (H_2: N_2: O_2 = 4.5 : 8.0 : 1.0), well-
converged concentration profiles were obtained after 1200 iterations.
At this stage, the burning velocities calculated with respect to
all stable species and hydrogen and hydroxyl radicals agreed to
within a few percent, while those calculated with respect to other
radicals differed by no more than one or two orders of magnitude.
Final temperature and mole fraction profiles are shown in figures
18 to 22. The final calculated burning velocity is 1.07 $m.s^{-1}$, a
value which agrees within expected limits of error with the
experimental burning velocity of 1.29 $m.s^{-1}$ determined in the same
flame by Rosenfeld and Sugden.[38]

III. SIMULATION PROGRAMME FOR FLAME Z8 CONTAINING UP TO 1.0% CYANOGEN

(1) Model Reaction Scheme for the Combustion of Cyanogen

Computer simulation of the breakdown of cyanogen in
hydrogen-nitrogen-oxygen flames was studied using a basic flame
of the composition Z8 (H_2: N_2: O_2 = 4.5 : 8.0 : 1.0). Combustion of
cyanogen was described by a set of seventeen additional reactions.

These were specified as input data to the flame programme, together with rate constants for the forward and reverse processes, molecular parameters for the chemical species produced and consumed and a value for the initial proportion of cyanogen in the unburnt gas. Calculation was resumed at the converged solution of the programme for flame Z8 containing no additives. After a further 100 to 200 iterations, the converged profiles through the reaction zone were considered to represent a solution of the programme for the same flame containing the given initial concentration of cyanogen.

The mechanism of seventeen reactions used to model the breakdown of cyanogen in hydrogen-nitrogen-oxygen flames is listed in tables VII and VIII. Wherever possible, rate constants were estimated from experimental data in the literature. In the absence of sufficient information from literature sources, arbitrary values were chosen and adjusted by a process of trial and error to give calculated results in agreement with those from the present experimental measurements.

Using an arbitrary figure of 4.0×10^{10} m^3 $kgmol^{-1}$ s^{-1} for the pre-exponential factor of reaction (13), the activation energy was chosen to correspond to the measured value of k_{13} at room temperature.[24] The rate constant k_{14} was taken from the results of Boden and Thrush[27] at 687 K. In the case of reaction (15), initial parameters for the forward rate constant were chosen to agree with an approximate value of k_{15} at room temperature,[39] after which the figures for pre-exponential factor and activation energy were adjusted to give the lowest possible ratio of HCN to carbon oxides in the breakdown products from C_2N_2. Parameters for the reverse reaction were determined from the equilibrium constant K_{15}. This was calculated statistically, using data from the JANAF tables[25] together with a value of 418 kJ mol^{-1} for the enthalpy

of formation of gaseous CN at absolute zero.[24]

The pre-exponential factor and activation energy for the rate constant k_{16} were taken from the results obtained by Albers and co-workers[23] over the temperature range 200 K to 500 K. This choice was influenced by the high yields of carbon oxides observed in mass spectrometric work. Since the ratio of HCN to CO/CO_2 mixture from C_2N_2 will be determined by the relative rates of reaction of CN radicals with H_2 and O_2, reactions (15) and (16) respectively, a high yield of carbon oxides indicates that (16) is the faster process at the temperature of the reaction zone. Boden and Thrush[27] give a value of $4.4 \times 10^9 \ m^3 \ kgmol^{-1} \ s^{-1}$ for k_{16} at 687 K. However, this figure is lower by a factor of four than the value of k_{16} calculated at the same temperature from the parameters in table VIII.

The rapid radical exchange reactions (17) to (19) and (26) to (29) were assumed to be temperature-independent. Using arbitrary initial rates of the order of $10^{10} \ m^3 \ kgmol^{-1} \ s^{-1}$, final rate constants were obtained by adjusting the trial values to give results as far as possible consistent with experimental observations. The rate of reaction (20) was taken from the room temperature data of Gordon and co-workers.[40] Parameters for reaction (21) were calculated by combining the results for k_{21} determined at 1500 K in the present work and at 687 K by Boden and Thrush.[27] In the notation of Chapter V, section III,

$$k_{21} = k_{14} \ (Chapter \ V),$$

$$= 1.08 \times 10^{11} \ e^{-\ (3.36 \times 10^4 \ kJ \ kgmol^{-1})/RT} \ m^3 \ kgmol^{-1} \ s^{-1}.$$

Rate constants for the remaining reactions (22) to (25) were obtained from the recommended values in the compilation of Baulch and co-workers.[37]

TABLE VII

Model Reaction Scheme for the Combustion of
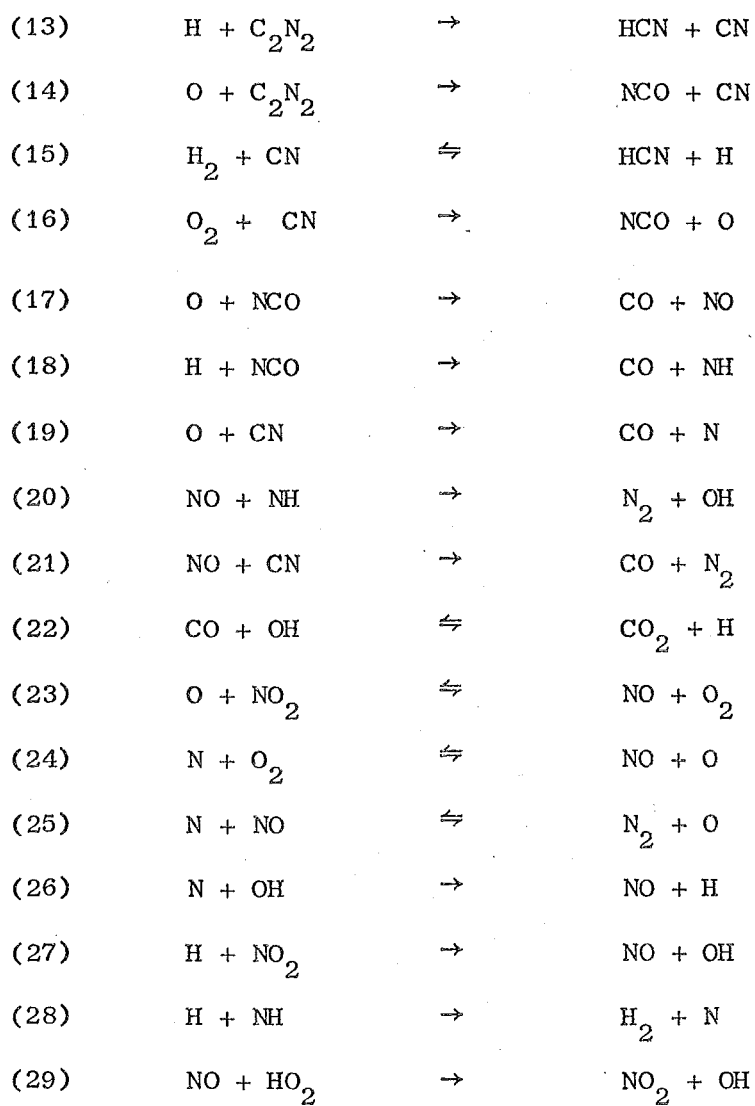
Cyanogen in Hydrogen-Nitrogen-Oxygen Flames

(13)	$H + C_2N_2$	$\rightarrow$	$HCN + CN$
(14)	$O + C_2N_2$	$\rightarrow$	$NCO + CN$
(15)	$H_2 + CN$	$\rightleftharpoons$	$HCN + H$
(16)	$O_2 + CN$	$\rightarrow$	$NCO + O$
(17)	$O + NCO$	$\rightarrow$	$CO + NO$
(18)	$H + NCO$	$\rightarrow$	$CO + NH$
(19)	$O + CN$	$\rightarrow$	$CO + N$
(20)	$NO + NH$	$\rightarrow$	$N_2 + OH$
(21)	$NO + CN$	$\rightarrow$	$CO + N_2$
(22)	$CO + OH$	$\rightleftharpoons$	$CO_2 + H$
(23)	$O + NO_2$	$\rightleftharpoons$	$NO + O_2$
(24)	$N + O_2$	$\rightleftharpoons$	$NO + O$
(25)	$N + NO$	$\rightleftharpoons$	$N_2 + O$
(26)	$N + OH$	$\rightarrow$	$NO + H$
(27)	$H + NO_2$	$\rightarrow$	$NO + OH$
(28)	$H + NH$	$\rightarrow$	$H_2 + N$
(29)	$NO + HO_2$	$\rightarrow$	$NO_2 + OH$

TABLE VIII

Rate Parameters for Reactions (13) to (29)

Reaction	Pre-exponential Factor (m^3 $kgmol^{-1}$ s^{-1})	Activation Energy (kJ $kgmol^{-1}$)	Reference	Temperature Range of Experimental Data (K)
Forward (13)	4.00×10^{10}	2.81×10^4	(24)	Room temperature
Forward (14)	2.50×10^{10}	4.60×10^4	(27)	687
Forward (15)	2.00×10^9	1.15×10^4	(39)	Room temperature
Reverse (15)	9.00×10^9	8.30×10^4	Calculated from K_{15}	
Forward (16)	3.30×10^{10}	4.20×10^3	(23)	200 - 500
Forward (17)	2.00×10^{10}	0.00		
Forward (18)	5.00×10^9	0.00		
Forward (19)	1.30×10^{10}	0.00		
Forward (20)	2.30×10^{10}	0.00	(40)	Room temperature
Forward (21)	1.08×10^{11}	3.36×10^4	Present work, Chapter V, section III	687 - 1500

Reaction	Pre-exponential Factor $(m^3\ kgmol^{-1}\ s^{-1})$	Activation Energy $(kJ\ kgmol^{-1})$	Reference	Temperature Range of Experimental Data (K)
Forward (22)	5.60×10^{8}	4.52×10^{3}	(37)	300 – 2000
Reverse (22)	5.60×10^{10}	9.83×10^{4}	(37)	1000 – 1350
Forward (23)	1.00×10^{10}	2.52×10^{3}	(37)	280 – 550
Reverse (23)	1.00×10^{9}	1.90×10^{5}	(37)	280 – 550
Forward (24)	$6.43 \times 10^{6}T$	2.62×10^{4}	(37)	300 – 2000
Reverse (24)	$1.55 \times 10^{6}T$	1.62×10^{5}	(37)	300 – 2000
Forward (25)	3.10×10^{10}	1.40×10^{3}	(37)	300 – 1600
Reverse (25)	1.36×10^{11}	3.16×10^{5}	(37)	300 – 1600
Forward (26)	2.00×10^{10}	0.00		
Forward (27)	3.00×10^{10}	0.00		
Forward (28)	2.00×10^{10}	0.00		
Forward (29)	1.00×10^{10}	0.00		

(2) Results of Computer Simulation on the Basis of the

Proposed Reaction Scheme

Computer simulation results for the combustion of 0.1%

cyanogen in flame Z8 are presented in figure 17. The calculated

mole fraction profiles for carbon-containing species are plotted as

a function of distance through the reaction zone, assuming for

clarity an equal spacing of the 36 grid points. Similar sets of

profiles were obtained at additive concentrations of 0.02%, 0.05%,

0.5% and 1.0%. As the percentage cyanogen in the flame was increased,

the most marked effect on the concentration profiles was a shift

towards the high temperature region of the reaction zone, 50%

decomposition of C_2N_2 occurring at grid point 17 for 0.02% cyanogen

as compared to grid point 30 for 1.0% cyanogen. The delay in

decomposition of the additive was accompanied by a small increase

in the ratio of HCN to carbon oxide product.

Calculated yields of HCN and CO/CO_2 mixture from C_2N_2 are

given in table IX. The corresponding ratios of HCN to carbon oxide

product, which range from 1.13 at 0.02% cyanogen to 1.36 at 1.0%

cyanogen, are consistent with production of HCN and CO by

reactions (13) and (16) to (18), under conditions where there is no

important contribution from reaction (15). The small rise in

product ratio with increasing additive concentration is probably due

to temperature changes. At higher initial proportions of cyanogen,

decomposition of the additive occurred at a later stage of the

reaction zone, where higher gas temperatures would enable

reaction (15) to compete more effectively with reaction (16).

FIGURE XVII

Mole Fraction Profiles through the Reaction Zone for Carbon-Containing Species

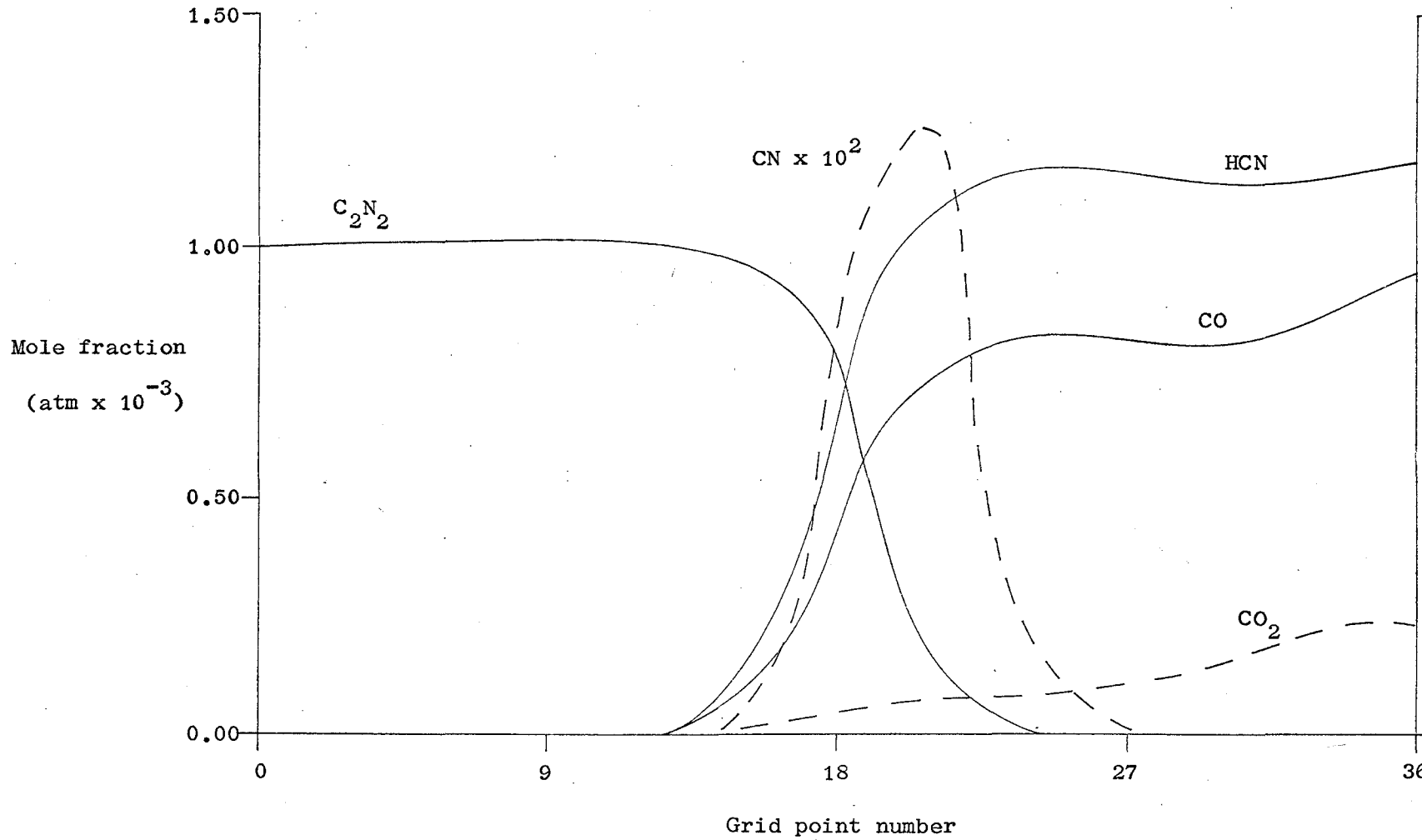Computer simulation results for flame Z8 containing 0.1% cyanogen

TABLE IX

Yields of HCN and Carbon Oxides from C_2N_2 in Flame Z8

Containing up to 1.0% Cyanogen

Mole Fraction of	Mole Fractions in Burnt Gas			Ratio [HCN]/[CO + CO_2]
C_2N_2 in Unburnt Gas	HCN	CO	CO_2	in Burnt Gas
(atm x 10^{-2})	(atm x 10^{-2})	(atm x 10^{-2})	(atm x 10^{-2})	
0.02	0.0231	0.0170	0.0035	1.13
0.05	0.0570	0.0418	0.0080	1.14
0.10	0.113	0.082	0.014	1.18
0.50	0.576	0.395	0.041	1.32
1.00	1.28	0.85	0.09	1.36

(3) Comparison of Experimental and Calculated Results

for the Combustion of Cyanogen

As described in Chapter V, experimental yields of HCN and

carbon oxides from C_2N_2 were determined in flame Z8 by mass

spectrometric analysis of the burnt gas stream. These results are

plotted in figure 9 as a function of percentage cyanogen added to

the flame.

The most important feature of the mass spectrometric

measurements is the small yields of HCN observed at low additive

concentrations. As the percentage cyanogen in the unburnt

composition is increased from 0.1% to 1.0%, the measured ratio of

HCN to CO/CO_2 mixture rises from 0.25 to 0.30, finally reaching

unity at 1.5% cyanogen. No comparable effect is observed in the

computer simulation results. As shown in table IX, when breakdown

of cyanogen is modelled by the system of reactions (13) to (29),

the calculated ratio of HCN to carbon oxide product is close to unity

for additive concentrations ranging from 0.02% to 1.0%. Hence the

proposed reaction scheme does not provide an adequate description

of the combustion of cyanogen in hydrogen flames.

In terms of the present mechanism, to account for HCN

yields lower than the corresponding yields of carbon oxides, HCN

produced in reaction (13) must be converted to CN or NCO radicals

by a process comparable in rate to the reaction of CN with molecular

oxygen. One possibility is the reaction of HCN with O atoms:

$$HCN + O \quad \rightarrow \quad CN + OH \ldots \ldots (30).$$
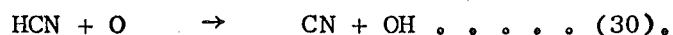
However, when this process was included in the reaction scheme of

table VII, together with an arbitrary value of $10^{10} \, m^3 \, kgmol^{-1} \, s^{-1}$

for the rate constant k_{30}, little change was observed in the calculated

yields of HCN. This effect was probably due to the low concentrations

of O atoms relative to HCN. As indicated by the profiles of figures
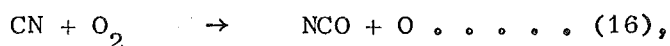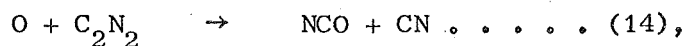
17 and 22, the peak O atom concentration in the reaction zone is

5×10^{-4} atm for a flame containing 0.1% cyanogen, while the final

concentration of HCN in the same flame is approximately 1×10^{-3} atm.

Further trial calculations were carried out to test the

possible conversion of HCN to CN by the reverse process (15), the

reaction of HCN with H atoms:

$$HCN + H \rightarrow CN + H_2 \quad . \quad . \quad . \quad . \quad . \quad (15r).$$
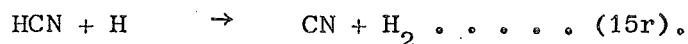
Since data for high temperature reaction rates are subject to large

errors of experimental measurement, the parameters given in table

VIII for the reverse reaction (15) were adjusted to give an

increase of 100% in the calculated value of the rate constant at

700 K. Once again, there was no significant decrease in the

calculated yield of HCN.

According to the results of computer simulation using these

and other trial mechanisms, there is no process occurring in the

reaction zone of flame Z8 which produces CN or NCO radicals from

HCN at a rate sufficiently fast to account for HCN yields lower than

the corresponding yields of carbon oxides. This suggests that HCN

is not formed in the primary decomposition of C_2N_2. Therefore,

from the present work, it appears that production of CN and NCO

radicals takes place by reactions (14) and (16):

$$O + C_2N_2 \rightarrow NCO + CN \quad . \quad . \quad . \quad . \quad . \quad (14),$$

$$CN + O_2 \rightarrow NCO + O \quad . \quad . \quad . \quad . \quad . \quad (16),$$

with no significant competition from reaction (13):

$$H + C_2N_2 \rightarrow HCN + CN \quad . \quad . \quad . \quad . \quad . \quad (13).$$
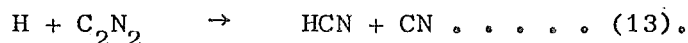
A recent study of the reaction of C_2N_2 with atomic hydrogen[23]

has given evidence that the initial step of this process leads to

formation of a cyclic intermediate:

$$H + C_2N_2 \rightarrow H(CN)_2 \quad . \quad . \quad . \quad . \quad . \quad (31).$$
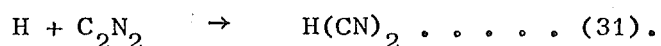
In a fuel-rich hydrogen-nitrogen-oxygen flame, this intermediate would be expected to decompose by further reaction with H atoms, either slowly to give CN radicals:
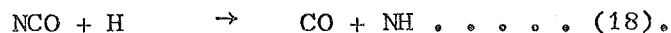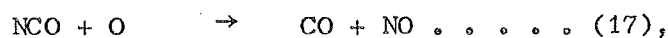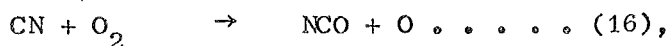
$$H(CN)_2 + H \rightarrow H_2 + 2CN \ldots \ldots (32),$$
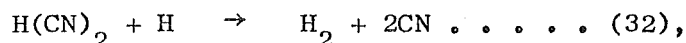
or more rapidly to regenerate C_2N_2:

$$H(CN)_2 + H \rightarrow H_2 + C_2N_2 \ldots \ldots (33).$$
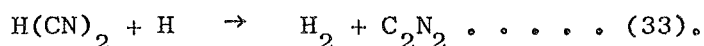
The present results support these observations. If the reaction of C_2N_2 with H atoms in flame Z8 follows pathways (31) and (33) rather than pathway (13), then breakdown of C_2N_2 will occur by O atom attack:

$$O + C_2N_2 \rightarrow NCO + CN \ldots \ldots (14),$$
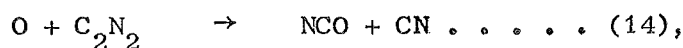
followed by rapid conversion of CN and NCO radicals to carbon oxides:

$$CN + O_2 \rightarrow NCO + O \ldots \ldots (16),$$

$$NCO + O \rightarrow CO + NO \ldots \ldots (17),$$

$$NCO + H \rightarrow CO + NH \ldots \ldots (18).$$

Production of HCN will be limited to processes of the type:

$$CN + H_2 \leftrightharpoons HCN + H \ldots \ldots (15),$$

$$NCO + H \leftrightharpoons HCN + O \ldots \ldots (34).$$
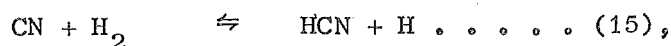
Provided decomposition of the additive occurs in the early reaction zone at temperatures below about 700 K, the reaction of CN with molecular hydrogen will be slower than the reaction of CN with molecular oxygen by at least one order of magnitude.[23] As a result, the ratio of HCN to carbon oxide product in the burnt gas stream will be less than unity. In future studies of the combustion of cyanogen in hydrogen flames, better correlation between calculated and experimental results may be obtained if the mechanism used in computer modelling assumes formation of the intermediate $H(CN)_2$ from the reaction of C_2N_2 with atomic hydrogen, breakdown of the additive to CN and NCO radicals occurring largely by reaction of C_2N_2 with atomic oxygen.

FIGURE XVIII

Mole Fraction Profiles through the Reaction Zone for H_2, O_2 and H_2O in Flame Z8

The curve for H_2 is displaced downward by 0.10 atm.
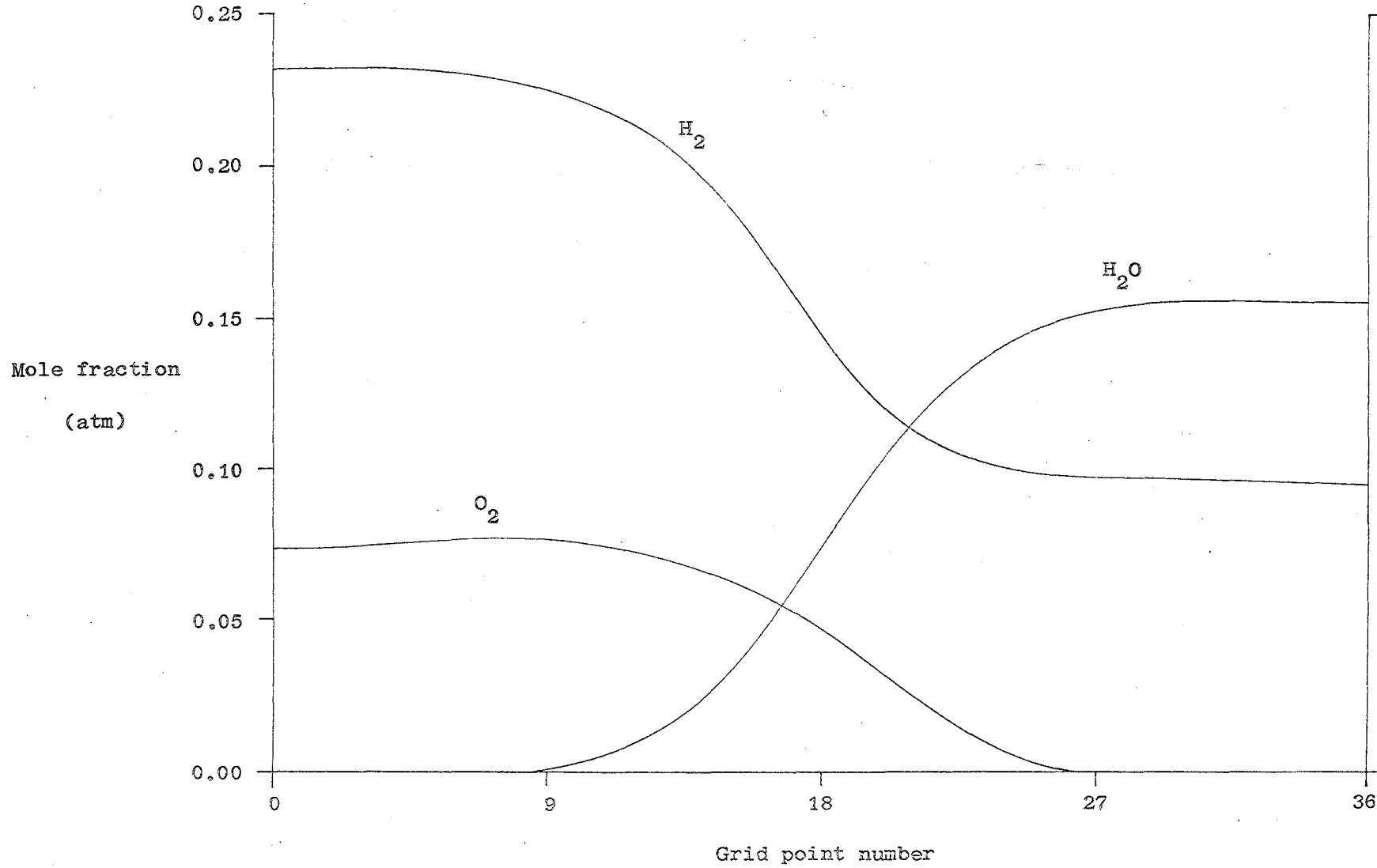
FIGURE XIX

<u>Temperature Profiles through the Reaction Zone of Flame Z8</u>

Computer simulation results   (a)   in the absence of additives;
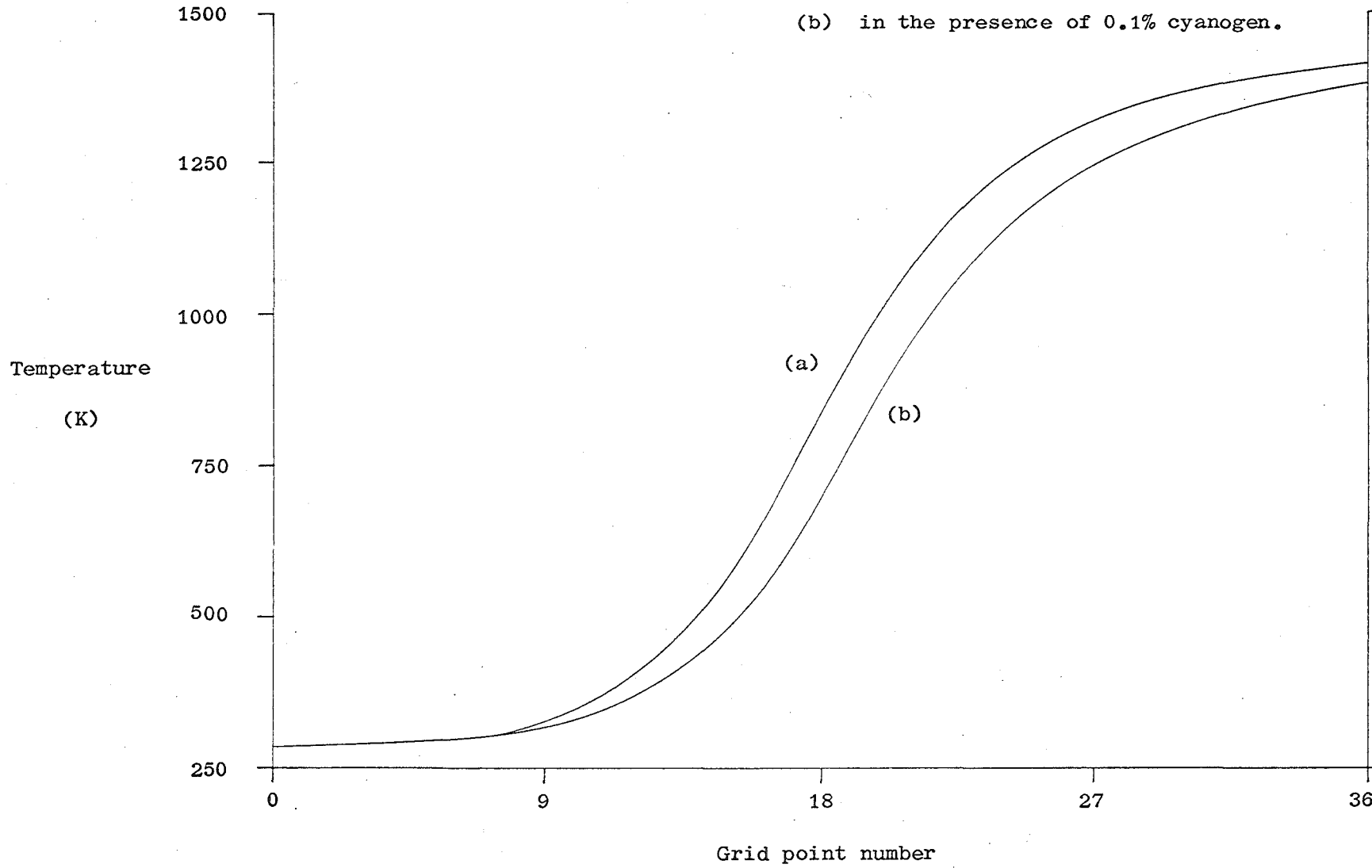
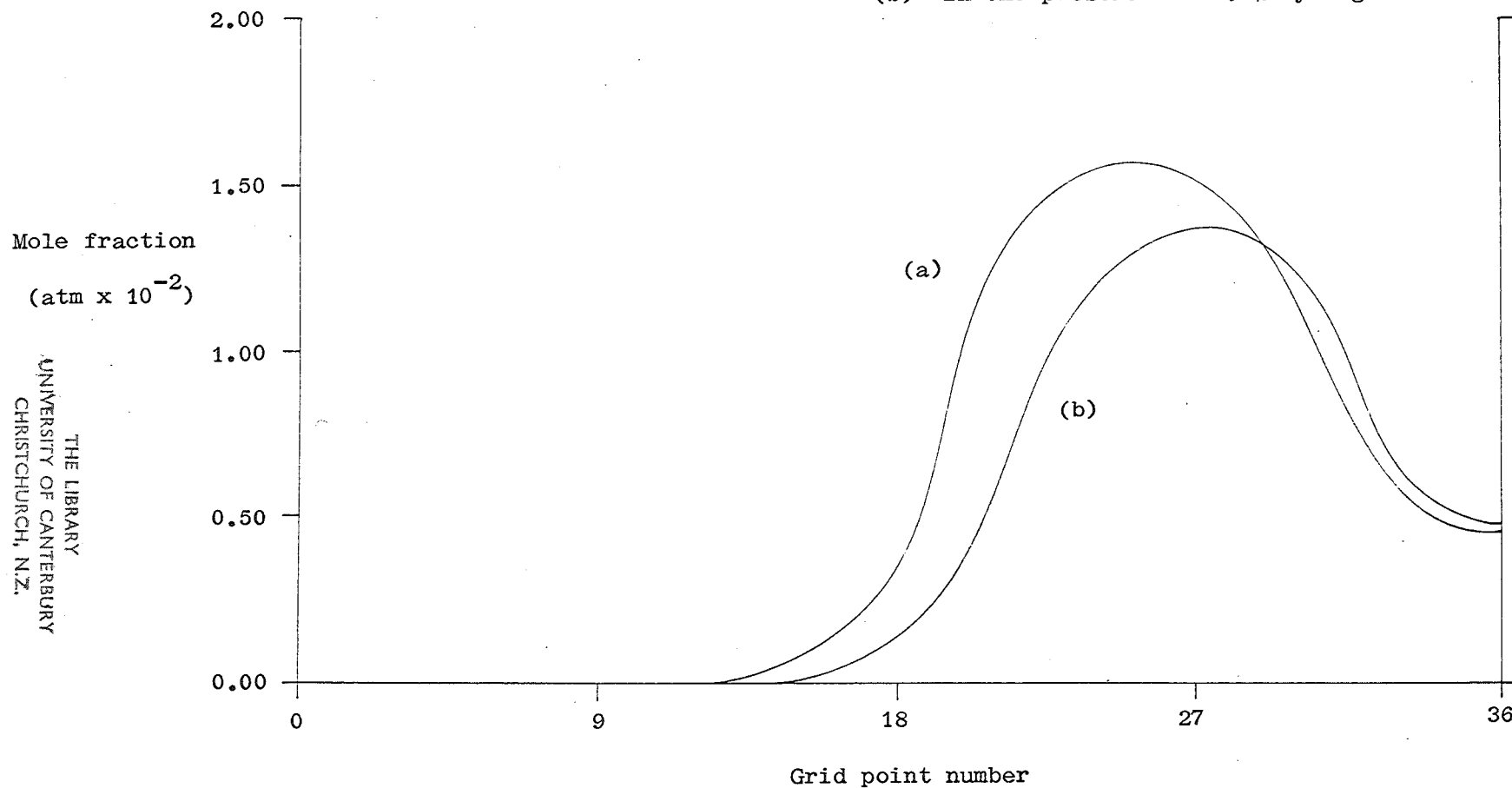(b)   in the presence of 0.1% cyanogen.

FIGURE XX

Mole Fraction Profiles through the Reaction Zone for H Radicals in Flame Z8

Computer simulation results (a) in the absence of additives;

(b) in the presence of 0.1% cyanogen.

FIGURE XXI

Mole Fraction Profiles through the Reaction Zone for OH Radicals in Flame Z8

Computer simulation results (a) in the absence of additives;
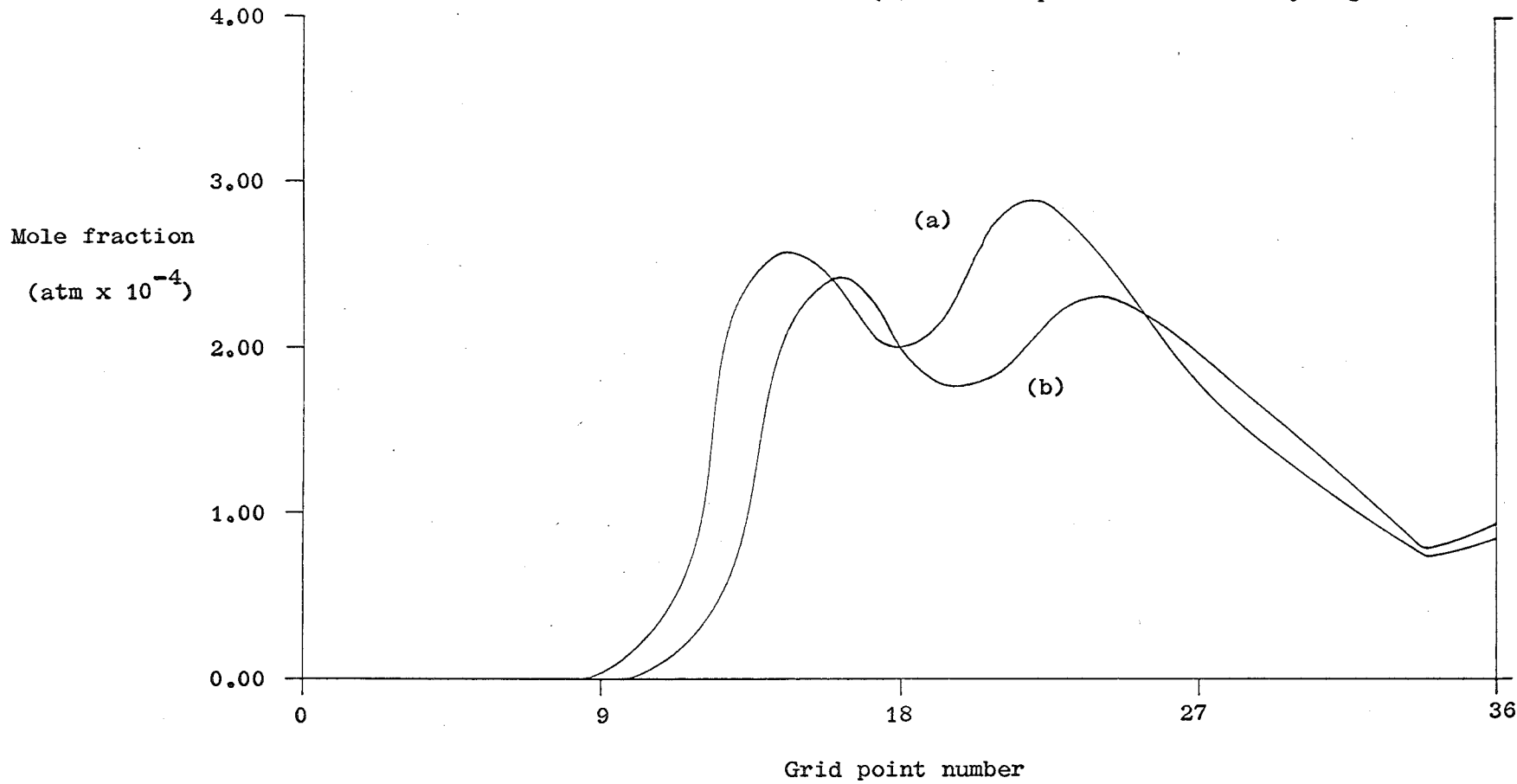
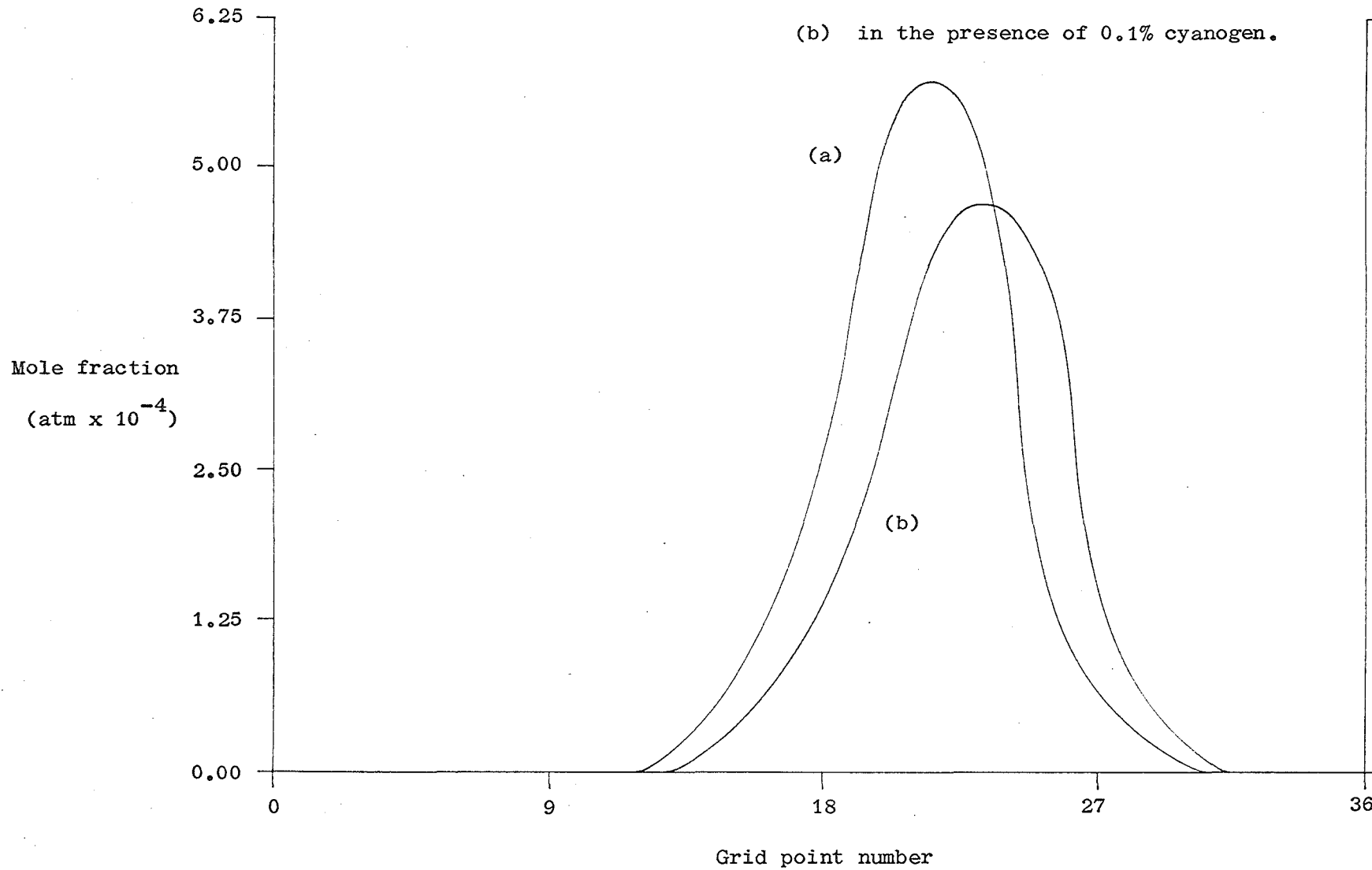(b) in the presence of 0.1% cyanogen.

FIGURE XXII

Mole Fraction Profiles through the Reaction Zone for O Radicals in Flame Z8

Computer simulation results (a) in the absence of additives;

(b) in the presence of 0.1% cyanogen.

(4) Effect of Cyanogen on Calculated Temperature and

Radical Concentration Profiles

Profiles through the reaction zone for temperature and the

mole fractions of H, OH and O radicals were calculated in flame Z8

containing initial proportions of cyanogen in the range 0.02% to

1.0%. Results at 0.1% cyanogen are presented in figures 19 to 22.

Although these profiles were determined using the reaction system

of tables VII and VIII to model the combustion of cyanogen, the

calculated results were in closer agreement with experimental data

than those obtained from the same mechanism for the yields of HCN

and carbon oxides from C_2N_2.

In figure 19, comparison of the temperature profile for

flame Z8 in the absence of additives with the corresponding

profile in the presence of 0.1% cyanogen indicates that introduction

of the additive leads to a decrease of 2% in the calculated

temperature of the burnt gases emerging from the reaction zone.

At 1.0% cyanogen, the calculated reduction in final flame

temperature is 9%. Experimentally, using the sodium reversal

method, a decrease of approximately 10% was observed in the burnt

gas temperature of the same flame for cyanogen concentrations

ranging from 1.0% to 1.5%.

As shown by the mole fraction profiles in figures 20, 21 and

22, the calculated values for the peak concentrations of H, OH and O

radicals are reduced by 15%, 17% and 18% respectively in the

presence of 0.1% cyanogen. The decrease in peak radical

concentrations is accompanied by a shift in the profiles towards the

high temperature region of the reaction zone. As the percentage

cyanogen in the flame is increased, the calculated mole fraction

profiles continue to decline, the total reduction at 1.0% cyanogen

amounting to approximately 30% for the peak concentrations of all

three species. In the burnt gas stream, the decrease in radical concentrations would be expected to be somewhat smaller. This prediction is supported by the experimental results of Chapter VI, section III, where a 10% reduction in H atom concentration was observed in the burnt gas region of flame Z8 for initial proportions of cyanogen in the range 1.0% to 1.5%.

CHAPTER VIII

THE REACTION OF NO WITH NH IN HYDROGEN-NITROGEN-OXYGEN FLAMES

I. INTRODUCTION

In the present study of the combustion of cyanogen in
hydrogen-nitrogen-oxygen flames, removal of nitric oxide produced
in breakdown of the additive was attributed to a rapid reaction of
NO with NH radicals:

$$NO + NH \quad \rightarrow \quad products \; . \; . \; . \; . \; . \; (1).$$
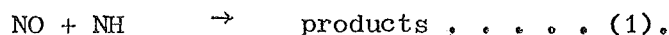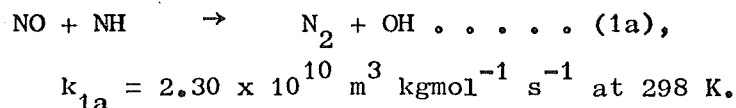
This assignment was supported by the results of computer simulation.
In flame Z8, combustion of cyanogen was modelled by a mechanism
in which the principal pathway for destruction of NO was the
process:

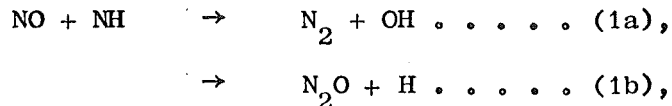$$NO + NH \quad \rightarrow \quad N_2 + OH \; . \; . \; . \; . \; . \; (1a).$$
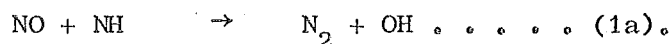
Calculated concentrations of NO in the burnt gas stream were
comparable to those observed experimentally. At 1.0% cyanogen, the
calculated ratio of NO to HCN product was 2.5×10^{-2}, while at the
same cyanogen concentration mass spectrometric analysis of the
burnt gases 1.0 mm above the reaction zone gave an experimental
NO to HCN ratio of approximately 5×10^{-2}.

Further evidence in support of a fast reaction of NO with NH
in hydrogen-nitrogen-oxygen flames has now been obtained from a
study of the processes occurring in a fuel-rich flame containing
small quantities of nitric oxide and ammonia. Destruction of
NO and NH reaches completion within the reaction zone of the flame.
This indicates a rate constant of the order of 10^{10} m^3 $kgmol^{-1}$ s^{-1},
a prediction which is consistent with the value of k_1 determined
at room temperature by Gordon and co-workers:[40]

$$NO + NH \quad \rightarrow \quad N_2 + OH \ \text{\textperiodcentered} \ \text{\textperiodcentered} \ \text{\textperiodcentered} \ \text{\textperiodcentered} \ \text{\textperiodcentered} \quad (1a),$$

$$k_{1a} = 2.30 \times 10^{10} \ m^3 \ kgmol^{-1} \ s^{-1} \ \text{at} \ 298 \ K.$$

To distinguish between the two possible reaction paths:

$$NO + NH \quad \rightarrow \quad N_2 + OH \ \text{\textperiodcentered} \ \text{\textperiodcentered} \ \text{\textperiodcentered} \ \text{\textperiodcentered} \ \text{\textperiodcentered} \quad (1a),$$

$$\rightarrow \quad N_2O + H \ \text{\textperiodcentered} \ \text{\textperiodcentered} \ \text{\textperiodcentered} \ \text{\textperiodcentered} \ \text{\textperiodcentered} \quad (1b),$$

isotopic labelling of the reactant NO has been combined with mass

spectrometric analysis of stable reaction products in samples from

the burnt gas stream. The predominant pathway appears to be the

process (1a). Within the detection limits of the present sampling

system, the product N_2O is not formed, while introduction of $N^{15}O$

into the nitric oxide supplied to the flame leads to an increase in

the measured concentration of $N^{15}N^{14}$ in the burnt gases emerging

from the reaction zone.

II. MASS SPECTROMETRIC STUDIES OF THE REACTION OF NO WITH NH IN

     A HYDROGEN-NITROGEN-OXYGEN FLAME

    (1)   Results at Mass 30 in Flame Z8 containing Nitric Oxide

         and Ammonia

The experimental results to be described in this chapter

were determined in a hydrogen-nitrogen-oxygen flame of the

composition Z8 (H_2: N_2: O_2 = 4.5 : 8.0 : 1.0). Using a total unburnt

gas flow, excluding additives, of 81.0 $cm^3 \ s^{-1}$, nitric oxide and

ammonia were introduced at flow rates ranging from 0.0 to 0.7 $cm^3 \ s^{-1}$

and 0.0 to 0.9 $cm^3 \ s^{-1}$ respectively. Argon was added as an internal

standard at a constant flow rate of 1.0 $cm^3 \ s^{-1}$. To minimise

corrosive effects, ammonia was introduced into the central flame gas

supply immediately prior to the burner, while nitric oxide was added

by mixing with the nitrogen stream to the central flame.

Samples for mass spectrometric analysis were withdrawn from the burnt gas region by means of the quartz probe and continuous flow sampling system described in Chapter III. The first series of measurements was taken at a distance of 1.0 mm from the reaction zone. Using a steady initial concentration of 0.90% nitric oxide in the unburnt composition, the mass spectrum was recorded for initial proportions of ammonia over the range 0.0% to 1.15%. Results were taken as the average of three scans at a given concentration of added ammonia. Background corrections were determined by recording the mass spectrum for the same initial proportions of ammonia in the absence of nitric oxide, while pressure fluctuations were taken into account by expressing the measured peak heights relative to the corresponding mass 40-Ar peaks.

In a second series of measurements, constant additive concentrations of 0.90% nitric oxide and 0.48% ammonia were maintained in the unburnt composition, while the position of the sampling probe in the burnt gas stream was varied in steps of 0.5 mm over the distance range 0.5 mm to 7.0 mm above the reaction zone. Peak heights were determined as the average of three scans at each sampling position. As in the previous set of experiments, corrections were applied for background in the absence of nitric oxide and for pressure fluctuations as indicated by changes in the argon peak as mass 40.

Results from the two series of experiments are presented in table X. In flame Z8 containing 0.90% nitric oxide, the measured value of the mass 30 - NO peak in samples taken 1.0 mm above the reaction zone decreases linearly with increasing ratio of ammonia to nitric oxide in the unburnt gas. At an additive ratio of unity,

TABLE X

Mass Spectrometric Results for the Concentrations of NO and N_2O in the Burnt Gas Region of Flame Z8

(1)   Profiles as a Function of Additive Ratio $[NH_3]/[NO]$

Sampling distance : 1.0 mm above reaction zone.

Mole Fractions in Unburnt Gas (atm x 10^{-2})		Ratio $[NH_3]/[NO]$ in Unburnt Gas	Peak Heights Relative to Argon in Burnt Gas	
NO	NH_3		Mass: 30(NO)	44(N_2O)
0.90	0.00	0.00	8.0	0.0
0.90	0.48	0.53	4.0	0.0
0.90	0.90	1.00	0.0	0.0
0.90	1.15	1.28	0.0	0.0

(2) Profiles as a Function of Distance from Reaction Zone

Mole fractions in unburnt gas: NO: 0.90×10^{-2} atm;

NH_3: 0.48×10^{-2} atm.

Distance from Reaction Zone (mm)	Peak Heights Relative to Argon in Burnt Gas	
	Mass: 30(NO)	44(N_2O)
0.5	5.7	0.0
1.0	6.0	0.0
1.5	6.1	0.0
2.0	5.9	0.0
2.5	5.8	0.0
3.0	5.6	0.0
4.0	5.8	0.0
5.0	6.2	0.0
6.0	5.7	0.0
7.0	6.0	0.0

the peak height at mass 30 is reduced to zero. Using constant

additive concentrations of 0.90% nitric oxide and 0.48% ammonia,

no significant change is observed in the mass 30 - NO peak as the

sampling position in the burnt gas region is varied from 0.5 mm

to 7.0 mm above the reaction zone.

According to these results, in a fuel-rich hydrogen-

nitrogen-oxygen flame, added nitric oxide is completely destroyed

by introduction of an equal concentration of ammonia. A rapid

reaction of NO with NH radicals:

$$NO + NH \quad \rightarrow \quad products \quad \circ \quad \bullet \quad \bullet \quad \bullet \quad \bullet \quad (1),$$
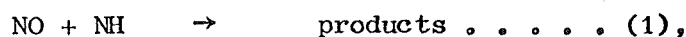
is consistent with the experimental data. To account for the

observed rate of nitric oxide removal, the process (1) must be

sufficiently fast to reach completion within the reaction zone of

the flame, a requirement which indicates a rate constant of the

order of 10^{10} m^3 $kgmol^{-1}$ s^{-1}. This prediction is supported by the

results of Gordon and co-workers[40] at room temperature. For

the reaction:

$$NO + NH \quad \rightarrow \quad N_2 + OH \quad \circ \quad \bullet \quad \circ \quad \circ \quad \circ \quad (1a),$$
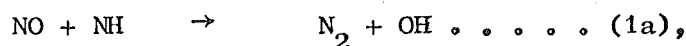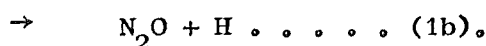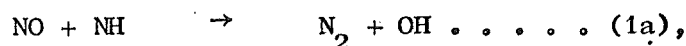
these authors give:

$$k_{1a} = 2.30 \times 10^{10} \, m^3 \, kgmol^{-1} \, s^{-1} \text{ at } 298 \text{ K.}$$

(2)   Results at Mass 44 in Flame Z8 containing Nitric Oxide

and Ammonia

In a fuel-rich hydrogen-nitrogen-oxygen flame, there are two

possible sets of products for the reaction of NO with NH radicals:

$$NO + NH \quad \rightarrow \quad N_2 + OH \quad \bullet \quad \circ \quad \bullet \quad \circ \quad \circ \quad (1a),$$

$$\rightarrow \quad N_2O + H \quad \circ \quad \circ \quad \bullet \quad \circ \quad \circ \quad (1b).$$

The two alternative reaction paths may be distinguished by mass

spectrometric methods. In the present work, the sampling system

did not enable mass spectrometric measurement of the

concentrations of unstable species such as H and OH radicals in

the burnt gas stream, while direct detection of the product N_2

was prevented by a strong background of nitrogen from the flame

gases. Therefore, results were restricted to the mass 44 – N_2O

peak. Table X gives the measured values of the peak height at

mass 44 in the burnt gas region of flame Z8 for an initial

nitric oxide concentration of 0.90% and initial proportions of

ammonia in the range 0.0% to 1.15%. The gas samples were taken

at a distance of 1.0 mm from the reaction zone. From these

measurements, after correction for the background of CO_2 in the

absence of additives, the mass 44 – N_2O peak remains at

approximately zero over the entire range of concentrations of

nitric oxide and ammonia. Thus N_2O was not observed as a product

from the reaction of NO with NH in flame Z8.

The detection limits of the sampling system for N_2O were

checked by addition of nitrous oxide to the unburnt gases of

flame Z8. Using initial proportions of additive ranging from

0.0% to 1.09%, samples for mass spectrometric analysis were withdrawn

from the burnt gas stream 1.0 mm above the reaction zone, the mass

spectrum being recorded as the average of three scans at a given

concentration of nitrous oxide. Corrections were applied as in

previous work for pressure changes and background in the absence

of additives.

Table XI gives the detection limits for nitrous oxide in

flame Z8. From the measured value of the mass 44 – N_2O peak at a

sampling distance 1.0 mm above the reaction zone, it was possible

to determine concentrations of nitrous oxide in the burnt gas stream

as low as 0.8×10^{-2} atm. This figure may be compared with the

TABLE XI

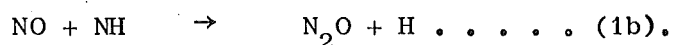Detection Limits for N_2O in the Burnt Gas Region of Flame Z8

Sampling distance: 1.0 mm above reaction zone.

Mole Fraction N_2O in Unburnt Gas (atm x 10^{-2})	Calculated Concentration N_2O in Burnt Gas (atm x 10^{-2})	Peak Height Relative to Argon in Burnt Gas Mass: $44(N_2O)$
0.77	0.83	7.0
0.88	0.95	8.0
1.09	1.17	9.0

maximum expected concentration of N_2O from the reaction of NO with

NH. For flame Z8 containing 0.90% nitric oxide and 0.90% ammonia,

assuming complete conversion of NO and NH to N_2O by process (1b),

the calculated concentration of nitrous oxide in the burnt gases

emerging from the reaction zone is 1.0×10^{-2} atm. Therefore,

the present experiments exceeded the detection limit for N_2O by a

factor of 1.25. Since N_2O was not observed as a product from the

reaction of nitric oxide with ammonia in flame Z8, it appears that

the reaction of NO with NH in a fuel-rich hydrogen-nitrogen-oxygen

flame proceeds by pathway (1a):

$$NO + NH \quad \rightarrow \quad N_2 + OH \ . \ . \ . \ . \ . \ (1a),$$
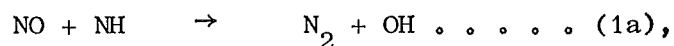
rather than by pathway (1b):

$$NO + NH \quad \rightarrow \quad N_2O + H \ . \ . \ . \ . \ . \ (1b).$$


III. USE OF ISOTOPE LABELLING TO STUDY THE REACTION OF NO WITH

   NH IN A HYDROGEN-NITROGEN-OXYGEN FLAME

Direct evidence to support the occurrence of process (1a),

as opposed to process (1b), in hydrogen-nitrogen-oxygen flames was

obtained from the results of isotope labelling. Measurements

were carried out as previously in the fuel-rich flame

Z8 (H_2: N_2: O_2 = 4.5 : 8.0 : 1.0). Nitric oxide and ammonia were

added to the unburnt gas stream at constant initial concentrations

of 0.91% and 0.47% respectively, while samples for mass spectro-

metric analysis were withdrawn from the burnt gas region at a

distance of 1.0 mm from the reaction zone.

Nitric oxide containing 50% $N^{15}O$ was trapped at liquid

nitrogen temperature in an evacuated flask partly filled with

silica gel. The mass spectrum was first recorded in the absence

of the labelled reactant. Sampling was then continued while the

nitric oxide supply to the flame was passed through the flask

containing $N^{15}O$, which at this stage was allowed to warm to room

temperature. At the end of the run, the mass spectrum was

recorded again in the absence of $N^{15}O$. The measured peak heights

in successive scans were corrected for pressure fluctuations by

comparison with the corresponding mass 40 - Ar peaks, while

background corrections were determined from a run for flame Z8

containing no additives.

As shown in table XII, the results of the isotope labelling

experiment are consistent with the occurrence of the reaction:

$$N^{15}O + N^{14}H \rightarrow N^{15}N^{14} + OH \ . \ . \ . \ . \ . \ (1a).$$
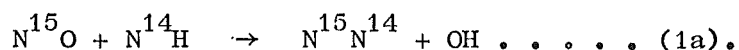
Introduction of the labelled reactant is followed by a rise in the

mass 31 - $N^{15}O$ peak. This is accompanied by an increase in the

peak at mass 29 due to $N^{15}N^{14}$, which persists until the concentration

of $N^{15}O$ in the nitric oxide supply has once again decreased to zero.

There is no evidence of a peak at mass 45 due to the alternative

product $N^{15}N^{14}O$.

According to the present mass spectrometric studies, when

nitric oxide and ammonia are added to a fuel-rich hydrogen-

nitrogen-oxygen flame, nitric oxide is removed in the reaction zone

of the flame by the fast process:

$$NO + NH \rightarrow N_2 + OH \ . \ . \ . \ . \ . \ (1a).$$
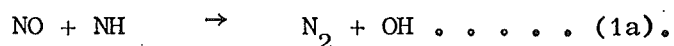
The alternative reaction path:

$$NO + NH \rightarrow N_2O + H \ . \ . \ . \ . \ . \ (1b),$$
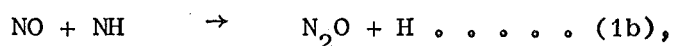
appears to be relatively unimportant. These results, which indicate

the formation of N_2 as the dominant stable product, are consistent

with calculated energy changes for the reaction of NO with NH.

Using data from the JANAF tables,[25] pathway (1b) is less

TABLE XII

Results from Isotopic Labelling of the Reactant NO in the

Reaction of NO with NH in Flame Z8

Sampling distance: 1.0 mm above reaction zone.

Mole fractions in unburnt gas: NO : 0.91×10^{-2} atm;

$\qquad NH_3$: 0.47×10^{-2} atm.

Scans (1) to (3) and (7) to (9) in absence of $N^{15}O$.

Scans (4) to (6) in presence of $N^{15}O$.

Scan Number	Peak Heights Relative to Argon in Burnt Gas			
	Mass: $29(N^{15}N^{14})$	$30(N^{14}O)$	$31(N^{15}O)$	$45(N^{15}N^{14}O)$
(1)	8.0	8.0	0.0	0.0
(2)	8.0	8.0	0.0	0.0
(3)	8.0	8.0	0.0	0.0
(4)	11.0	9.0	3.0	0.0
(5)	10.5	7.0	2.0	0.0
(6)	10.0	6.5	1.0	0.0
(7)	8.5	8.0	0.0	0.0
(8)	8.5	8.0	0.0	0.0
(9)	8.0	8.0	0.0	0.0

exothermic than pathway (1a) by 262.5 kJ mol^{-1}.

In future studies of the reaction of NO with NH in hydrogen-nitrogen-oxygen flames, it would be useful to obtain direct spectroscopic evidence for the presence of NH radicals in the reaction zone, possibly through laser fluorescence experiments. Further measurements involving isotopic labelling of reactants would also be of value. In the present work, since no further N^{15}O was available, the labelled experiment was limited to a single run and it was not possible to obtain reproducible data for the identification of N$_2$ as the dominant reaction product.

CHAPTER IX

SUMMARY

The aim of the present work was to study the combustion of trace additives in fuel-rich hydrogen-nitrogen-oxygen flames. Experimental results determined by mass spectrometric and spectroscopic methods were to be compared with the theoretical predictions of computer modelling to give information on the processes occurring in the breakdown of compounds such as cyanogen or nitric oxide in the combustion zone. Reaction rates and equilibria in the burnt gas stream were also to be investigated. The intention was to combine mass spectrometric profiles of stable species with flame photometric profiles of unstable atoms and free radicals to follow the progress of a reaction as a function of either time from primary combustion or initial additive concentration in the unburnt gas.

Preliminary studies consisted of a series of experiments to determine the chemical composition of the solid oxide particles formed in hydrogen-nitrogen-oxygen flames by the transition metals chromium, vanadium and iron. X-ray powder diffraction established the chromium and vanadium oxides as Cr_2O_3 and V_2O_3 respectively. Since the oxide composition appeared to be unaffected by changes in flame temperature or hydrogen to oxygen ratio, it was concluded that the particles formed by a given transition metal are characteristic of the metal rather than the flame, consisting in general of the solid oxide with the highest thermodynamic stability. Adsorption of gaseous sulphur dioxide at the surface of metal oxide particles was considered unlikely to be important under flame conditions.

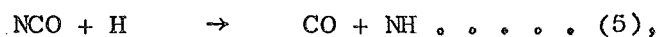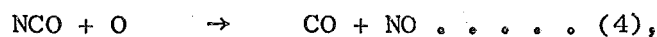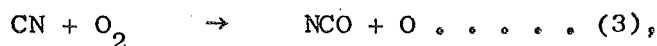Breakdown of cyanogen in the fuel-rich flame Z8

$(H_2: N_2: O_2 = 4.5 : 8.0 : 1.0)$ was investigated experimentally by

mass spectrometric measurement of the concentrations of stable

combustion products in the burnt gases emerging from the reaction

zone. The relative yields of HCN and carbon oxides from C_2N_2 were

found to depend on the percentage cyanogen added to the flame. For

additive concentrations ranging from 0.0% to 1.5% of the unburnt

composition, the measured ratio of HCN to CO/CO_2 product showed a

slow rise from 0.25 at 0.1% to 0.30 at 1.0% cyanogen, followed by

a more rapid increase to a value of approximately unity at 1.5%

cyanogen. These results were later compared with those obtained by

computer simulation. Using a model reaction scheme based on the

mechanism of Rentzepis and Sugden,[20] concentration profiles

through the reaction zone were calculated for the combustion of

cyanogen in flame Z8 over the composition range 0.02% to 1.0%

additive in the unburnt gas. The calculated ratio of HCN to

carbon oxide product was in all cases greater than unity. Thus the

present mechanism, which assumed production of HCN in the main

primary reaction:

$$H + C_2N_2 \rightarrow HCN + CN \quad \dots \dots (1),$$
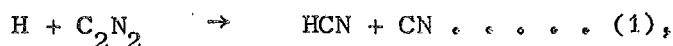
was inconsistent with the low yields of HCN observed in mass

spectrometric sampling. It was concluded that primary decomposition

of C_2N_2 must occur largely by reaction with atomic oxygen:

$$O + C_2N_2 \rightarrow NCO + CN \quad \dots \dots (2).$$
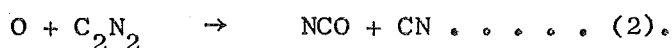
Conversion of CN and NCO radicals to carbon oxides would then take

place by the fast processes:

$$CN + O_2 \rightarrow NCO + O \quad \dots \dots (3),$$

$$NCO + O \rightarrow CO + NO \quad \dots \dots (4),$$

$$NCO + H \rightarrow CO + NH \quad \dots \dots (5),$$

while formation of HCN would be limited to relatively slow reactions

of the type:

$$CN + H_2 \rightleftharpoons HCN + H \ldots \ldots (6).$$

Further work to develop a model reaction scheme which accurately simulates the processes occurring in the combustion of cyanogen in hydrogen flames is now being undertaken by Professor L.F. Phillips of this department. The revised calculations are based on a mechanism in which initial decomposition of C_2N_2 occurs by attack of atomic oxygen. As suggested by the results of a recent experimental study,[23] the reaction of C_2N_2 with atomic hydrogen is assumed to lead to formation of a cyclic intermediate:

$$H + C_2N_2 \rightarrow H(CN)_2 \ldots \ldots (7),$$
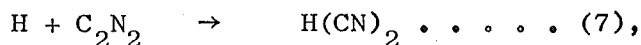
destruction of the intermediate by further reaction with H atoms giving either CN radicals or C_2N_2:

$$H(CN)_2 + H \rightarrow H_2 + 2CN \ldots \ldots (8a),$$

$$\rightarrow H_2 + C_2N_2 \ldots \ldots (8b).$$
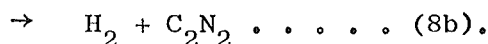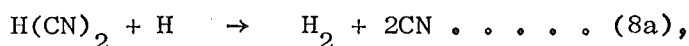
Breakdown of C_2N_2 to CN and NCO radicals therefore takes place by processes which do not involve the production of HCN. As a result, the calculated yields of HCN are expected to be lower than the corresponding yields of CO/CO_2 mixture, in closer agreement with the present experimental ratios of HCN to carbon oxide product.

In the combustion of cyanogen in flame Z8, mass spectrometric analysis of the burnt gas stream indicated that nitric oxide formed in breakdown of the additive is destroyed by a process sufficiently fast to reach equilibrium within a millisecond of the reaction zone. Removal of nitric oxide was attributed to a rapid reaction with NH radicals:

$$NO + NH \rightarrow products \ldots \ldots (9).$$
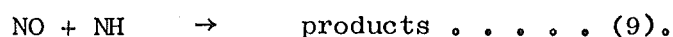
This prediction was later confirmed by mass spectrometric measurement of NO profiles in the burnt gases of the same flame containing the additives nitric oxide and ammonia in initial concentrations of 0.90%

and 0.0% to 1.15% respectively. The reaction of NO with NH was found

to reach completion within the combustion zone. Preliminary

experiments using isotopic labelling of the reactant NO gave evidence

for the production of molecular nitrogen by the process:

$$NO + NH \rightarrow N_2 + OH \ . \ . \ . \ . \ . \ (9a),$$
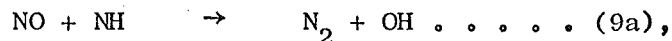
as opposed to formation of nitrous oxide by the alternative pathway:

$$NO + NH \rightarrow N_2O + H \ . \ . \ . \ . \ . \ (9b).$$
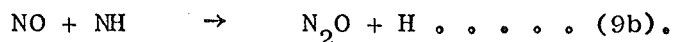
Within the detection limits of the sampling system, nitrous oxide

was not observed as a stable reaction product. Thus the results

were consistent with removal of nitric oxide by process (9a), the

rate constant being of the order of 10^{10} m^3 $kgmol^{-1}$ s^{-1}, comparable

to the rates of other radical exchange reactions which are

equilibrated in the combustion zone of a hydrogen flame.

A section of the work dealt with the reaction of NO with CN

radicals:

$$CN + NO \rightarrow N_2 + CO \ . \ . \ . \ . \ . \ (10).$$
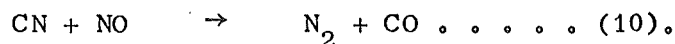
In flame Z8 containing 1.1% cyanogen and 2.0% nitric oxide, mass

spectrometric profiles of HCN and NO as a function of time from the

reaction zone were combined with the photometric profile of H atom

concentration to determine a value for the rate constant k_{10} at the

burnt gas temperature:

$$k_{10} = 7.5 \times 10^9 \ m^3 \ kgmol^{-1} \ s^{-1} \ at \ 1500 \ K.$$

Combined spectroscopic and mass spectrometric results were

also used to determine metal cyanide dissociation energies in a

study of the formation of alkali metal cyanides in hydrogen-nitrogen-

oxygen flames. Measurements were carried out in flame Z8 at a

distance of 4.0 mm from the reaction zone. At a given initial

concentration of cyanogen, the ratio of metal cyanide to free

metal atoms was obtained from the emission intensity at the metallic

resonance lines, while the corresponding concentration of HCN was

taken from the mass spectrometric profile for the yield of HCN from C_2N_2 as a function of percentage cyanogen added to the flame. This enabled a value to be calculated for the equilibrium constant of the reaction:

$$M + HCN \rightleftharpoons MCN + H \ . \ . \ . \ . \ . \ (11).$$
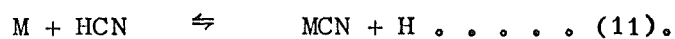
Combination of K_{11} with the partition functions for reactants and products gave the enthalpy of reaction at absolute zero and thus the dissociation energy of the metal cyanide.

ACKNOWLEDGEMENTS

REFERENCES

(1)   McEWAN, M.J. Thesis, Ph.D., University of Canterbury, 1965.

(2)   PHILLIPS, L.F. Thesis, Ph.D., University of Cambridge, 1960.

(3)   PADLEY, P.J. Thesis, Ph.D., University of Cambridge, 1959.

(4)   SUTTON, M.M. Thesis, Ph.D., University of Leeds, 1966.

(5)   SMITH, S.K. and GORDON, A.S. J. Chem. Phys. 22, 1954. 1150p.

(6)   FRIEDMAN, R. and CYPHERS, J. J. Chem. Phys. 23, 1955. 1875p.

(7)   FRISTROM, R.M., PRESCOTT, R. and GRUNFELDER, C. Combustion

      and Flame 1, 1957. 102p.

(8)   MAVRODINEANU, R. and BOITEUX, H. "Flame Spectroscopy".

      New York, Wiley, 1965.

(9)   DE VOSS, J.C. Physica 20, 1954. 690p.

(10) GAYDON, A.G. "The Spectroscopy of Flames". London, Chapman

      and Hall, 1957.

(11) PADLEY, P.J. and SUGDEN, T.M. Seventh Symposium (International)

      on Combustion. London, Butterworths, 1959. 235p.

(12) KALLEND, A.S. Combustion and Flame 11, 1967. 81p.

(13) KELLEY, R. and PADLEY, P.J. Nature 216, 1967. 258p.

(14) BULEWICZ, E.M., JONES, G. and PADLEY, P.J. Combustion and

      Flame 13, 1969. 409p.

(15) BULEWICZ, E.M. and PADLEY, P.J. Combustion and Flame 15, 1970.

      203p.

(16) A.S.T.M. Data File. Swarthmore, Pennsylvania, American Society

      for Testing Materials, Joint Committee on Powder Diffraction

      Standards, 1945.

(17) COTTON, F.A. and WILKINSON, G. "Advanced Inorganic Chemistry".

      2d. ed. New York, Interscience, 1966.

(18) NIELSEN, M.L., HAMILTON, P.M. and WALSH, R.J. Symposium on

      Ultrafine Particles, Indianapolis, 1961. 181p.

(19) KERR, J.A., CALVERT, J.G. and DEMERJIAN, K.L. Chemistry in Britain 8, 1972. (6) 252p.

(20) RENTZEPIS, P.M. and SUGDEN, T.M. Nature 202, 1964. 448p.

(21) BULEWICZ, E.M., PADLEY, P.J. and SMITH, R.E. Fourteenth Symposium (International) on Combustion. Pittsburgh, The Combustion Institute, 1973. 329p.

(22) VAN TIGGELEN, A., PEETERS, J. and VINCKIER, C. Thirteenth Symposium (International) on Combustion. Pittsburgh, The Combustion Institute, 1971. 311p.

(23) ALBERS, E.A. and others. Fifteenth Symposium (International) on Combustion. Pittsburgh, The Combustion Institute, in press.

(24) DUNN, M.R., FREEMAN, C.G., McEWAN, M.J. and PHILLIPS, L.F. J. Phys. Chem. 75, 1971. 2662p.

(25) JANAF Thermochemical Tables, NSRDS-NBS 37. 2d. ed. Washington, D.C., National Bureau of Standards, 1970.

(26) JANAF Thermochemical Tables, 1974 Supplement. Washington, D.C., National Bureau of Standards, 1974.

(27) BODEN, J.C. and THRUSH, B.A. Proc. Roy. Soc. A305, 1968. 93, 107pp.

(28) BULEWICZ, E.M., PHILLIPS, L.F. and SUGDEN, T.M. Trans. Faraday Soc. 57, 1961. 914p.

(29) HERZBERG, G. "Infrared and Raman Spectra". New York, Van Nostrand, 1945.

(30) GAYDON, A.G. "Dissociation Energies". London, Chapman and Hall, 1968.

(31) GAYDON, A.G. and WOLFHARD, H.G. "Flames". London, Chapman and Hall, 1953.

(32) BULEWICZ, E.M. and SUGDEN, T.M. Trans. Faraday Soc. 52, 1956. 1475p.

(33) SPALDING, D.B. and STEPHENSON, P.L. Proc. Roy. Soc. A324, 1971. 315p.

(34) PATANKAR, S.V. and SPALDING, D.B. "Heat and Mass Transfer in Boundary Layers". 2d. ed. London, Intertext, 1970.

(35) DAY, M.J., DIXON-LEWIS, G. and THOMPSON, K. Proc. Roy. Soc. A330, 1972. 199p.

(36) STEPHENSON, P.L. and TAYLOR, R.G. Combustion and Flame 20, 1973. 231p.

(37) BAULCH, D.L., DRYSDALE, D.D., HORNE, D.G. and LLOYD, A.C. "Evaluated Kinetic Data for High Temperature Reactions". London, Butterworths, 1972. 5v.

(38) ROSENFELD, J.L.J. and SUGDEN, T.M. Combustion and Flame 8, 1964. 37p.

(39) IWAI, T., PRATT, D.W. and BROIDA, H.P. J. Chem. Phys. 49, 1968. 919p.

(40) GORDON, S., MULAC, W. and NANGIA, P. J. Phys. Chem. 75, 1971. 2087p.

(41) MALTE, P.C. and PRATT, D.T. Fifteenth Symposium (International) on Combustion. Pittsburgh, The Combustion Institute, in press.

(42) THOMPSON, D., BROWN, T.D. and BEER, J.M. Fourteenth Symposium (International) on Combustion. Pittsburgh, The Combustion Institute, 1973. 787p.

(43) SAROFIM, A.S. and POHL, J.H. Fourteenth Symposium (International) on Combustion. Pittsburgh, The Combustion Institute, 1973. 739p.

(44) ZELDOVICH, YA.B. Acta Physicochim. URSS 21, 1946. 577p.

(45) BOWMAN, C.T. Combustion Science Technology 3, 1971. 37p.

(46) ENGLEMAN, V.S., BARTOK, W., LONGWELL, J.P. and EDELMAN, R.B. Fourteenth Symposium (International) on Combustion. Pittsburgh, The Combustion Institute, 1973. 755p.

(47) TAKAGI, T., OGASAWARA, M., FUJII, K. and DAIZO, M. Fifteenth Symposium (International) on Combustion. Pittsburgh, The Combustion Institute, in press.

(48) FENIMORE, C.P. Thirteenth Symposium (International) on Combustion. Pittsburgh, The Combustion Institute, 1971. 373p.

(49) NEWHALL, H.K. and SHAHED, S.M. Thirteenth Symposium (International) on Combustion. Pittsburgh, The Combustion Institute, 1971. 381p.

(50) BOWMAN, C.T. Fourteenth Symposium (International) on Combustion. Pittsburgh, The Combustion Institute, 1973. 729p.

(51) BOWMAN, C.T. and SEERY, D.J. "Emissions from Continuous Combustion Systems". Cornelius, W. and Agnew, W.G. ed. New York, Plenum Press, 1972. 123p.

(52) IVERACH, D., BASDEN, K.S. and KIROV, N.Y. Fourteenth Symposium (International) on Combustion. Pittsburgh, The Combustion Institute, 1973. 767p.

(53) EBERIUS, K.H. Fourteenth Symposium (International) on Combustion. Pittsburgh, The Combustion Institute, 1973. 775p.

(54) YAMAGISHI, K. and others. Fifteenth Symposium (International) on Combustion. Pittsburgh, The Combustion Institute, in press.

(55) MERRYMAN, E.L. and LEVY, A. Fifteenth Symposium (International) on Combustion. Pittsburgh, The Combustion Institute, in press.

(56) FENIMORE, C.P. Combustion and Flame 19, 1972. 289p.

(57) DE SOETE, G.G. Fifteenth Symposium (International) on Combustion. Pittsburgh, The Combustion Institute, in press.

(58) APPLETON, J.P. and HEYWOOD, J.B. Fourteenth Symposium (International) on Combustion. Pittsburgh, The Combustion Institute, 1973. 777p.

(59) HEYWOOD, J.B. and others. Journal of the American Institute

of Aeronautics and Astronautics 9, 1971. (5) 841p.

(60) FLETCHER, R.S. and others. "The Control of Oxides of Nitrogen

Emissions from Aircraft Gas Turbine Engines". Cambridge,

Mass., Northern Research and Engineering Corporation, 1971. 3v.

(61) CORNELIUS, W. and AGNEW, W.G. "Emissions from Continuous

Combustion Systems". New York, Plenum Press, 1972.

(62) AIRESEARCH COMPANY. "Exhaust Emissions Test AiResearch

Aircraft Propulsion and Auxiliary Power Gas Turbine Engines".

AiResearch Company, 1971.

(63) CERNANSKY, N.P. and SAWYER, R.F. Fifteenth Symposium

(International) on Combustion. Pittsburgh, The Combustion

Institute, in press.